DISTRIBUTED STATE ESTIMATION WITH THE MEASUREMENTS OF PHASOR MEASUREMENT UNITS

by

XUAN YANG

A thesis submitted to
The University of Birmingham
for the degree of
DOCTOR OF PHILOSOPHY

School of Electronic,
Electrical and Computer Engineering
The University of Birmingham
July 2013

To my parents

ACKNOWLEDGEMENTS

ABSTRACT

The world-wide application of Phasor Measurement Units (PMUs) brings great benefit to power system state estimation. The synchronised measurements from PMUs can increase estimation accuracy, synchronise states among different systems, and provide greater applicability of state estimation in the transient condition. However, the integration of synchronised measurements with state estimation can introduce efficiency problems due to the substantial burden of data.

The research is divided into two parts: finding a solution to cope with the computational efficiency problem and developing a transient state estimation algorithm based on synchronised measurements from PMUs.

The computational efficiency problems constitute important considerations in the operation of state estimation. To improve the low computational efficiency, two distributed algorithms are proposed in Chapters 4 and 5. In these two algorithms, the modelling, structure, and solution are described, and the corresponding procedures of bad data processing are presented. Numerical results on the IEEE 30-bus, 118-bus and 300-bus systems can verify the effectiveness of the two proposed algorithms.

A novel transient state estimation algorithm based on synchronised measurements is proposed in Chapter 6. Considering the scanning cycle and sampling rate of PMU measurements, the proposed algorithm can estimate transient states in a practical way. The performance of the proposed algorithm is demonstrated in a transient simulation on the IEEE 14-bus system.

Table of Contents

List of Figures

List of Tables

List of Abbreviations

DSELC   Distributed State Estimation with Linear Coordination

DSSE   Distributed Space State Estimation

EI   Estimation Identification

EMS   Energy Management System

FACTS   Flexible AC Transmission System

FDSELC   Fast Distributed State Estimation with Linear Coordination

GPS   Global Positioning System

HTI   Hypothesis Testing Identification

IEEE   Institute of Electrical and Electronics Engineers

LNR   Largest Normalised Residual

PMU   Phasor Measurement Unit

RTU   Remote Terminal Unit

SCADA   Supervisory Control and Data Acquisition

TSE   Transient State Estimation

WAMS   Wide Area Measurement System

WLS   Weight Least Square

CHAPTER 1 INTRODUCTION

1.1 Research Background

1.1.1 Status of Power System Development

In the late 18th century, the first commercial use of electricity for arc lamps lighted the world, and this was the beginning of what would change traditional life. Electricity was soon widespread, and a multitude of new appliances driven by electricity were invented, which could make life better. Currently, the power system transmitting power from suppliers to consumers is becoming one of the largest industries in the world.

Normally, the modern power system can be divided into three main parts: generation, transmission network and consumers. The electricity is produced in generated stations by different types of sources such as fossil fuels and renewable sources. Thereafter, this electricity is transmitted to consumers spared in different locations through a complex and huge network comprising of a large number of components including overhead transmission lines and underground cables, transformers, power electronics devices, etc,.

The network is named as the transmission network, and this network is typically classified into three main subsystems depending on different levels of voltage (from high to low). These three subsystems are transmission system, sub-transmission

system and distribution system. The transmission system connects major generating stations and main load centrals and it is the backbone of the modern power system. The electricity is transmitted from the transmission system to sub-transmission and distribution systems, and then dispatched to consumers. This thesis also focuses on the transmission system.

The capacity of power systems depends on customer demand. The increasing needs of electricity in daily life and modern industry spur the expansion of power system capacity. For instance, in the UK, the amount of electricity generated increased continuously from 1973 to 2007, as illustrated in Fig. 1.1. The same situation happened around the world at the same time, and it is even more apparent in the developing countries such as China and Brazil. This growth of capacity requires larger and more reliable power systems, and increases the complexity of these systems correspondingly.
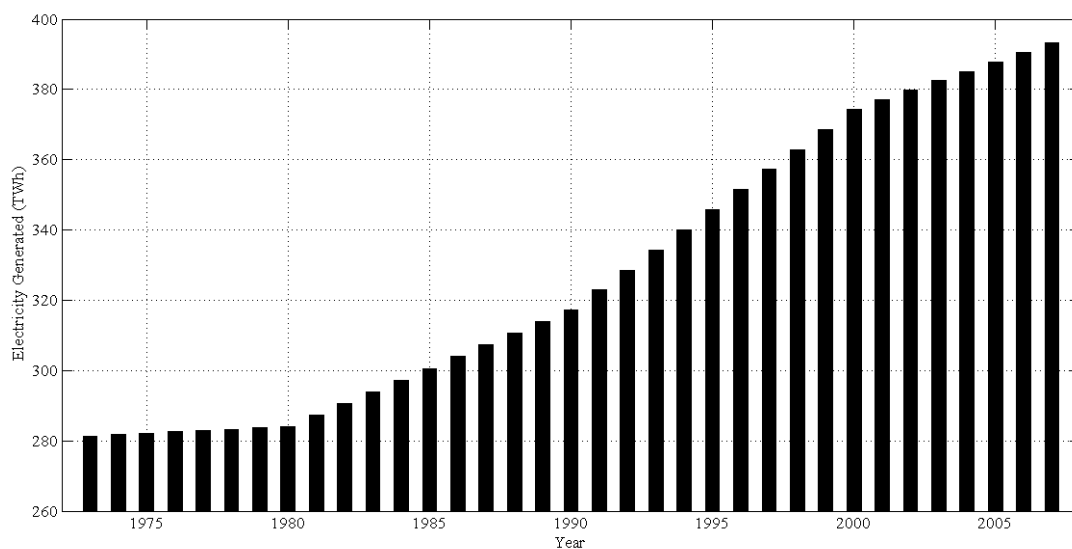
Fig. 1. 1. Electricity generated in the UK from 1973~2007

Another important factor concerning the complexity is the integration of renewable energy sources with modern power systems. The traditional dominant resources to generate electricity are coal and oil [1]. As typical fossil fuels, they have negative effects on the environment, such as the greenhouse effect, air pollution, etc. This problem became more notable in the last decade of the 20th century, and it soon attracted high attention around the world. The calls for environmental protection propel the international community to speed up the research into renewable technologies. Since then, the share of renewable energy sources in electricity generation has been raised sharply. In the UK, the capacity of renewable sources has been tripled during the last ten years, as shown in Fig. 1.2 [2], as well as the U.S., France, Germany, China, and other countries [3, 4].
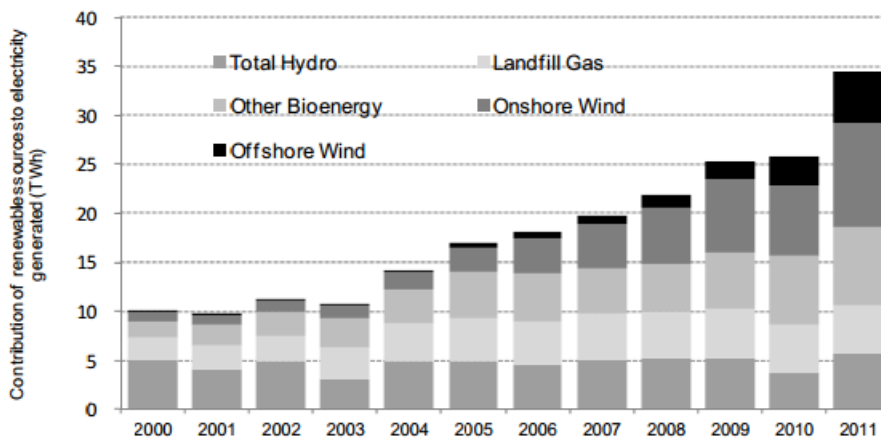
Fig. 1. 2. Electricity generated by main renewable sources in the UK from 2000~2011

With increasing penetration of renewable energy sources, multiple challenges appear in the control, protection, and operation of power systems. The financial and regulatory restricts have forced electricity utilities to employ new technology such as

Flexible AC Transmission System (FACTS) devices, which increases the complexity further, and thus higher security level becomes necessity. However, the existing power system cannot satisfy the increasing security requirements in some extreme situations. Even in the developed countries, more than ten severe blackouts happened in the last decade. For example, in 2003, the Northeast Blackout in the U.S. and Canada shocked the world, and led to economic losses of about 6 billion dollars [5]. This event reemphasise the importance of power system security.

The security of power system refers the ability to survive imminent disturbances without interruption to customer service [6]. It requires system operators to react correctly in case of contingencies and/or disturbance. Of all the functions in power system operation, the security analysis of power system is an essential one in control centres. To enhance the security analysis, the Energy Management System/Supervisory Control and Data Acquisition (EMS/SCADA), a successful analytical tool, was developed in 1990s. It is widely employed in power industry to monitor and control modern power systems.

The EMS/SCADA system includes three parts [7]. The first part is the EMS system comprising several functions to control and manage power system. In case of disturbances, the EMS system has to react correctly in time, or a serious blackout might occur. The SCADA system is the second part, which contains a number of monitoring devices at substations and measuring instruments in networks. It is responsible for capturing raw measurements of power systems and transmitting them

to control centres. The last part provides planning and analysis functions to aid power systems in control and off-line analysis.

Conventionally, in the SCADA system, Remote Terminal Units (RTUs) are used to capture raw measurements. In practice, measurement errors cannot be avoided in telemeter data because of the inevitable conditions such as inaccurate transducer calibration, noise in communication channels, unbalanced phases, etc [8]. So, these raw measurements cannot be directly used in the EMS functions or the planning and analysis functions until the background noise and gross errors in them are filtered, and this process is known as state estimation [7]. Fig 1.3 shows the typical configuration of the EMS/SCADA system, and how state estimation acts as a bridge between the EMS and SCADA systems.

1.1.2 Power System State Estimation

Power system state estimation is "indeed a systematic procedure-a mathematical procedure-to process the set of real-time measurements to come up with the best estimate of the current state of the system" [8]. It utilises redundant measurements from the SCADA system to compute the on-line states of buses in an estimator. The estimator is the hardware to perform state estimation. Normally, RTUs provide these raw measurements, including active and reactive power flows, active and reactive power injections and voltage magnitudes [8]. State estimation calculates the voltage magnitudes and phase angles of buses. These states (voltage magnitudes and phase angles) can be transmitted to and utilised in power system monitoring, controlling,

dispatching, security analysis, etc.
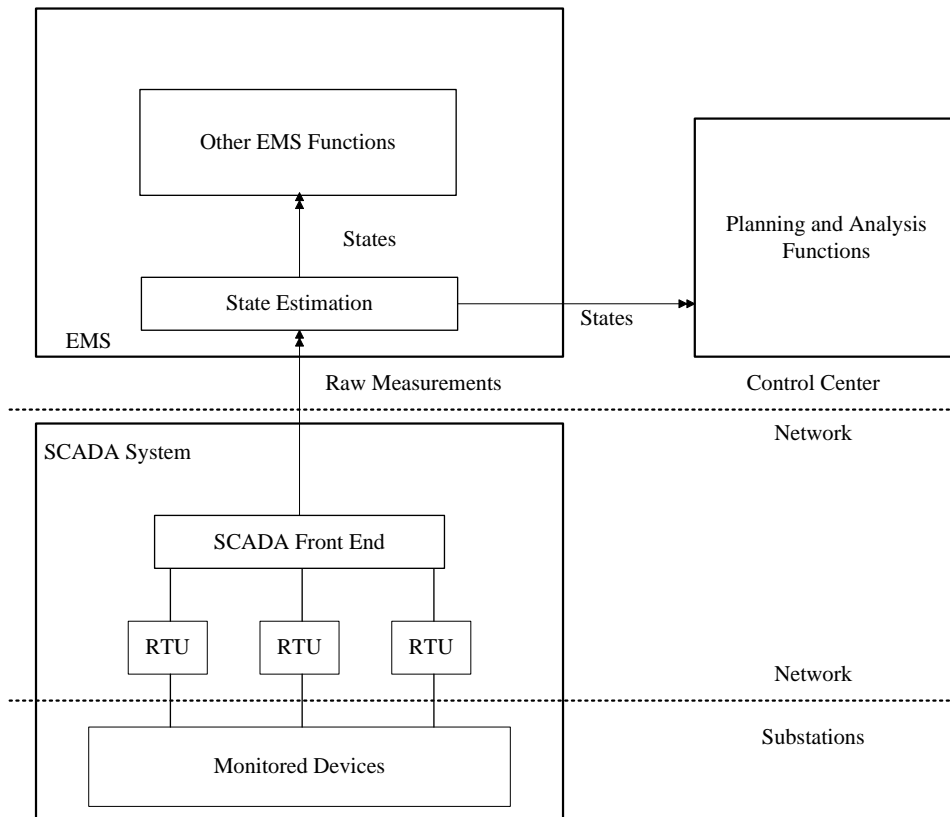
Fig. 1. 3. Typical configuration of the EMS/SCADA system

The concept of state estimation was first proposed by Fred Schweppe in 1970 [9-11]. These publications are considered as the starting point of state estimation, and their importance has long been recognised in industry [12]. Since Schweppe's proposals, state estimation has become an attractive topic, and a large amount of progress has been achieved to enhance its performance.

Typically, state estimation can be classified as static and transient state estimation according to the model employed. Static state estimation stands in a dominant position in the development of state estimation due to its reduced requirement of hardware. In this situation, the majority of researches are focused on static state

estimation, whilst the publications about transient state estimation are rare. So far, all the practical estimators have employed static state estimation, and conventional state estimation, to some extent, can be considered as the static state estimation.

Currently, state estimation is becoming the foundation of the EMS/SCADA system, and it is an indispensable part in control centres of power systems. The real-time results of state estimation can determine the accuracy of several functions in power system control and protection. In practical operation, the reliability is the most important factor in estimators, and several auxiliary procedures are integrated into estimators to guarantee the reliability. A practical state estimator contains the following functions [7], and a simple function diagram is shown as Fig 1.4.

- Topology Processor: Collects the status of circuit breakers and switches, and configures the topology of network.

- Observability Analysis: Determines the observability of the system and recognises unobservable islands if any exist.

- Estimation: Estimates optimal states from redundant measurements and system model.

- Bad Data Processing: Detects the existence of bad data in measurements and identifies bad data.

- Parameter and Structural Error Processing: Estimates network parameters, detects structural errors in network configuration and locates errors if any exist.
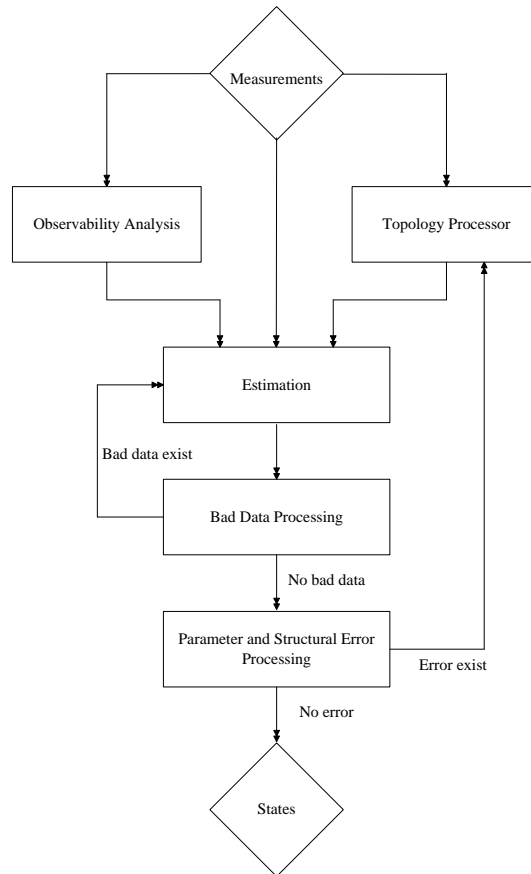
Fig. 1. 4. Function diagram of practical state estimation

This thesis is mainly focused on the procedures of estimation and bad data processing. More details about other procedures can be referred in a more comprehensive introduction [7].

In addition to the reliability, the accuracy and efficiency of state estimation are also critical, and they can be enhanced from two aspects. The first aspect is software. In this aspect, the accuracy and efficiency of state estimation are improved by the research of estimation model and the introduction of other mature techniques to state estimation. Different algorithms have been proposed in this aspect and an obvious progress has been achieved.

However, hardware development limits the software improvement in state estimation. The evolution of state estimation algorithms cannot satisfy the increasing demand for the accuracy and efficiency, especially in an extremely huge and complex power system. Hence, the hardware of state estimation also needs advancement. A typical example of this advancement occurred in the 1980s. The birth of Phasor Measurement Units (PMUs) brought a hardware breakthrough in state estimation. PMU measurements are more accurate and have a faster sampling speed than conventional RTU measurements. These characteristics not only improve the accuracy and efficiency of state estimation, but also enable a multitude of potential applications in state estimation.

1.1.3 Phasor Measurement Units (PMUs)

PMUs are novel measurement tools providing synchronised phasor measurements. The PMU measurements consist of the voltage and current phasors with time-tags from the Global Positioning System (GPS) signals [13]. In the 1980s, the PMU was invented by Arun Phadke at Virginia Tech. The configuration of the early PMU is illustrated in Fig. 1.5 [13].

Compared with conventional RTU measurements, PMU measurements have three advantages in principal [14]. They are in the form of phasors containing the information of magnitudes and phase angles. These phase angle measurements from PMUs can benefit power system monitoring, control and protection. On the contrary, RTU measurements are formed by magnitudes only. In addition, PMU measurements

9

are synchronised and time-stamped by the GPS signals. These measurements have precise time tags at the source, and the transmission speed of the measurements is no longer a critical parameter [13]. Finally, PMU measurements are more accurate and have a faster sampling rate. This can lead to several potential applications in power system operation.
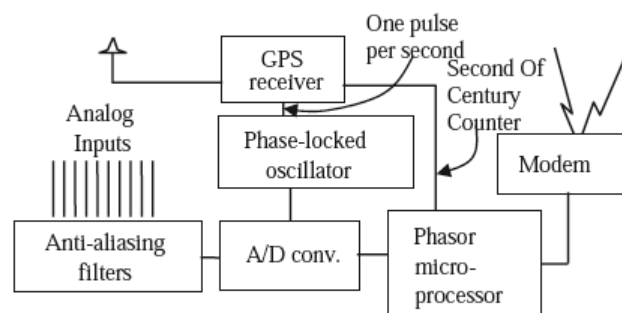
Fig. 1. 5. Configuration of the PMU

As a consequence of the progress of PMUs, more applications based on PMU measurements have been proposed [13]. A multitude of PMUs can form the Wide Area Measurements System (WAMS). This WAMS is helpful in power system operation, and some countries have installed the WAMS in their power system [15]. In the UK, the WAMS has also attracted much attention by its improvement in the real-time view of power systems. Details about the employment of WAMS and PMUs in the UK can be referred to in [16].

However, there are still some challenges in the application of PMUs. A major one is the comparatively high cost. Although the cost of PMUs is decreasing in these years, the price is still beyond expectations, and PMUs, in the near future, cannot be

employed at every substation. The most likely condition is that both PMUs and conventional RTUs would exist together in the SCADA system. Additionally, the utilisation of PMU measurements is still under development and power industry are still confused on how to use PMU measurements.

1.1.4 PMU Measurements in State Estimation

Although PMU measurements have obvious advantages, they cannot be employed in the EMS functions directly due to some inevitable conditions and potential errors. They are still raw measurements, and need to be filtered in state estimation. It is certain that the accurate and fast sampled PMU measurements can improve the performance of state estimation. Therefore, even before the birth of PMUs, the consideration of phasor measurements in state estimation had been discussed [17].

PMU measurements can enhance state estimation in the following aspects: the phase angle measurements from PMUs can improve the accuracy of the phase angle estimation, and provide the reliability of estimators [18]; the unique time-tags of PMU measurements can be used to synchronise the estimated results from different systems [19]; the more accurate PMU measurements can enhance the accuracy of state estimation, and their faster sampling rate can also increase the redundancy degree of state estimation [13].

To take the advantages of PMU measurements, scholars have proposed a number of methods to integrate them with state estimation. A successful example is the linear state estimation algorithm [13]. Without iterative process, the linear approach has

higher computational efficiency compared with conventional methods of state estimation. However, there is an inherent drawback in this linear approach that all the measurements must be provided from PMUs, and this drawback limits the application of this method in practical.

1.2 Motivations and Contributions

There are two main challenges in state estimation. One is utilising PMU measurements to improve the performance of estimators [17]. The other is solving the problems caused by the integration of PMU measurements with state estimation. The solution to the first challenge has been progressed in recent years, whilst there are still many problems unsolved in the latter challenge.

In the integration of PMU measurements with state estimation, two difficulties need to be overcome. The first difficulty is a limited number of PMUs can be installed in the power system. A reasonable placement of PMUs is necessary to achieve better observability and higher estimation accuracy [20]. Many algorithms have been proposed to discuss the placement, and consequently this problem has been mitigated. The second difficulty is the low computational efficiency caused by the integration [21]. It seems certain that the introduction of PMU measurements can improve the estimation accuracy, but at same time, this can lead to a huge computational burden. This problem constitutes a very important consideration in the practical application of state estimation with both RTU and PMU measurements, and it has not as yet been fully solved. This is one of the primary motivations for this thesis. Two algorithms are

proposed to mitigate this problem, and their effectiveness is verified by numerical simulations.

The linear estimation approach based on PMU measurements has impressively high computational efficiency. This characteristic is more meaningful in a huge and complex power system. However, the inherent drawback that all the measurements are required to be provided from PMUs restricts the practical application of this method [13]. To deal with this problem, the thesis proposes a method to create a suitable environment to satisfy the requirement. Therefore, it is possible to perform the linear approach with a limited number of PMUs in practice.

Additionally, transient state estimation is also discussed in this thesis. In practice, the operation of a power system is dynamic, and disturbances and faults are unavoidable. However, current research on transient state estimation is still theoretical due to hardware limitations. Fortunately, the appearance of PMUs changes the situation. A novel transient state estimation algorithm based on fast sampled PMU measurements is proposed. This algorithm can provide the flexibility for practical application of transient estimator.

In conclusion, the main contributions of this thesis can be summarised as follows:

1. Presentation of a method to perform linear estimation with a limited number of PMUs, and a corresponding procedure to detect and identify bad data in this method.

2. Proposal of a novel algorithm, namely the Distributed State Estimation with Linear Coordination (DSELC), utilising distributed configuration and linear estimation approach to mitigate the problem of low computational efficiency caused by the integration of PMU measurements with state estimation.

3. Introduction of PMU measurements in the fast decoupled state estimator, and description of a procedure to deal with bad data in this case.

4. Proposal of the Fast Distributed State Estimation with Linear Coordination (FDSELC) algorithm, which is developed from the DSELC algorithm and takes advantages of fast decoupled estimator, to further improve computational efficiency.

5. Proposal of a novel algorithm of transient state estimation using actual PMU measurements, called Distributed Space State Estimation (DSSE), which makes it possible to apply the transient state estimator in practice.

The DSELC algorithm is summarised in [21], and the FDSELC algorithm is presented in [22] and more details of this algorithm is described in [23]. The DSSE algorithm is proposed in [24].

1.3 Thesis Outline

This thesis consists of four parts. Part I provides general background information in state estimation and PMUs in three chapters (Chapters 1, 2 and 3). Part II of the thesis (Chapters 4 and 5) proposes two distributed state estimation algorithms, which are

used to solve the problem of the low computational efficiency in state estimation. In Part III (Chapter 6), a newly developed algorithm is proposed to perform the transient state estimation with PMU measurements. Part IV (Chapter 7) concludes this thesis. Details in each chapter are listed as follows:

- Chapter 2: The literature review on the historical development of state estimation and PMUs is presented.

- Chapter 3: The classical methods of static state estimation and bad data processing are reviewed.

- Chapter 4: The DSELC algorithm is proposed in this chapter. The method to perform the linear estimation method with a limited number of PMUs is presented, and the procedure of bad data processing for the linear estimation is also described.

- Chapter 5: The FDSELC algorithm is proposed in this chapter. The integration of PMU measurements with the fast decoupled state estimation is introduced, and the procedure of bad data processing in this case is also discussed.

- Chapter 6: The DSSE algorithm is proposed in this chapter. The transient state estimation models and corresponding differential equations are provided.

- Chapter 7: The thesis is summarised and future research topics are discussed.

CHAPTER 2 LITERATURE REVIEW

This chapter outlines the history of PMUs at first, and describes the related applications of PMUs in power systems. Then, the development of conventional state estimation is tracked, and some typical algorithms in state estimation are reviewed. Finally, the development of the use of PMU measurements in state estimation is described.

2.1 Phasor Measurement Units

Compared with conventional RTUs, PMUs are more accurate and have faster sampling rate. These advantages can enhance the power system in monitoring, controlling and protection. Since the 1990s, the development of PMUs has experienced a rapid progress in academia and industry. This section presents the historical development of PMUs and their applications in power system. More details can be referred to in [13].

2.1.1 Historical Development of PMUs

The invention of PMUs was based on the synchronised phasor measurement technology and the Global Positioning System (GPS) [25]. The synchronised technology was developed from the technology of phase angle measurement and the concept of positive-sequence voltages and currents [13]. Until the early 1980s, the measurement of phase angle could not be captured directly. The synchronisation of the reference time between different positions was a challenge. The first attempt to

synchronise clock was proposed in [26], where the LORAN C signal was used to perform the synchronisation. At the same time, other approaches determined reference time by the Harrisburg radio time signal [27] and the Geostationary Operational Environmental Satellite signals [28]. In these attempts, local phase angles were obtained through the next positive-going zero-crossing phase according to the reference signal, and these angles were then coordinated with a common reference angle. However, these methods were not suitable for practical applications, because they did not consider the information of magnitudes, and thus could not form phasor measurements. In spite of these flaws, these attempts contributed to the framework of PMUs.

As a consequence of the development of the positive-sequence voltages and currents, phasor measurements became possible. The importance of the positive-sequence voltages and currents was first emphasized in [29]. Combined the positive-sequence measurements with the technology of phase angle measuring, the concept of phasor measurements was identified in 1983 [30], and it was considered as the starting point of modern technology of synchronised phasor measurements. The advance of this technology provided the theoretical foundation of PMUs [31].

Similarly, the GPS [25] became mature in the 1980s. It was a better means to synchronise power systems and provide reference time. With the aid of GPS signals, the first prototype of PMUs was invented in Virginia Tech in the early 1980s [13]. In 1991, commercial PMUs were produced by Macrodyne [32], and the first practical

application of PMUs was then to record events at Plant Scherer in Georgia [33].

Due to their obvious merits, PMUs gained worldwide favour [15, 34], and their measurements were standardised soon. The Institute of Electrical and Electronics Engineers (IEEE) published the first standard of PMU measurements in 1995 [35], and unified the formats of these measurements and their transmissions. Ten years later, this standard was revised to adjust the progress of PMUs [36]. The latest standard was issued in 2011 [37, 38] covering measurement provisions and data communications of PMUs.

2.1.2 Application of PMUs in Power Systems

Initially, PMUs were considered as monitoring instruments, and their measurements were used to record events and to monitor the operation of power systems. In the last two decades, PMUs have extended their application range. Currently, PMU measurements are widely employed in the protection and control of power systems. These applications are introduced in this section, and [39] provides more details.

- Power system monitoring

The fundamental function of PMUs is to monitor the operation of power systems. During the early stage, PMUs were generally used as event recorders [33] or digital system disturbance recorders [39]. Meanwhile, it was found that PMUs can easily observe frequency oscillations. Thus, a frequency monitoring network comprising of PMUs was established to enhance the frequency monitoring of power systems [40].

After the shock of the Northeastern U.S. blackout in 2003, PMU measurements were found to be of great value in the post-mortem analysis. The final report of this blackout mentioned that power systems "require use of time-synchronised data recorders", and recommended that all power utilities employed PMUs consequently [5]. Currently, the Wide Area Measurement System (WAMS) comprising PMUs is proposed and implemented in power systems around the world [15]. Through the WAMS, power system monitoring can be more reliable.

- Power system protection

In addition to power system monitoring, PMUs can also benefit power system protection, especially in the adaptive protection and fault location technique.

As for the adaptive protection, two kinds of protection methods can be improved by PMU measurements: the multi-terminal differential protection and the out-of-step protection. The multi-terminal differential protection utilised the phase angle measurements from PMUs to reduce the cost of the synchronizing equipments [41]. Regarding the out-of-step protection, the real-time phasor measurements from PMUs can revise the values of parameters in the out-of-step blocking and tripping on-line. This revision can improve the performance of protection in terms of both accuracy and speed [42].

PMU measurements are also introduced to the fault location technique. In traditional estimation of fault location, there is a problem that the source or fault impedances would change in case of faults. This problem can lower the accuracy of the estimation.

The synchronised measurements from PMUs can guarantee the accuracy [43]. A practical operation in Taiwan power utility verified the effectiveness [44].

- Power system control

PMU measurements have a place in power system control as well. Conventional control was mainly based on local signals and measurements. These local terms limited the performance of the control at the wide area level. PMU measurements can form a wide area control system to mitigate this problem. A typical application of this system is in the small-signal instability [45]. Furthermore, based on this system, some new controllers such as the supervisory level power system stabilizer [46] and the wide area damping controller [47] were proposed to enhance the stability and robustness of the power system.

2.2 State Estimation

Typically, state estimation can be classified as static and transient state estimation according to different models. The development of these two kinds of estimation is briefly introduced in this section, and some important algorithms in them are also described. Several publications [8, 19, 48-50] provide outlines of state estimation, and more comprehensive information can be referred to in [7, 51].

2.2.1 Static State Estimation

Compared with the transient one, static state estimation has lower hardware requirements, which makes its implementation simple in practical power systems. As

a result, static state estimation attracted more attention in the development of state estimation. To some extent, conventional state estimation can be considered as the static state estimation.

Based on the load flow calculation and estimation theory, static state estimation was first proposed in 1970 [9-11]. It was defined as "a data processing algorithm for converting redundant meter readings and other available information into an estimate of the static-state vector", and as such it was used to deal with the uncertainties of measurements. In the practical operation, bad data was always appeared in the static state estimation, which had negative impacts such as the decrease in the estimation accuracy. A procedure, called bad data processing, was proposed to suppress this bad data in [52].

a)   Estimation process

Estimation process is the fundamental function in the static state estimation, and it determines states from redundancy measurements of the power system. A multitude of algorithms have been proposed to conduct this function. One successful method is the Weight Least Square (WLS) algorithm.

•   Development of the WLS algorithm

The WLS algorithm was proposed to solve the static state estimation, but its effect was not recognised by industry initially [9]. Fortunately, a revised version, based on the operational experience from power utilities, was developed soon and widely

accepted [53, 54]. Since then, the research on the WLS algorithm has progressed greatly, and several aspects in the WLS estimation, including the sensitivity of measurements [55], the convergence quality of the estimation [56, 57], the effects of weighting matrix [58], and the uncertainty of measurements [59, 60] have been investigated. These contributions promoted the development of the concept, model and solution of the WLS algorithm.

More methods have been proposed to improve the performance and provide greater applicability of the WLS algorithm. For instance, the fast decoupled load flow technique was introduced into the WLS estimation to reduce memory storage and improve computational efficiency [61]. A generalised state estimation considering the topology and parameter information was developed to provide greater applicability of the WLS algorithm [51, 62], and a more robust algorithm for the generalised state estimation was proposed by applying mixed integer nonlinear program in the last decade [63]. Recently, a modified WLS estimation utilising historical measurements to calculate the auto tuning weights for new measurements was presented in [64], and higher estimation accuracy can be obtained.

- Alternative Formulations of the WLS algorithm

From the practical perspective, some inherent drawbacks in the WLS algorithm, such as unsatisfied convergence in a large system, limit its application. In addition, the WLS estimation is prone to be ill-conditioned, and the estimation is numerically unstable in this condition [7, 8]. To improve the robustness, researchers have proposed

alternative formulations of the WLS algorithm. This improvement is mainly achieved through two methods: the Orthogonal Factorisation and the Equality-Constrained.

In the WLS estimation, a crucial reason for the divergence problem is the intrinsically ill-conditioned gain matrix [7]. The Orthogonal Factorisation methods were developed to avoid this ill-conditioned gain matrix by the factorisation of the Jacobian matrix [65-69]. The Golub's approach was first introduced to factorise the Jacobian matrix in [65]. This approach improved the numerical stability of the WLS algorithm, but at the same time, it brought a huge computational burden. Based on the Givens rotation, a fast approach was proposed to solve this problem [66]. In addition, the row ordering technique was introduced to improve efficiency [69]. In these two attempts, the Jacobian matrix was reduced by rows, and the computational burden can be reduced effectively.

Another reason for the divergence problem is the use of virtual measurements in the WLS estimation, such as zero injections. The corresponding weights of these virtual measurements are very high, and this can tend to make the gain matrix ill-conditioned [70]. On the other hand, these virtual measurements cannot be ignored, because the estimation accuracy may be decreased without them [71]. The Equality-Constrained methods were proposed to model these virtual measurements as equality-constraints [70-74]. Thus, these measurements can be excluded from the Jacobian matrix, and their large weights can be avoided. The Lagrangian multiplier was first introduced to solve the equality-constraints model in [72]. This method was effective, but it had an

unsymmetrical matrix, which might lead to the computational difficulty. Subsequently, a matrix with the positive definite coefficient was employed to simplify the computation processes and improve the robustness [73]. This method was further enhanced by the symbolic optimal ordering and the unique signed-Cholesky factorisation in [74].

b)   Bad Data Processing

The bad data processing contains two processes: bad data detection and identification. The detection is to check the existence of bad data in the measurements of the state estimation. If the bad data is detected, the identification process starts to locate this bad data. The concept of the bad data processing was first defined in [52]. Three detection theories and two identification tests were proposed in [75] to deal with the bad data in the WLS estimation. One of them, the Largest Normalised Residual (LNR) test, can identify the single bad data easily and reliably, and thus it was widely accepted soon.

However, there are two drawbacks blocking the practical application of approaches in [75]. At first, the determination of the threshold in the detection process is difficult. A method, namely the Chi-square method, can be used to solve this problem [7]. This method is based on the fact that the objective function in the WLS estimation has a Chi-squares distribution. The other drawback is the lower accuracy of the bad data identification in case of multiple bad data. To increase the accuracy, the LNR test was revised to adjust multiple bad data.

The first attempt modified the LNR test by geometric integration [76]. A novel algorithm was also established to introduce the measurement dependencies to the LNR test to recognise multiple bad data [77]. On the other hand, some scholars indicated that this modification of LNR test was inferior to satisfaction due to the inherent drawbacks of the test. In this situation, two improved methods, named as Estimation Identification (EI) [78] and Hypothesis Testing Identification (HTI) [79, 80], were developed to replace the LNR test in bad data identification. In the EI approach, an inverse of the reduced residual sensitivity matrix was calculated and utilised to identify multiple bad data [78]. The HTI method estimated the errors of residuals to locate multiple bad data [79, 80]. The HTI approach had less computational burden than the EI approach [81]. Furthermore, several methods for multiple bad data identification in some special systems were proposed, such as in an unobservable system [82] and in a non-uniquely observable system [83].

In addition, the alternative formulation of the WLS estimation can be also used to eliminate bad data. For instance, the state estimation problem was reformulated as a linear problem rather than a least square problem, and linear solution can be used to solve the problem correspondingly [84]. This approach reserved the degree of noise filtering and provided the capability of bad data rejection.

2.2.2 Transient State Estimation

The static state estimation is executed on the static model of the power system, and it was reasonable in the early stage due to hardware limitations. However, the dynamics

of the power system could not be treated as static one in the practical situation. When some disturbances or faults happen, the power system experiences a transient process, and the static state estimation cannot satisfy the requirement of accuracy in this process. Hence, the transient state estimation is necessary, and some methods have been proposed to deal with the transient state estimation.

Initially, a discrete nonlinear observer was utilised to perform the transient state estimation [85]. This method adopted the nonlinear differential equations to represent the transient model of the power system, and these equations were then discretised by the Taylor expansion. The above process became the foundation of the transient state estimation. Considering the synchronised machine, another attempt was published in [86]. An invariant imbedding non-linear dynamic method was used to estimate transient states in this attempt.

In the last decade, the progress of computer made the simulation of transient state estimation possible. Based on the state-space theory and the first-order differential equations, the Transient State Estimation (TSE) algorithm was proposed in [87]. Numerical simulations verified its effectiveness, but this algorithm was difficult to apply in practical power systems, because its hardware requirements cannot be satisfied. Another novel method was proposed to guide upgrading existed static state estimator to adjust the transient condition [88]. This method was useful, but it cannot solve the problem fundamentally.

The potential use of PMU measurements in transient state estimation was discussed in

the latest proposal [89]. This proposal recognised the capability of PMU measurements for capturing transients, and attempted to utilise these measurements, instead of solutions of conventional static state estimation, to form snapshots of power systems during the transient condition. However, the proposal focused on identifying transient incidents by PMU measurements rather than considering these measurements in the transient state estimation. Therefore, so far, no method can be used to perform the transient state estimation in practices.

2.2.3 Algorithms in State Estimation

To achieve higher accuracy and efficiency, a multitude of algorithms have been proposed in state estimation. According to different configurations, these algorithms are usually divided into two groups, centralised algorithms and distributed algorithms. Generally, the distributed algorithms are developed from centralised ones to reduce computational burden. Some typical algorithms in these two groups are briefly introduced in this section.

a) Centralised Algorithms

In the centralised algorithms, the estimation for the overall system is performed at one time, and this can simplify the structure of these algorithms. The objectives of these centralised algorithms can be also divided into two categories.

The first category is to increase the applicability of the estimation. This is always achieved by considering the models of devices or special systems in the estimation.

For instance, some centralised algorithms were proposed to combine the model of the multi-terminal system or FACTS devices in the estimation [90-94]. The existing algorithms of transient state estimation [85-87] are all belonged to this category, because the transient model of power systems is considered in them.

The other algorithms are to improve the performance of the estimation. Two main options can achieve this target. Some algorithms are proposed to improve the estimation model, such as the optimisation of solutions and factorisation of matrices in the estimation. The alternative formulations of the WLS algorithm [65-74] described above belong to this type. The other option is to introduce other mature techniques to the estimation. For example, the fast load flow technique was introduced in state estimation to improve computational efficiency [61, 95-97].

b)   Distributed Algorithms

The distributed algorithms are derived from the centralised algorithms to enhance computational efficiency [9]. The states in these algorithms are normally estimated in each subsystem individually, and this can reduce the computational burden in local estimations. In recent years, as a result of the rising of Smart Grids and the power industry reformation, the distributed configuration has attracted more attention than ever before [19]. It is certain that the distributed algorithms will be more significant in future state estimation. An early survey about these distributed algorithms was described in [98], and a more comprehensive introduction was presented in [49]. In this thesis, all the three algorithms proposed utilise the distributed configuration.

According to computational configuration, the structure of distributed algorithms could be divided into the hierarchical configuration and the decentralised configuration.

- Hierarchical Configuration

The hierarchical algorithms are constructed of the subsystem level and the coordination level. A large system is divided into a number of subsystems, and these subsystems constitute the subsystem level. The local estimation in each subsystem is performed separately. These local solutions are then coordinated at the upper level. Thus, the estimated results are only communicated between local estimators and the coordinator. This communication scheme is illustrated in Fig. 2.1.
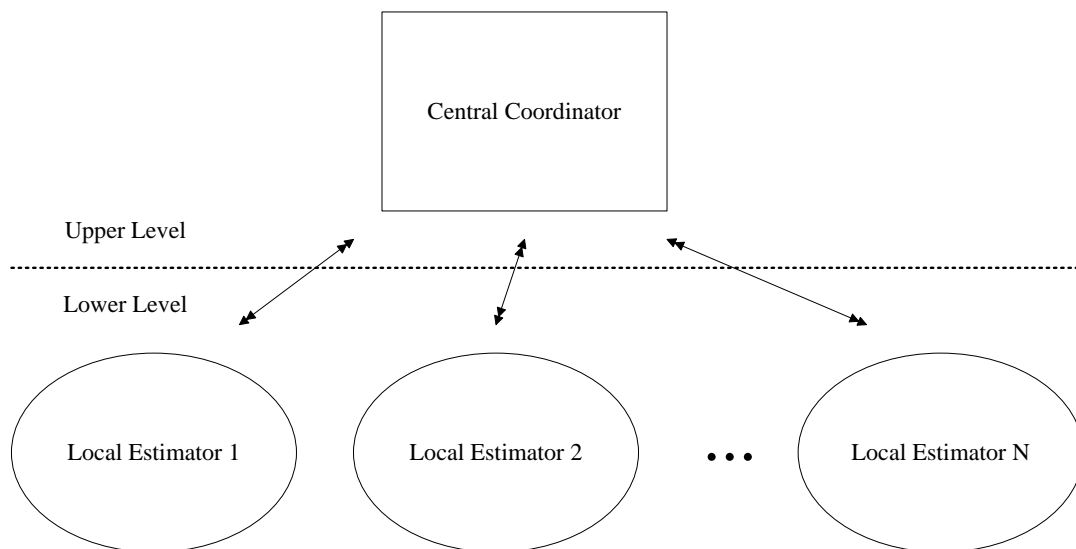
Fig. 2. 1. Communication scheme in hierarchical configuration

The hierarchical algorithms can be further divided into two groups by different coordination schemes. One group coordinates local results only once [99-105], and the other one conducts the coordination repeatedly [106-110].

The first group attracts more attention due to its simple implementation. The proposed algorithms in Chapters 4 and 5 belong to this group. In this group, the first method to re-estimate local results was published in [99], and this method utilised an overlapping strategy to decompose the large system. A novel algorithm was then proposed to replace the decomposition strategy as a non-overlapping one [100]. The data process cost and local computer memory can be reduced in this method. A faster and more flexible algorithm was developed in [101] to further reduce computational burden and hence improve computational efficiency. These three algorithms were formulated, demonstrated and compared in [102].

A reduced model with tie-line measurements was introduced to the hierarchical configuration to coordinate local results [104]. Most recently, [105] suggested a simple and efficient methodology to reduce the bandwidth requirements. This method only utilised the processed measurements other than raw measurements in the estimation.

- Decentralised configuration

As for the decentralised algorithms, the coordination process is not necessary. Local estimations are performed with the aids of boundary measurements from neighbouring subsystems. The data is only communicated between adjacent subsystems, as shown in Fig. 2.2.

Compared with the hierarchical algorithms, the decentralised algorithms require less

on hardware, and their calculations are comparatively simple. So, the initial distributed state estimation algorithm employed this configuration [9]. Afterwards, some important progress promoted the development of decentralised algorithms [106, 111-113]. The mature decentralised algorithm was proposed in [106]. The solutions from neighbouring systems were assumed to be optimised, and this assumption was the theoretic basis to discard the coordination.
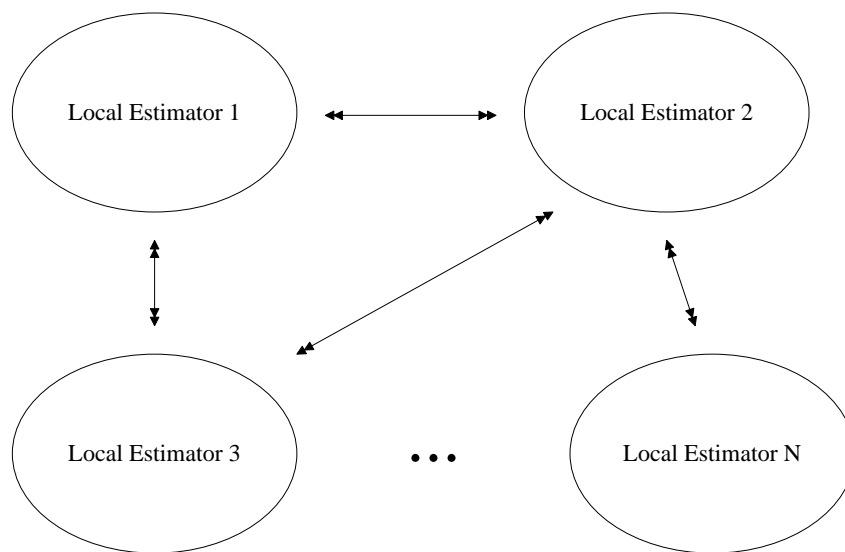
Fig. 2. 2. Communication scheme in decentralised configuration

However, the convergence problem becomes worse in the decentralised algorithms, and the synchronisation problem between local estimators is more serious. The convexity assumptions were introduced to the decentralised algorithms to deal with the convergence problem [111]. A revised algorithm was proposed in [112], and it was more suitable for hardware implementation and on-chip execution. In 2007, a novel decentralised procedure was proposed based on the optimisation technique [113], and the robustness and applicability of this method were both improved.

2.3 State Estimation with PMU Measurements

Considering the accurate synchronised phasor measurements from PMUs, the performance of state estimation could be improved apparently. Since the birth of PMUs, researchers began to integrate PMU measurements with state estimation. Thereafter, the integration of PMU measurements into state estimation has been an attractive topic, and its development is reviewed in this section.

• Development of the integration

The first attempt to use synchronised phasor measurements in state estimation was addressed in [17, 18], even before the invention of PMU hardware. The modified estimation model contained phasor measurements, and the corresponding results were observed to be more accurate. Moreover, the modified gain matrix became more sparse and constant, and the computational efficiency of the estimation could be improved consequently. In the last decade, with the progress of the manufactory, PMUs have been widely employed in practical power systems [15]. In this situation, the integration of PMU measurements with state estimation attracts more attention, and several publications have been proposed to promote this integration [114-117].

One important application of synchronised measurements in state estimation is to synchronise different estimators. This is more meaningful in the distributed algorithms. The first attempt to introduce PMU measurements in distributed algorithms was proposed in [118]. This method employed conventional hierarchical configuration and overlapping strategy to decompose the large system. Based on this

algorithm, a novel approach with a non-overlapping decomposition strategy was presented in [119]. This method can improve computational efficiency. The proposed algorithms in Chapter 4 and 5 are developed from these algorithms. In a recent publication [120], the diakoptics theory was combined with the distributed estimation. In this approach, PMU measurements were used to coordinate phase angles in each subsystem.

- Potential research for the integration

Currently, it is certain that PMUs will play a more important role in the Smart Grid [121]. As for future state estimation, PMU measurements would replace conventional RTU measurements. However, this cannot be achieved in the near future, because the cost of PMUs is still high. Additionally, RTUs have already been widely applied, and it would be a huge waste to discard all RTU measurements. The most likely condition is that both RTU and PMU measurements are utilised in state estimation at the same time. This compromise can increase the estimation accuracy apparently, but at the same time, two problems would be appeared.

The first problem is that only a limited number of PMUs can be installed in the power system. In recent decade, several methods have been proposed to find an optimal placement of the limited number of PMUs [20, 122-128]. With these contributions, a reasonable placement of PMUs could be obtained to achieve higher accuracy and better observability in state estimation. Thus, this problem is, to some extent, solved.

The other problem is the huge computational burden caused by the use of RTU and

PMU measurements together in the estimation. The computational efficiency is reduced then and this low efficiency may be unacceptable in the practical application. Existing distributed algorithms could mitigate this problem partly, but their efficiency was still not satisfied. Two algorithms are proposed in Chapters 4 and 5 to solve this problem, and their effectiveness are demonstrated by numerical simulations.

In addition, researches only tried to integrate PMU measurements with the static state estimation. Actually, the value of PMU measurements in the transient state estimation is also great. The characteristics of PMU measurements make it possible to implement the transient state estimation in practical power systems. Based on this potential application, a novel algorithm of the transient state estimation with PMU measurements is proposed in Chapter 6. This algorithm can provide greater applicability in the transient state estimation.

CHAPTER 3 CONVENTIONAL STATIC STATE ESTIMATION

3.1 Static State Estimation

State estimation can be classified as static and transient state estimation according to different models (static model and dynamic model). The static model of power system requires less on calculation and hardware. On the contrary, it is still a challenge to estimate states with the dynamic model even now. Therefore, static state estimation usually attracted more attention in the development of state estimation. The algorithms proposed in Chapter 4 and Chapter 5 also belong to static state estimation. This chapter introduces the fundamental concept, model, and solution of the static state estimation, and presents a corresponding procedure of bad data processing.

3.1.1 States and Measurements

The objective of state estimation is to determine the states of buses from the redundancy measurements of the power system. Two essential elements in state estimation are measurements and states. In static state estimation, the state of each bus includes the voltage magnitude and the phase angle. This state can be defined as:

$$x_i = \begin{bmatrix} v_i & \theta_i \end{bmatrix}^T \tag{3.1}$$

where

x_i state at Bus i;

v_i voltage magnitude at Bus i;

θ_i phase angle at Bus i;

All the measurements in conventional static state estimation are provided from RTUs. These RTU measurements are comprised of voltage magnitudes, active and reactive power flows, and active and reactive power injections, denoted by the subscript v, pf, qf, $pinj$ and $qinj$, respectively. Typically, RTU measurements z can be defined as:

$$z = \begin{bmatrix} z_v & z_{pf} & z_{qf} & z_{pinj} & z_{qinj} \end{bmatrix} \tag{3.2}$$

3.1.2 Measurement Model and Estimation Model

The measurement model in static state estimation demonstrates the relationship between the states and the measurements. Combined all these nonlinear relationships, the measurement model of the overall system can be obtained. This model and its compact form are expressed as [9]:

$$\begin{bmatrix} z_1 \\ z_2 \\ \vdots \\ z_m \end{bmatrix} = \begin{bmatrix} h_1(x_1, x_2, \cdots, x_n) \\ h_2(x_1, x_2, \cdots, x_n) \\ \vdots \\ h_m(x_1, x_2, \cdots, x_n) \end{bmatrix} + \begin{bmatrix} e_1 \\ e_2 \\ \vdots \\ e_n \end{bmatrix} \tag{3.3}$$

$$z = h(x) + e \tag{3.4}$$

where

z_i	measurement i;
$h_i(.)$	nonlinear function relating measurement i to states;
e_i	error of measurement i.
z	$m \times 1$ vector of measurements;
x	$n \times 1$ vector of states ($n < m$);
h	$m \times 1$ vector of nonlinear functions relating z to x;
e	$m \times 1$ vector measurement errors.

The covariance matrix of measurement errors, denoted by R, is introduced to solve the measurement model above. The configuration of this covariance matrix is shown in

(3.5), and it is formed on the corresponding standard deviation of independent measurements. It should be noticed that the measurement errors e_i is Gaussian noise, i.e. $E(e_i)=0$, and $e_i \sim N(0,R_{ii})$, where R_{ii} is the ith diagonal entry in the covariance matrix R.

$$R = \text{cov}(e) = \begin{bmatrix} \sigma_1^2 & & & \\ & \sigma_2^2 & & \\ & & \ddots & \\ & & & \sigma_m^2 \end{bmatrix} \tag{3.5}$$

where

R $m \times m$ covariance matrix of measurement errors, and this matrix is a diagonal matrix;

σ_i standard deviation of measurement i.

Afterwards, the estimation model of static state estimation is discussed. The estimation model is developed from the measurement model, and it represents the relationship between the measurements and the estimated results. Similar to the measurement model in (3.3) and (3.4), the estimation model and its compact form are formulated by:

$$\begin{bmatrix} z_1 \\ z_2 \\ \vdots \\ z_m \end{bmatrix} = \begin{bmatrix} h_1(\hat{x}_1, \hat{x}_2, \cdots, \hat{x}_n) \\ h_2(\hat{x}_1, \hat{x}_2, \cdots, \hat{x}_n) \\ \vdots \\ h_m(\hat{x}_1, \hat{x}_2, \cdots, \hat{x}_n) \end{bmatrix} + \begin{bmatrix} r_1 \\ r_2 \\ \vdots \\ r_m \end{bmatrix} \tag{3.6}$$

$$z = h(\hat{x}) + r \tag{3.7}$$

where

$\hat{x}_i$ estimated states at Bus i;

r_i residual of measurement i;

$\hat{x}$ $n \times 1$ vector of estimated states, and this vector is the estimated solution;

r $m \times 1$ vector of residuals ($m > n$).

The residuals of static state estimation demonstrate the differences between the estimated measurements and the exact ones. As for each measurement, the magnitude of the residual r_i indicates the deviation extent between the estimated value and the actual value of measurement i. The sum of all these magnitudes or the absolute values of these residuals is used to show the progress of state estimation. When this sum reaches its minimum value, the estimation is finished, and the estimated states in (3.7) at the last iteration are the final estimated results.

3.2 Conventional Solution for Static State Estimation

There are several approaches can be used to obtain the minimum sum of residuals. The Weight Least Square (WLS) algorithm is a popular one due to its greater applicability. The WLS algorithm aims to minimise the sum of the square weighted residuals. This aim can lead to an objective function $J(x)$, which is formulated as [7]:

$$J(x) = (z - h(x))^T \cdot R^{-1} \cdot (z - h(x)) \qquad (3.8)$$

When the above objective function reaches its minimum value, the estimated results of the WLS algorithm, denoted by $\hat{x}$, are obtained. Substituted (3.7) into (3.8), the minimum value of the objective function is expressed as:

$$J(\hat{x}) = (z - h(\hat{x}))^T \cdot R^{-1} \cdot (z - h(\hat{x})) = r^T \cdot R^{-1} \cdot r = \sum_{i=1}^{m} r_i^2 R_{ii} \qquad (3.9)$$

To solve this minimised problem, the first order differential of $J(x)$ is introduced in (3.10), and it is denoted as $g(x)$ [7]. When the minimum value of J(x) is obtained, $g(x)$

equals 0.

$$g(x) = \frac{\partial J(x)}{\partial x} = -H^T(x) \cdot R^{-1} \cdot (z - h(x)) \qquad (3.10)$$

In (3.10), *H(x)* is called the Jacobian matrix, which is the first order differential of the nonlinear function in (3.4), i.e. *H(x)=∂h(x)/∂x*. The Jacobian matrix is very meaningful in the WLS algorithm and the corresponding bad data processing. Fig. 3.1 illustrates the configuration of the Jacobian matrix. Concrete equations to calculate each entry in the Jacobian matrix can be referred to in Appendix 1.2.

	v_1	$\cdots$	v_n	θ_1	$\cdots$	θ_n
z_1	$\dfrac{\partial z_1}{\partial v_1}$	$\cdots$	$\dfrac{\partial z_1}{\partial v_n}$	$\dfrac{\partial z_1}{\partial \theta_1}$	$\cdots$	$\dfrac{\partial z_1}{\partial \theta_n}$
$\vdots$			$\cdots$			
z_i	$\dfrac{\partial z_i}{\partial v_1}$	$\cdots$	$\dfrac{\partial z_i}{\partial v_n}$	$\dfrac{\partial z_i}{\partial \theta_1}$	$\cdots$	$\dfrac{\partial z_i}{\partial \theta_n}$
$\vdots$			$\cdots$			
z_m	$\dfrac{\partial z_m}{\partial v_1}$	$\cdots$	$\dfrac{\partial z_m}{\partial v_n}$	$\dfrac{\partial z_m}{\partial \theta_1}$	$\cdots$	$\dfrac{\partial z_m}{\partial \theta_n}$

Fig. 3. 1 Configuration of the Jacobian matrix

Thereafter, the (3.10) can be reformulated in (3.11) if the Taylor series of *g(x)* is expanded at the vector x^k and higher order components are ignored [7].

$$g(x) = g(x^k) + \frac{\partial g(x^k)}{\partial x} \cdot (x - x^k) = g(x^k) + G(x^k) \cdot (x - x^k) = 0 \qquad (3.11)$$

where

 $G(x)$ gain matrix, and $G=\partial g/\partial x$.

In (3.11), substituted x with x^{k+1}, an iterative equation can be obtained, as shown in

(3.12) [7]. The gain matrix $G(x)$ is introduced to denote the first order differential of

$g(x)$. At the vector x^k, this gain matrix is formulated in (3.13).

$$g(x^{k+1}) = g(x^k) + G(x^k) \cdot (x^{k+1} - x^k) = 0$$
$$\Rightarrow x^{k+1} - x^k = -G(x^k)^{-1} \cdot g(x^k)$$

    (3.12)

$$G(x^k) = \frac{\partial g(x^k)}{\partial x} = H^T(x^k) \cdot R^{-1} \cdot H(x^k)$$

    (3.13)

where

 k iteration index;
 x^k estimated states at iteration k;

Finally, an iterative solution of the WLS algorithm is obtained by (3.10), (3.12), and

(3.13). This solution is expressed in (3.14), and it is called the Normal Equation. It

can calculate the vector Δx at each iteration of the WLS algorithm.

$$G(x^k) \cdot \Delta x^{k+1} = H^T(x^k) \cdot R^{-1} \cdot (z - h(x^k))$$

    (3.14)

where

 Δx^{k+1} $\Delta x^{k+1} = x^{k+1} - x^k$.

This iterative calculation process would stop when the maximum value in Δx is

smaller than the convergence limit, which is normally chosen as 1e-6.

3.3 Bad Data Processing

Measurement errors are always existed in practical estimators due to the limited

accuracy of meters and the loss in the telecommunication medium. Small

measurement errors are treated as Gaussian noise and their impacts can be neglected.

On the other hand, some extremely large measurement errors caused by the wrong

connections of meters, the failures of telecommunication system, and the incorrect

measurements, etc., can damage the estimation. The measurements with these large

errors are regarded as the bad data in state estimation.

The bad data can be classified as single bad data and multiple bad data. The single

bad data is common in practical condition, and its detection and identification are

simple. Because this thesis is mainly focused on the estimation process, only the

single bad data is focused, and the multiple bad data will be considered in future. If

the bad data exists, the estimation accuracy would decrease and the estimated results

may be unacceptable. The bad data should be filtered first to guarantee the accuracy

of results, and this procedure is called the bad data processing. This procedure always

contains the processes of bad data detection and identification.

Regarding the WLS algorithm, the bad data can be only detected after the finish of the

estimation due to the iterative estimation process in the algorithm. All the estimated

results are checked by a detection process to determine the existence of the bad data.

If there is bad data in the estimation, an identification process is conducted to locate

and eliminate this bad data.

3.3.1 Bad Data Detection

A successful and widely applied approach to detect bad data in the WLS algorithm is

the Chi-squares approach. This approach is easy to implement and has a low computational burden. The precondition of the Chi-squares approach is that the objective function of the WLS algorithm conforms to the Chi-squares distribution. This is demonstrated by the following process. The objective function of the WLS algorithm is rewritten and simplified at first, as shown in (3.15) and (3.16).

$$J(x) = \sum_{i=1}^{m} R_{ii}^{-1} (z_i - h_i(x))^2 \qquad (3.15)$$

$$J(x) = \sum_{i=1}^{m} R_{ii}^{-1} \cdot e_i^2 = \sum_{i=1}^{m} (\frac{e_i}{\sqrt{R_{ii}}})^2 = \sum_{i=1}^{m} (e_i^N)^2 \qquad (3.16)$$

where

e_i error of measurement i;
R_{ii} i^{th} diagonal entry in the covariance matrix of measurement errors;
e_i^N normalised error of measurement i.

Because the measurement error e_i is Gaussian noise with the variance of R_{ii}, the normalised measurement error e_i^N in (3.16) conforms to the Standard Normal Distribution [7], i.e. $e_i^N \sim N(0,1)$. Hence, the objective function of the WLS algorithm is demonstrated to obey the Chi-squares distribution. The Chi-squares distribution has m-n degrees of freedom, where m is the total number of measurements and n is the total number of states. This is the theoretical foundation of the Chi-square approach in bad data detection. The Chi-square approach is executed according to the following steps.

Step 1, calculate the objective function by (3.9) with the estimated results of the WLS estimation, as $J(\hat{x})$;

Step 2, obtain the detection threshold from the Chi-squares distribution table with the detection confidence probability p and the degrees of freedom m-n. Denote this threshold as $\chi^2_{m-n,p}$.

Step 3, compare $J(\hat{x})$ with $\chi^2_{m-n,p}$.

If $J(\hat{x}) \geq \chi^2_{m-n,p}$, there is bad data in the WLS estimation.

Otherwise, the measurements are free of bad data.

3.3.2 Bad Data Identification

The bad data identification is more challengeable than detection, because it requires a more complex calculation and analysis to locate the bad data. The Largest Normalised Residual (LNR) approach is a simple and reliable method to identify the single bad data. This approach utilises the normalised residual of each measurement. At first, the residual i is the difference between the actual value and the estimated value of measurement i, and it can be calculated as:

$$r_i = z_i - h_i(\hat{x}) \tag{3.17}$$

Afterwards, the residual sensitivity matrix S is introduced to present the relationship between the residuals and the measurement errors in the WLS algorithm. This relationship is presented as:

$$r = S \cdot e \tag{3.18}$$

According to the property of the WLS algorithm, the residual sensitivity matrix can be

formulated as follows [7], where I is the identity matrix.

$$S = I - H \cdot G^{-1} \cdot H^T \cdot R^{-1} \tag{3.19}$$

Because each measurement error conforms to Gaussian distribution, $e_i \sim N(0,R_{ii})$, the mean value and covariance of the residuals can be solved from (3.18) as [7]:

$$E(r) = E(S \cdot e) = S \cdot E(e) = 0 \tag{3.20}$$

$$Cov(r) = E(r \cdot r^T) = S \cdot R = \Omega \tag{3.21}$$

where

Ω covariance matrix of residuals

Therefore, the residuals in the WLS algorithm also obey the Gaussian distribution, i.e. $r \sim N(0,\Omega)$. Compared with the diagonal covariance matrix of measurement errors R, the residual covariance matrix Ω is an off-diagonal matrix. This is because the measurements in the estimation are independent, whilst the residuals may be correlated. This residual covariance matrix is calculated from (3.19) and (3.21) as:

$$\Omega = S \cdot R = R - H \cdot G^{-1} \cdot H^T \tag{3.22}$$

The diagonal entries of Ω are used to compute the normalised values of residuals. For each measurement, the normalised value of residual is calculated by its absolute value and the corresponding diagonal entry in Ω as: [7]

$$r_i^N = \frac{|r_i|}{\sqrt{\Omega_{ii}}} \tag{3.23}$$

where

r_i^N normalised residual of measurement i;

Ω_{ii} i^{th} diagonal entry in the covariance matrix of residuals

These normalised residuals can identify the bad data. Detailed process of the LNR approach is summarised as follows:

Step 1, calculate the residual for each measurement by (3.17), as r_i;

Step 2, form the residual covariance matrix, Ω, by (3.22);

Step 3, compute the normalised residual for each measurement by (3.23), denoted by r_i^N;

Step 4, find the measurement j with the largest normalised residual r_j^N.

Step 5, compare the r_j^N with the selected identification threshold, ε.

If $r_j^N > \varepsilon$, the measurement j is recognised as bad data.

If not, all the measurements are free of bad data, and the bad data detection process need to be repeated.

Once the bad data is identified, it would be filtered in the estimation. Then, the state estimation and the procedure of bad data processing are repeated until no bad data exists.

CHAPTER 4 COORDINATED ALGORITHM FOR DISTRIBUTED STATE ESTIMATION WITH PMU MEASUREMTNS

4.1 Introduction

As a consequence of the introduction of power electronic devices and communication technology, the power system is becoming extremely large, and its operation is more complex. In addition, the power system may face more serious conditions such as earthquakes and the threat of terrorism, and therefore it demands higher security levels. These higher security levels may lead to a higher requirement for state estimation in reliability, estimation accuracy and computational efficiency. Conventional methods of state estimation cannot satisfy these increasing demands of accuracy and efficiency. However, the appearance of PMUs now makes it possible to improve existing static state estimation.

PMU measurements have a multitude of advantages, such as higher accuracy and a faster sampling rate, compared with conventional RTU measurements. It seems likely that PMU measurements would replace all RTU measurements in the estimation, but this cannot be achieved in the near future. The high cost of PMUs always limits their installations at every substation. On the other hand, RTUs have already been widely applied in power systems. It is very wasteful to discard all RTU measurements. The most likely condition is that both RTU and PMU measurements will be utilised in

state estimation at the same time.

Considering both RTU and PMU measurements in the estimation, the accuracy can be improved, but at the same time the computational efficiency is decreased as more measurements involved. This decrease is more obvious in a large scale power system. One attempt to solve this problem was presented in [118], where the distributed concept was introduced in state estimation. This approach can improve the efficiency to some extent, but it was inferior to satisfaction.

To improve the efficiency, this chapter proposes a novel algorithm, named as Distributed State Estimation with Linear Coordination (DSELC). The DSELC algorithm can mitigate the low efficiency problem, and case studies validate the effectiveness.

4.2 Distributed State Estimation with Linear Coordination (DSELC) Algorithm

The DSELC algorithm can estimate the states of buses from both RTU and PMU measurements. A distributed configuration is employed in this algorithm. This configuration is established on two levels: the subsystem level and the coordination level (the lower level and the upper level).

At the subsystem level of the DSELC algorithm, the overall system is decomposed into several subsystems, and in each subsystem, the WLS estimation is performed individually. Afterwards, some local results are transmitted to the upper level and

coordinated there. The linear estimation approach based on PMU measurements is used to coordinate these local solutions.

4.2.1 Decomposition Strategy

In the distributed configuration, decomposition strategy is used to decompose the large system into a number of subsystems. In the DSELC algorithm, a non-overlapping decomposition strategy is employed, and the subsystems formed through this strategy are connected by tie-lines. The information between subsystems is only exchanged via tie-lines in this algorithm. Thus, each subsystem can be treated as an independent one, and the estimation in each subsystem can be performed individually. Fig. 4.1 illustrates the non-overlapping decomposition strategy, and more details are introduced in [49].
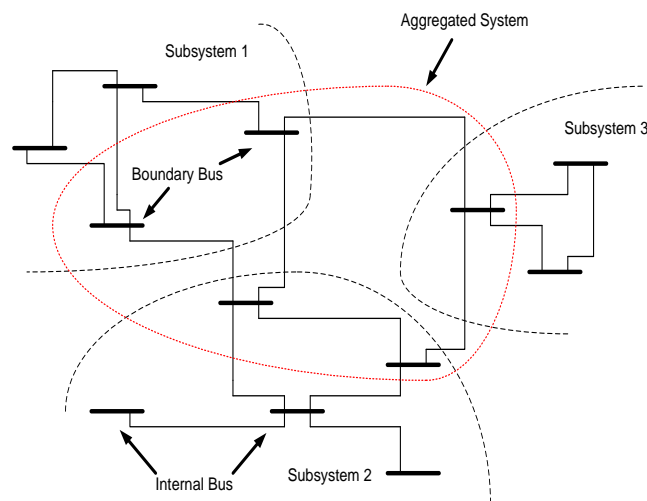
Fig. 4. 1. Non-overlapping decomposition strategy

In Fig. 4.1, buses are classified into two categories: internal buses and boundary buses. In the DSELC algorithm, PMUs are only installed at the suitable boundary buses to

achieve the minimum cost, and there is at least one PMU installed in each subsystem.

- Internal buses: buses are not terminals of tie-lines;

- Boundary buses: terminal buses of tie-lines.

In addition, three types of measurements are also classified as:

- Internal measurements: measurements associated with internal buses and internal branches, denoted by z^{int};

- Boundary measurements: measurements at boundary buses, denoted by z^{bod};

- Tie-line measurements: tie-line flow measurements, denoted by z^{tie};

In each subsystem, the states of internal buses can be well estimated by the local estimation, because all the measurements related to these buses are considered in this estimation. On the other hand, the states of boundary buses need to be coordinated at the upper level due to the lack of tie-line measurements in the estimation at the lower level. In this situation, all the boundary buses and the tie-lines between these buses can form an aggregated system, where the coordination is executed.

The linear estimation approach is used to coordinate the local results of boundary buses at the upper level. This method has greatly improved computational efficiency, but its requirement is very strict that all the measurements in this approach need to be provided from PMUs. The requirement is hard to meet in the overall system, because there are only a limited number of PMUs can be installed. However, it is possible to

meet this requirement in the aggregated system when an appropriate decomposition strategy and a reasonable placement of PMUs are employed.

Thus, the applicability of the linear estimation approach is improved by the DSELC algorithm. This is one of the major contributions in the proposed algorithm. Detailed descriptions of the DSELC algorithm at both levels are presented in the next part.

4.2.2 DSELC Algorithm

In the DSELC algorithm, two different estimation approaches are performed at two levels. In each subsystem, the WLS approach estimates local states from RTU and PMU measurements. At the coordination level, PMU measurements and the pseudo measurements from local estimations are utilised to coordinate the states of boundary buses by the linear estimation approach.

PMUs are only installed at suitable boundary buses in the DSELC algorithm to meet the following requirements: there is at least one PMU should be implemented in each subsystem and all tie-lines in the aggregated system should be measured by PMUs.

- Subsystem Level:

At the subsystem level, the states in each subsystem are estimated by the WLS estimation locally. According to the classification of states and measurements in the last sub-section, the states and measurements at this level can be defined as follows. The superscript *sub* denotes the variables at the subsystem level.

$$x^{sub} = \begin{bmatrix} x^{int} & x^{bod} \end{bmatrix}^T \tag{4.1}$$

$$z^{sub} = \begin{bmatrix} z^{int} & z^{bod} \end{bmatrix}^T = \begin{bmatrix} z_{RTU}^{int} & z_{PMU}^{int} & z_{RTU}^{bod} & z_{PMU}^{bod} \end{bmatrix}^T \tag{4.2}$$
$$= \begin{bmatrix} z_{RTU}^{sub} & z_{PMU}^{sub} \end{bmatrix}^T$$

In the above equations, x^{int} and x^{bod} are the states of internal and boundary buses, respectively. The subscripts *RTU* and *PMU* mean the variables associated with RTU and PMU measurements. RTUs can provide the measurements of voltage magnitudes, active and reactive power flows, active and reactive power injections. These power injection measurements are not considered in the DSELC algorithm, because they do not affect the estimation accuracy obviously, but at the same time, they would lead to significant complexity. PMU measurements constitute of voltage and current phasors. These phasor measurements can be treated as voltage magnitudes, phase angles, the real part and imaginary part of current phasors to adjust the nonlinear estimation process. Detailed information of RTU and PMU measurements in the DSELC algorithm are described in (4.3) and (4.4).

$$z_{RTU} = \begin{bmatrix} z_v & z_{pf} & z_{qf} & z_{pinj} & z_{qinj} \end{bmatrix} \tag{4.3}$$

$$z_{PMU} = \begin{bmatrix} z_v & z_a & z_{i\,Re} & z_{i\,Im} \end{bmatrix} \tag{4.4}$$

Therefore, the measurement model at the subsystem level of the DSELC algorithm can be achieved.

$$\begin{bmatrix} z_{RTU}^{sub} \\ z_{PMU}^{sub} \end{bmatrix} = \begin{bmatrix} h_{RTU}^{sub}(x^{sub}) \\ h_{PMU}^{sub}(x^{sub}) \end{bmatrix} + \begin{bmatrix} e_{RTU}^{sub} \\ e_{PMU}^{sub} \end{bmatrix} \tag{4.5}$$

$$z^{sub} = h^{sub}(x^{sub}) + e^{sub} \tag{4.6}$$

where

x^{sub} vector of states at the subsystem level;

z^{sub} vector of measurements at the subsystem level;

h^{sub} vector of nonlinear functions relating measurements to states at the subsystem level;

e^{sub} vector of measurement errors at the subsystem level.

Two matrices, denoted by R_{RTU}^{sub} and R_{RTU}^{sub}, are introduced to present the covariance of RTU and PMU measurements at this level. Because all the measurement errors are regarded as Gaussian noise, these two covariance matrices have the same configuration as (3.5), and the entries in them depend on the standard deviations of RTU and PMU measurements.

The measurement model at the subsystem level (4.5) can be solved by the WLS approach. The WLS approach is comparatively applicable to combine PMU measurements with the estimation, because the modifications on existing WLS estimators are simple and the cost of these modifications is small. However, the huge computational burden in this approach should be considered in the practical operation as well.

According to Section 3.2, the modified gain matrix and Normal Equation considering both RTU and PMU measurements are formulated as:

$$G^{sub} = \begin{bmatrix} H_{RTU}^{sub} \\ H_{PMU}^{sub} \end{bmatrix}^{T} \cdot \begin{bmatrix} R_{RTU}^{sub} & 0 \\ 0 & R_{PMU}^{sub} \end{bmatrix}^{-1} \cdot \begin{bmatrix} H_{RTU}^{sub} \\ H_{PMU}^{sub} \end{bmatrix} \qquad (4.7)$$

$$G^{sub} \cdot \Delta x^{sub} = \begin{bmatrix} H_{RTU}^{sub} \\ H_{PMU}^{sub} \end{bmatrix}^{T} \cdot \begin{bmatrix} R_{RTU}^{sub} & 0 \\ 0 & R_{PMU}^{sub} \end{bmatrix}^{-1} \cdot \begin{bmatrix} z_{RTU}^{sub} - h_{RTU}^{sub}(x^{sub}) \\ z_{PMU}^{sub} - h_{PMU}^{sub}(x^{sub}) \end{bmatrix} \qquad (4.8)$$

where

H^{sub} Jacobian matrix at the subsystem level;

Equations (4.7) and (4.8) can estimate states in each subsystem individually. The states of internal buses are well estimated, because all the measurements associated with these buses are involved in the above estimation. On the other hand, without the flow measurements on tie-lines, the states of boundary buses need to be coordinated in the aggregated system at the upper level. However, the interties in the aggregated system are limited. This makes the redundancy degree at a low level, and the estimation accuracy may be unacceptable. Under this situation, the estimated results of boundary buses in subsystems are imported into the coordinator as pseudo measurements, which can increase the redundancy to a satisfied level.

- Coordination Level:

At the coordination level, all states are from the boundary buses, and they are all expressed in the phasor form as follows. The superscript *cor* means the variables at the coordination level.

$$X^{cor} = X^{bod} \tag{4.9}$$

The measurements considered at this level are boundary measurements and tie-line measurements, and they are also in the phasor form. PMUs provide all these phasor measurements (Z_{PMU}^{cor}), including the voltage phasors of boundary buses (Z_{PMU}^{bod}), and the current phasors of tie-lines (Z_{PMU}^{tie}). To guarantee the observability of the aggregated system, PMUs should be installed at suitable boundary buses.

The pseudo phasor measurements (Z_{Psu}^{cor}) are introduced in the coordination, and these measurements are formed from the local solutions of boundary buses (Z_{Psu}^{cor}). Finally, the phasor measurements employed at the coordination level are expressed as:

$$Z^{cor} = \begin{bmatrix} Z^{bod} & Z^{tie} \end{bmatrix}^T = \begin{bmatrix} Z_{PMU}^{bod} & Z_{Psu}^{cor} & Z_{PMU}^{tie} \end{bmatrix}^T \qquad (4.10)$$

Afterwards, the measurement model at this level of the DSELC algorithm is formulated. The measurement errors of PMU and pseudo phasor measurements are regarded as Gaussian noise. Thus, they have diagonal covariance matrices R_{PMU}^{cor} and R_{Psu}^{cor}, respectively.

$$\begin{align}
\begin{bmatrix} Z_{PMU}^{bod} \\ Z_{PMU}^{tie} \\ \cdots \\ Z_{Psu}^{cor} \end{bmatrix} &= \begin{bmatrix} B_{PMU}^{bod} \\ B_{PMU}^{tie} \\ \cdots \\ B_{Psu}^{cor} \end{bmatrix} \cdot X^{cor} + \begin{bmatrix} e_{PMU}^{bod} \\ e_{PMU}^{tie} \\ \cdots \\ e_{Psu}^{cor} \end{bmatrix} \\
&\Rightarrow \begin{bmatrix} Z_{PMU}^{cor} \\ \cdots \\ Z_{Psu}^{cor} \end{bmatrix} = \begin{bmatrix} B_{PMU}^{cor} \\ \cdots \\ B_{Psu}^{cor} \end{bmatrix} X^{cor} + \begin{bmatrix} e_{PMU}^{cor} \\ \cdots \\ e_{Psu}^{cor} \end{bmatrix} \\
&\Rightarrow Z^{cor} = B^{cor} \cdot X^{cor} + e^{cor}
\end{align} \qquad (4.11)$$

where

B transform matrix relating phasor measurements to phasor states;

Focused on the measurement model at the coordination level in (4.11), PMU measurements Z_{PMU}^{cor} contain the voltage phasor of boundary buses (Z_{PMU}^{bod}) and the current phasor of tie-lines (Z_{PMU}^{tie}). For Z_{PMU}^{bod}, the corresponding transform matrix B_{PMU}^{bod} is a binary matrix. If the voltage phasor measurement and the state are from the same bus, the entry is 1, otherwise the entry is 0. As for Z_{PMU}^{tie}, the related

transform matrix B_{PMU}^{tie} is also linear, and it only includes the admittance of tie-lines. B_{PMU}^{bod} and B_{PMU}^{tie} construct the transform matrix of PMU measurements, denoted by B_{PMU}^{cor}, and this combined transform matrix is also linear.

In addition, because the pseudo phasor measurements are all voltage phasors of boundary buses, their transform matrix B_{Psu}^{cor} is a binary matrix as well. Therefore, the overall transform matrix in the coordination B^{cor} is still a linear matrix. The measurement model in (4.11) is a linear model, and it has a linear solution:

$$X^{cor} = \left(\begin{bmatrix} B_{PMU}^{cor} \\ B_{Psu}^{cor} \end{bmatrix}^T \cdot \begin{bmatrix} R_{PMU}^{cor} & 0 \\ 0 & R_{Psu}^{cor} \end{bmatrix}^{-1} \cdot \begin{bmatrix} B_{PMU}^{cor} \\ B_{Psu}^{cor} \end{bmatrix}\right)^{-1} \cdot \begin{bmatrix} B_{PMU}^{cor} \\ B_{Psu}^{cor} \end{bmatrix}^T \cdot \begin{bmatrix} R_{PMU}^{cor} & 0 \\ 0 & R_{Psu}^{cor} \end{bmatrix}^{-1} \cdot \begin{bmatrix} Z_{PMU}^{cor} \\ Z_{Psu}^{cor} \end{bmatrix} \quad (4.12)$$

Through the above equation, the estimated results at the coordination level are solved. It should be noticed that the solutions from (4.12) are in the phasor form, and they are used to calculate the magnitude and phase angle of boundary buses. Without the iterative calculation process, the linear estimation approach has higher computational efficiency.

The results of internal buses at the lower level and the results of boundary buses at the upper level constitute the final solutions of the DSELC algorithm. Fig. 4.2 illustrates the function diagram of the DSELC estimation.

The DSELC algorithm is proposed to mitigate the low efficiency problem when both RTU and PMU measurements are considered in state estimation. The proposed algorithm can improve the computational efficiency from the following two aspects:
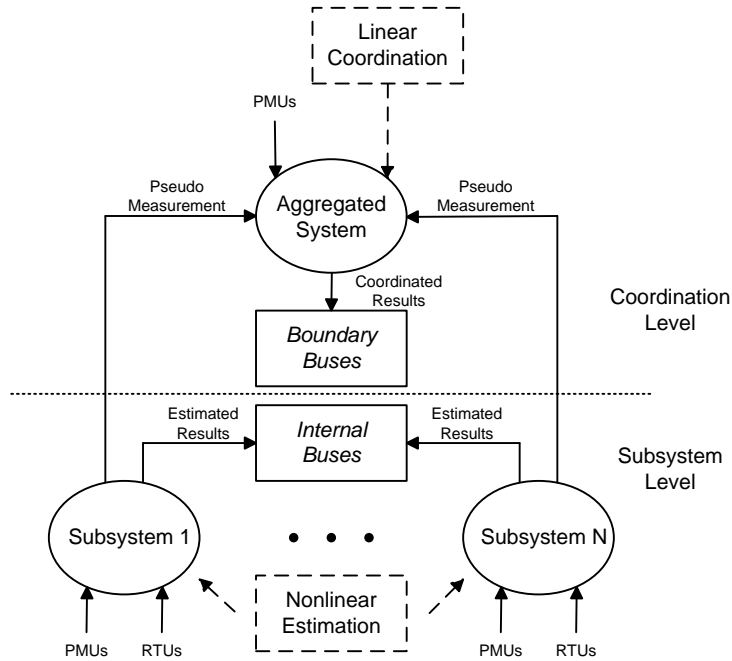
Fig. 4. 2. Function diagram of the DSELC algorithm

The DSELC algorithm employs a distributed configuration to reduce the computational burden in local estimations. The parallel computation process can be performed at the subsystem level directly, and this can further improve computational efficiency.

Additionally, a virtual aggregated system is established at the upper level, where the linear estimation approach is able to be executed. Without any iterative calculation, the computational efficiency at the coordination level of the DSELC algorithm is also improved.

4.2.3 Bad Data Processing

In the practical operation, a developed algorithm of static state estimation algorithm must be able to detect and identify bad data. The proposed DSELC algorithm can

meet this requirement, and its procedure of bad data processing is presented in this section. Because the distributed configuration is employed in the DSELC algorithm, the bad data detection and identification are performed at two levels independently.

- Subsystem level:

At the subsystem level, a number of subsystems are separated from the overall system, and the estimation in each subsystem is performed independently. Thus, the corresponding procedure of bad data processing in each subsystem can be executed individually. The conventional Chi-squares approach and LNR approach in Section 3.3 are used to detect and identify the bad data.

To detect the bad data at this level, the values of objective function in local estimations are calculated by (3.9) at first. These values are compared with the corresponding threshold to detect the existence of bad data. The details of the Chi-squares approach are described in Section 3.3.1. Because there are several subsystems at this level, the bad data detection process should be applied in each subsystem respectively. It means the Chi-squares approach would be executed in all subsystems to guarantee that all bad data can be detected at this level.

If the bad data is detected at this level, the LNR approach is used to identify the bad data. In this approach, the normalised residual for each measurement is calculated by (3.23). The measurement with the largest normalised residual is regarded as the bad data. This identification process is presented specifically in Section 3.3.2. Because the bad data was detected and located in a certain subsystem by the Chi-square approach,

the LNR approach is only performed in that subsystem.

- Coordination level:

The linear estimation approach is employed to coordinate the states of boundary buses at the coordination level. Because this approach is not based on the WLS algorithm, conventional Chi-squares approach and LNR approach are not suitable for detecting and identifying bad data at this level. Some modifications are necessary in these approaches to adjust the linear estimation.

Because the residuals obtained in the linear estimation are in the phasor form, the result of the objective function at this level is a complex number rather than an integral number in conventional WLS algorithm. The magnitude of this complex result can be used to detect the bad data. The modified objective function and the covariance matrix of phasor measurement errors at the coordination level of the DSELC algorithm are formulated as:

$$\left|J(\hat{X})\right| = \left|(Z^{cor} - B^{cor} \cdot \hat{X}^{cor})^T \cdot R^{cor^{-1}} \cdot (Z^{cor} - B^{cor} \cdot \hat{X}^{cor})\right| \qquad (4.13)$$

$$R^{cor} = \begin{bmatrix} R_{PMU}^{cor} & 0 \\ 0 & R_{Psu}^{cor} \end{bmatrix} \qquad (4.14)$$

The solution of (4.13) is used to compare with the corresponding detection threshold. The following process is the same as conventional Chi-squares approach in Section 3.3.1. Thus, the bad data at the coordination level of the DSELC algorithm can be detected through the above process.

If the bad data is detected, a modified LNR approach is conducted to identify the bad data. The residuals at this level are different from those in conventional LNR approach, because the measurements and states at this level are in the phasor form. Hence, the residuals at this level are also calculated in the phasor form as:

$$r_i^{cor} = Z_i^{cor} - B_i(\hat{X}^{cor}) \tag{4.15}$$

Afterwards, because the Jacobian and gain matrices are not used in the linear estimation approach, two virtual matrices are formed in the identification process to simulate the Jacobian and gain matrices in conventional LNR approach. A virtual Jacobian matrix H^{cor} is built to simulate the Jacobian matrix in the WLS algorithm in Section 3.3.2. Different from the Jacobian matrix in Fig. 3.1, this virtual matrix has a modified configuration. The states considered in H^{cor} are voltage magnitudes and phase angles, whilst the measurements in this matrix remain the phasor form. Fig. 4.3 illustrates the configuration of the virtual matrix. The equations to calculate entries in Fig. 4.3 are formulated in Appendix A.1.2. It should be noticed that all the entries in this matrix are also complex values.

The virtual gain matrix G^{cor} can be calculated from the virtual Jacobian matrix as:

$$G^{cor} = H^{cor^T} \cdot R^{cor^{-1}} \cdot H^{cor} \tag{4.16}$$

After the calculation of the virtual Jacobian matrix and the virtual gain matrix, the covariance matrix of residuals Ω^{cor} at this level is formulated by the following equation. The entries in Ω^{cor} are also complex numbers, and the absolute values of

these entries are used in the next step to identify bad data.

$$\Omega^{cor} = R^{cor} - H^{cor} \cdot G^{cor^{-1}} \cdot H^{cor^{T}} \tag{4.17}$$

$$
\begin{array}{c|cccc|c|ccc|c}
 & v_1 & \cdot & \cdot & \cdot & v_n & \theta_1 & \cdot & \cdot & \cdot & \theta_n \\
\hline
Z_1 & \dfrac{\partial Z_1}{\partial v_1} & \cdot & \cdot & \cdot & \dfrac{\partial Z_1}{\partial v_n} & \dfrac{\partial Z_1}{\partial \theta_1} & \cdot & \cdot & \cdot & \dfrac{\partial Z_1}{\partial \theta_n} \\
\cdot & & & & & & & & & & \\
\cdot & & & & & \cdot\;\cdot\;\cdot & & & & & \\
\cdot & & & & & & & & & & \\
Z_i & \dfrac{\partial Z_i}{\partial v_1} & \cdot & \cdot & \cdot & \dfrac{\partial Z_i}{\partial v_n} & \dfrac{\partial Z_i}{\partial \theta_1} & \cdot & \cdot & \cdot & \dfrac{\partial Z_i}{\partial \theta_n} \\
\cdot & & & & & & & & & & \\
\cdot & & & & & \cdot\;\cdot\;\cdot & & & & & \\
\cdot & & & & & & & & & & \\
Z_m & \dfrac{\partial Z_m}{\partial v_1} & \cdot & \cdot & \cdot & \dfrac{\partial Z_m}{\partial v_n} & \dfrac{\partial Z_m}{\partial \theta_1} & \cdot & \cdot & \cdot & \dfrac{\partial Z_m}{\partial \theta_n}
\end{array}
$$

Fig. 4. 3. Configuration of the virtual Jacobian matrix

The normalised residual for each phasor measurement at this level is solved from r^{cor} and Ω^{cor} by the following equation.

$$r_i^{N,cor} = \frac{\left| r_i^{cor} \right|}{\sqrt{\Omega_{ii}^{cor}}} \tag{4.18}$$

The results of normalised residuals are compared with each other to find the maximum one. The phasor measurement with this maximum normalised residual is identified as bad data. The following process is the same as conventional LNR approach in Section 3.3.2.

Finally, the bad data can be detected and identified at both levels in the DSELC algorithm individually. The effectiveness of this bad data processing is verified in the following case studies.

4.3 Case Studies

There are four aims in these case studies: The feasibility of the proposed DSELC algorithm is validated at first. The proposed algorithm is then compared with other centralised and distributed state estimation algorithms in estimation accuracy and computational efficiency. The bad data processing in the DSELC algorithm is also verified by numerical tests. At last, case studies demonstrate that the estimation accuracy of the WLS estimation can be improved by PMU measurements.

These case studies are simulated in the MATLAB R2009b on the desktop with an Intel Core 2 Quad CPU with 2.83 GHz.

4.3.1 Test Systems and Case Description

The test systems used in the case studies are the IEEE 30-bus and 118-bus system. Details about these systems can be referred to in [129, 130]. Four scenarios are established to test different centralised and distributed state estimation algorithms. They are defined as follows:

- Scenario 1: Centralised state estimation by the WLS algorithm [9] with RTU measurements only.

- Scenario 2: Centralised state estimation by the WLS algorithm with both RTU and PMU measurements.

- Scenario 3: Distributed state estimation by the algorithm in [118] with both RTU and PMU measurements.

- Scenario 4: Distributed state estimation by the proposed DSELC algorithm with both RTU and PMU measurements.

According to the above definitions, Scenario 1 and 2 apply centralised state estimation algorithms. The WLS approach is performed in these two scenarios with different sets of measurements. Scenario 1 considers RTU measurements only, whilst both RTU and PMU measurements are employed in Scenario 2.

Regarding Scenario 3 and 4, distributed state estimation algorithms are performed. Two levels, the subsystem level and the coordination level, are established in both scenarios. At the lower level of these two scenarios, the same approach is used to estimate states in each subsystem individually. However, different approaches are executed at the upper level to coordinate the state of boundary buses. Scenario 3 applies the nonlinear WLS based approach to perform the coordination, whilst Scenario 4 utilises the linear estimation approach.

According to four scenarios, four cases can be formed on the IEEE 30-bus and 118-bus system, respectively. Table 4.1 shows the relationship between scenarios and cases.

Test system	Centralised state estimation		Distributed state estimation	
	Scenario 1	Scenario 2	Scenario 3	Scenario 4
IEEE 30-bus	Case A	Case B	Case C	Case D
IEEE 118-bus	Case E	Case F	Case G	Case H

Table 4. 1. Case description in Chapter 4

In the following case studies, RTU measurements are comprised of bus voltage magnitudes and the power flows at the sending and receiving ends of branches. PMUs can provide the voltage and current phasor measurements. These phasor measurements can be directly used in the linear estimation approach, but in the nonlinear WLS based estimation, these measurements need to be processed before the use. The voltage phasors are transformed to voltage magnitudes and phase angles, and the current phasors are divided into the real and imaginary part separately.

The measurements from RTUs and PMUs are sampled as many as possible to guarantee the best estimation accuracy. In these case studies, the accuracy of RTU measurements is about 0.1% and the accuracy of PMU measurements is about 0.025% [131, 132]. To simulate practical conditions, White Gaussian noise is added into all the measurements. The average results of 1,000 tests are utilised to evaluate the performance of each case.

In distributed scenarios (Scenario 3 and 4), the non-overlapping strategy in Section 4.2.1 is employed to decompose the test system. The IEEE 30-bus system is decomposed into three subsystems geographically, and each subsystem has 10 buses. The decomposition scheme of this system is illustrated in Fig. 4.4. Four PMUs are

installed at Bus 4, 10, 15 and 28 to meet the requirement of the DSELC algorithm.
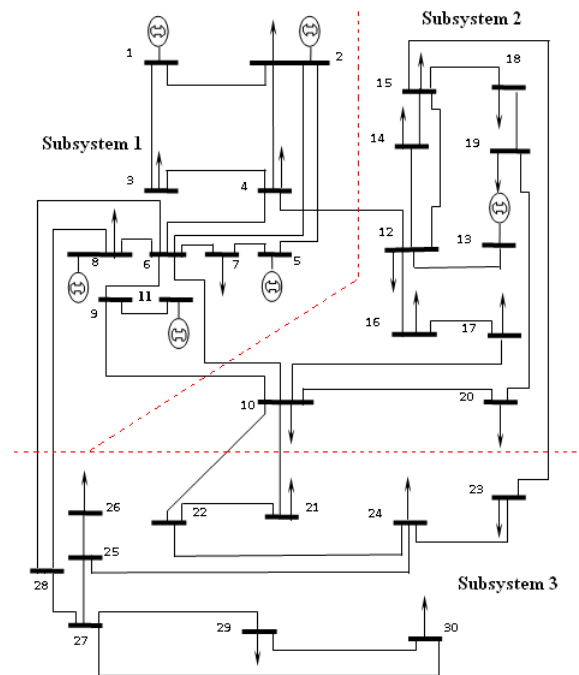
Fig. 4. 4. Decomposition scheme on the IEEE 30-bus system

In state estimation, redundancy is one crucial parameter affecting the estimation accuracy. The degree of redundancy is calculated from the number of the measurements and states in the system. Because the distributed configuration is employed in Case C & D, the redundancy in each subsystem and the aggregated system is independent in these two cases. These redundancy degrees are listed in Table 4.2, where 'S', 'M', and 'R' denote the number of states, measurements and the degree of redundancy, respectively.

Regarding the IEEE 118-bus system, the large system is divided into four subsystems, and there are about 30 buses in each subsystem. PMUs are installed at Bus 15, 17, 19, 23, 38, 49, 59, 64, 69, 80, 82 and 100 to meet the requirement of the DSELC

algorithm. Fig. 4.5 shows the decomposition scheme applied on the IEEE 118-bus system.

	Case C			Case D		
	S	M	R	S	M	R
Subsystem 1	20	65	3.25	20	65	3.25
Subsystem 2	20	66	3.30	20	66	3.30
Subsystem 3	20	53	2.65	20	53	2.65
Aggregated System	22	70	3.18	11	19	1.73

Table 4. 2. Redundancy degrees in Case C and Case D
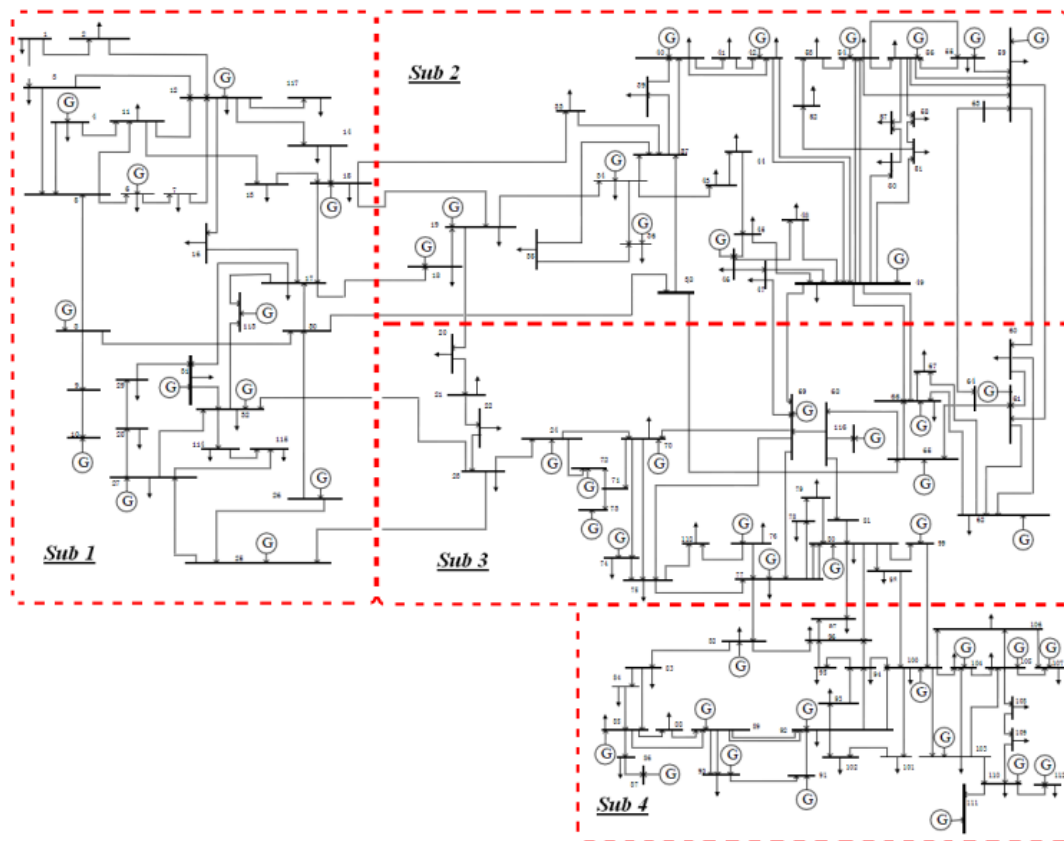
Fig. 4. 5. Decomposition scheme on the IEEE 118-bus system

Because the distributed state estimation algorithm [118] and the proposed DSELC algorithm are performed in Case G and H, respectively, these two cases also employ

the distributed configuration in Fig. 4.5. The degrees of redundancy in each subsystem and the aggregated system in these cases are summarised in the following table.

	Case G			Case H		
	S	M	R	S	M	R
Subsystem 1	58	201	3.46	58	201	3.46
Subsystem 2	60	244	4.07	60	244	4.07
Subsystem 3	60	222	3.70	60	222	3.70
Subsystem 4	58	219	3.78	58	219	3.78
Aggregated System	58	178	3.07	29	49	1.69

Table 4. 3. Redundancy degrees in Case G and Case H

Finally, the overall degree of redundancy in each case is summarised in Table 4.4. In centralised cases (Case A, B, E and F), the difference between the number of states in Case A and B is 2, and it is the same with Case E and F. This is reasonable because a Slack bus is selected in Case A and E to balance the phase angle in the system. However, this Slack bus is not necessary in Case B and F, because these two cases consider the phase angle measurements from PMUs. These phase angle measurements can synchronise the phase angle in the system directly. This is one of the great benefits brought by PMU measurements in state estimation.

	IEEE 30-bus system				IEEE 118-bus system			
	Case A	Case B	Case C	Case D	Case E	Case F	Case G	Case H
S	58	60	82	71	234	236	294	265
M	193	232	254	203	861	1006	1064	935
R	3.33	3.87	3.10	2.86	3.68	4.26	3.62	3.53

Table 4. 4. Overall redundancy degrees in Chapter 4

4.3.2 Feasibility of the DSELC Algorithm

According to the definitions of scenarios and Table 4.1, Case D and H apply the proposed DSELC algorithm. Thus, if Case D and H can estimate states in an acceptable accuracy, the feasibility of the proposed algorithm is validated. The estimation accuracy on both voltage magnitudes and phase angles in Case D and H are analysed in this case study.

To assess the estimation accuracy, the error level is introduced for both voltage magnitudes and phase angles, shown as (4.19) and (4.20). E_{Vi} and E_{Ai} denote the error level for the voltage magnitude and the phase angle at Bus i, respectively. It is certain that smaller value of the error level means higher estimation accuracy.

$$E_{Vi} = \left| \frac{V_i^{Est} - V_i^{Tru}}{V_i^{Tru}} \right| \tag{4.19}$$

$$E_{Ai} = \left| \theta_i^{Est} - \theta_i^{Tru} \right| \tag{4.20}$$

The superscript *Est* in (4.19) and (4.20) denotes the estimated results, and the superscript *Tru* means the exact values from the simulation. The error level at all buses in Case D is compared with that in Case A, where the conventional WLS algorithm is performed considering RTU measurements only. The Fig. 4.6 illustrates this comparison.

It is not difficult to find that the error level for voltage magnitudes and phase angles in Case D are generally smaller than those in Case A. This means the estimation accuracy in the proposed DSELC algorithm is higher than that in the conventional

WLS algorithm with RTU measurements on the IEEE 30-bus system. A similar conclusion can be obtained on the IEEE 118-bus system. Case H (DSELC algorithm) has higher estimation accuracy compared with Case E (WLS algorithm).
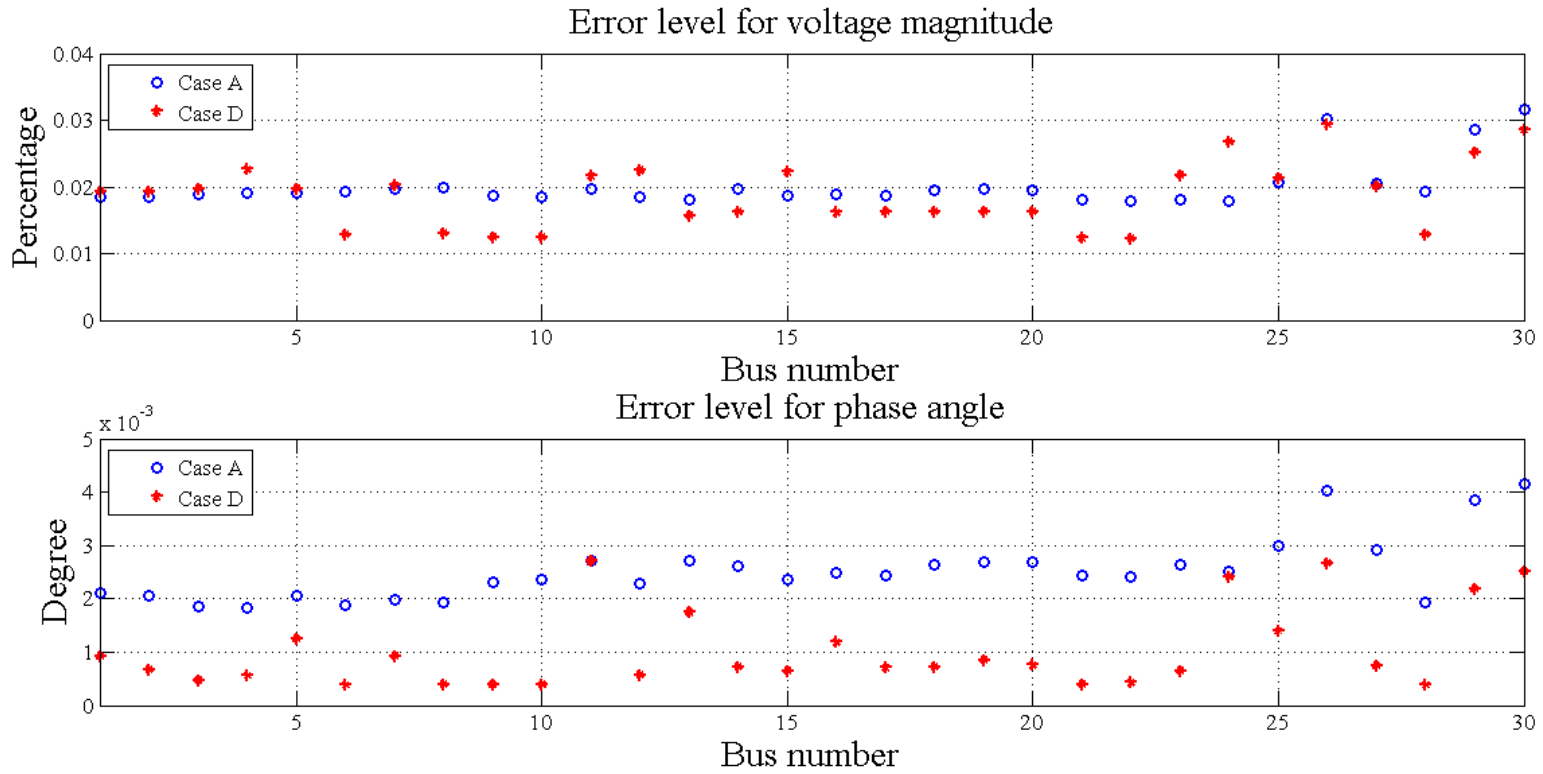
Fig. 4. 6. Comparison of error level between Case A and Case D

The conventional WLS algorithm with RTU measurements is a widely applied approach of state estimation. The DSELC algorithm is more accurate than this conventional WLS algorithm in both IEEE 30-bus and 118-bus systems. Therefore, the proposed DSELC algorithm is feasible.

4.3.3 Comparison of Estimation Accuracy

The estimation accuracy is one of fundamental criterions to evaluate the performance of state estimation algorithms. In this case study, the estimation accuracy of the

proposed DSELC algorithm is compared with other algorithms. The accuracy is assessed by the overall error level, which is calculated by the average value of the error level at all buses. Correspondingly, two overall error level are introduced: one is for the voltage magnitude (E_V), and the other is for the phase angle (E_A), shown in (4.21) and (4.22), respectively. It should be noticed that E_V is a normalised value, whilst E_A is an absolute value.

$$E_V = \frac{1}{n} \cdot \sum_{i=1}^{n} \left| \frac{V_i^{Est} - V_i^{Tru}}{V_i^{Tru}} \right| \tag{4.21}$$

$$E_A = \frac{1}{n} \cdot \sum_{i=1}^{n} \left| \theta_i^{Est} - \theta_i^{Tru} \right| \tag{4.22}$$

The overall error level in each case is calculated by the above equations. Fig. 4.7 shows the comparison of the overall level among the cases based on the IEEE 30-bus system (Case A, B, C and D).

Case B has the lowest E_V and E_A in Fig. 4.7. This means Case B has the best estimation accuracy for both voltage magnitudes and phase angles. It is reasonable because higher redundancy can lead to higher estimation accuracy in principle. According to Table 4.4, Case B has the highest redundancy among the four cases based on the IEEE 30-bus system.

A similar conclusion can be obtained by the comparison among the cases on the IEEE 118-bus system (Case E, F, G and H), shown as Fig. 4.8. In these cases, Case F has the highest redundancy in Table 4.4, and thus the overall error level for both voltage magnitudes and phase angles in this case are lower than those in any other case.
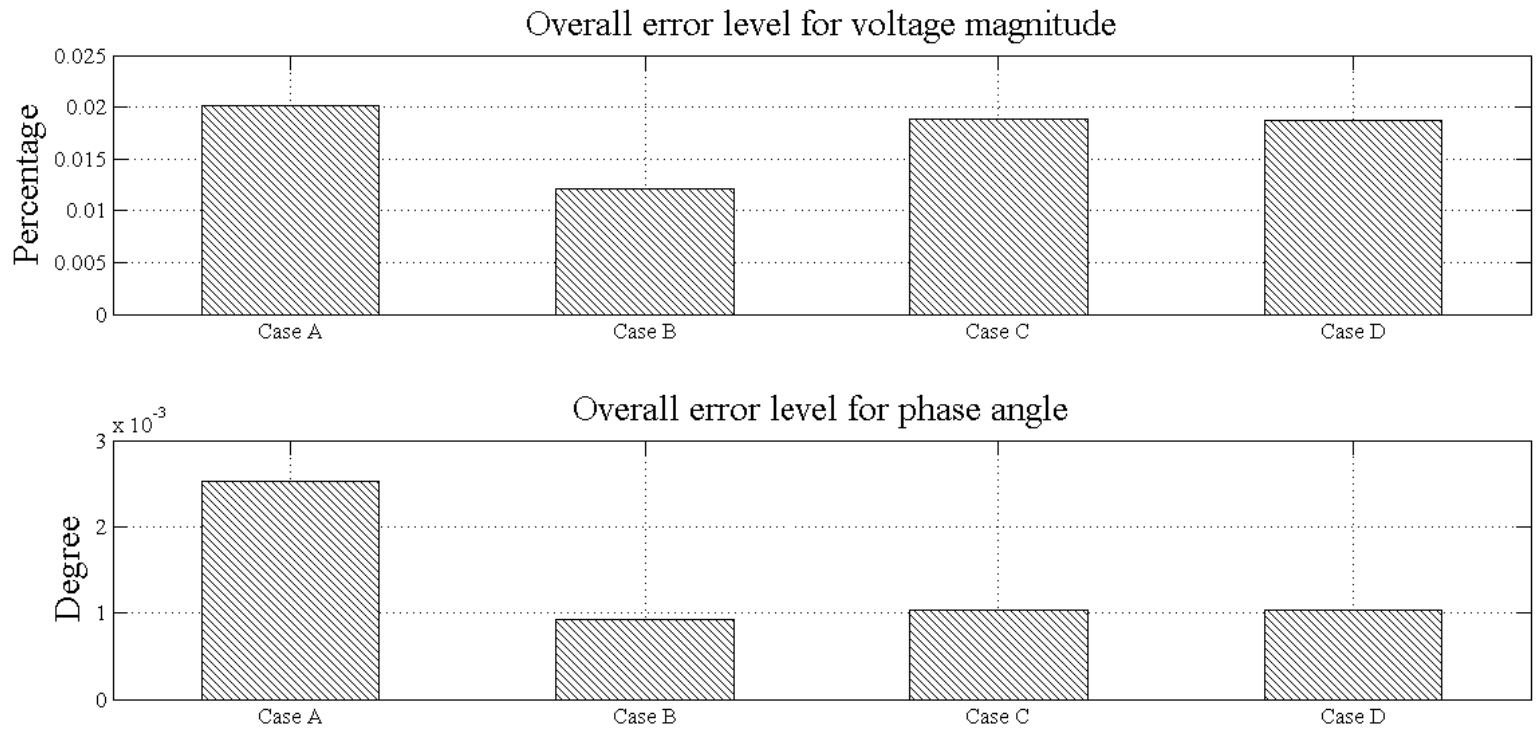
Fig. 4. 7. Comparison of overall error level on the IEEE 30-bus system
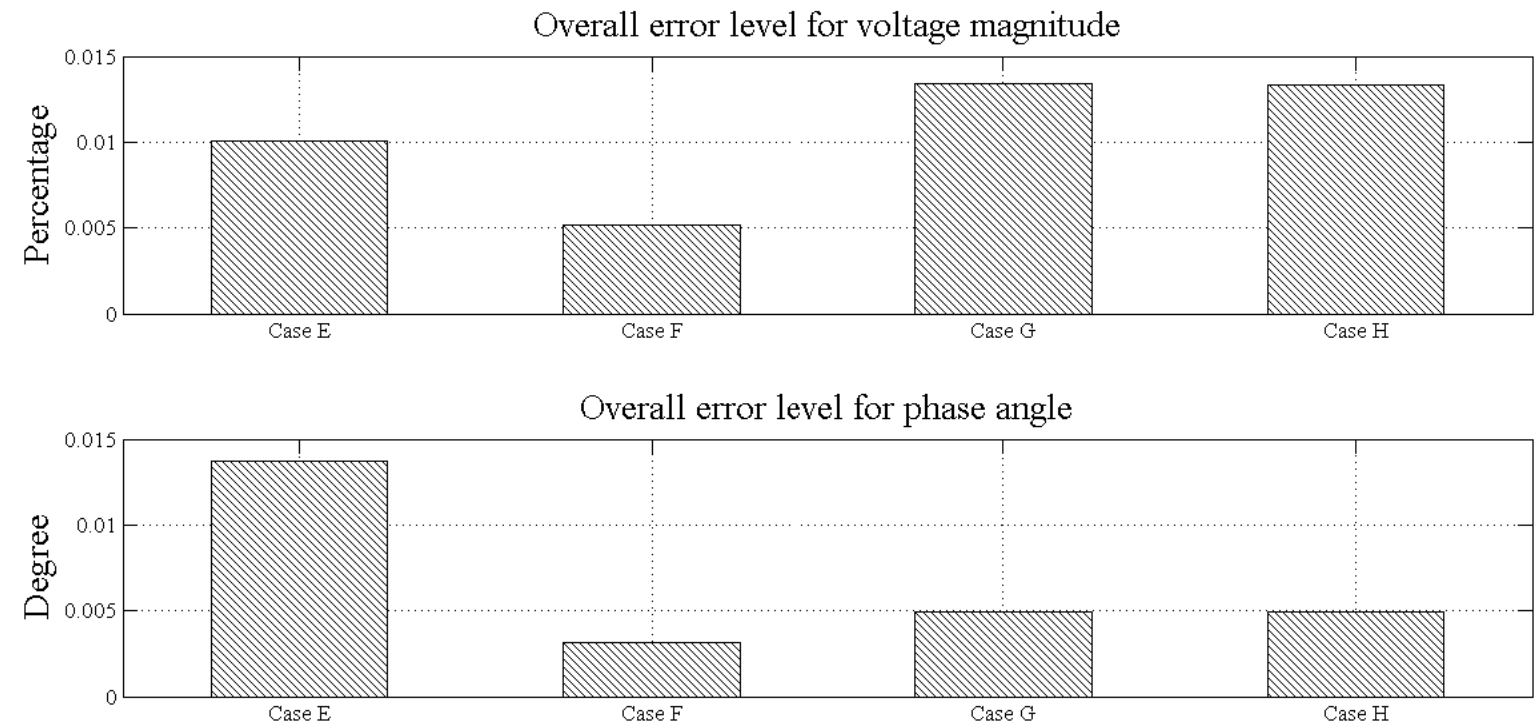
Fig. 4. 8. Comparison of overall error level on the IEEE 118-bus system

The estimation accuracy of the proposed DSELC algorithm can be also demonstrated in this case study. Compared the DSELC algorithm (Case D and H) with the distributed state estimation algorithm (Case C and G) in Fig. 4.7 and 4.8, the overall error level are very close in these two algorithms. It can deduce that the proposed DSELC algorithm has similar estimation accuracy with the distributed state estimation algorithm.

Thereafter, the DSELC algorithm is compared with centralised algorithms. The estimation accuracy of the DSELC algorithm is lower than that of the centralised WLS algorithm with both RTU and PMU measurements (Case B and F). This is because the redundancy in the cases of the DSELC algorithm is lower than that in Case B and F as in Table 4.4. Actually, the differences of the overall error level between these two algorithms are small. On the IEEE 30-bus system, the difference for the estimation accuracy of voltage magnitudes are smaller than 0.007%, and the difference associated with phase angles are 0.001 degree. On the IEEE 118-bus system, these differences increase to 0.009% and 0.002 degree. These small differences can be ignored in the industry application. Therefore, the estimation accuracy of the DSELC algorithm is acceptable compared with other centralised and distributed state estimation algorithms.

4.3.4 Comparison of Computational Efficiency

The objective of the proposed DSELC algorithm is to solve the problem of low efficiency in the state estimation considering both RTU and PMU measurements.

Compared with other centralised and distributed algorithms in this case study, the DSELC algorithm has much improved computational efficiency. This improvement is demonstrated in this case study.

Because both Scenario 3 and 4 employ the distributed configuration, these two scenarios are executed in parallel scheme naturally. In this parallel scheme, all local estimations are performed at the same time, and the solution time at the subsystem level depends on the subsystem with the largest computational burden. In addition, due to hardware limitations, the communication time between different estimators and the coordinator is not considered in these two scenarios.

All the cases are simulated in the MATLAB R2009b on the desktop with Intel Core 2 Quad CPU Q9550 of 2.83 GHz. The CPU time in each case is recorded to compare computational efficiency. The test results are listed in the following table, and the time unit is millisecond. The normalised values of CPU time are listed in brackets, and the time of Scenario 1 (Case A and E) is chosen as the standard in each test system.

	Centralised State estimation		Distributed State Estimation	
IEEE 30-bus	Case A	Case B	Case C	Case D
	2.0311 (100%)	2.6694 (131.4%)	1.1140 (54.85%)	0.6679 (32.88%)
IEEE 118-bus	Case E	Case F	Case G	Case H
	65.5631 (100%)	113.923 (173.8%)	5.2335 (7.98%)	2.8190 (4.30%)

Table 4. 5. Comparison of computational efficiency in Chapter 4

From the above table, the CPU time in the distributed scenarios (Scenario 3 and 4) is much smaller than that in these centralised scenarios (Scenario 1 and 2). It can

demonstrate that the distributed algorithms have improved computational efficiency. This improvement is attributed to two reasons: The distributed configuration can significantly reduce the computational burden in local estimations, and the parallel calculation process can further improve computational efficiency. According to Table 4.5, this improvement of the computational efficiency becomes more obvious in a larger system.

Compared Scenario 3 (Case C and Case G) with Scenario 4 (Case D and Case H), the computational time in Scenario 4 is smaller, which means the DSELC algorithm has higher computational efficiency than the distributed algorithm. The key reason for this improvement is that the linear estimation approach is employed at the coordination level of the DSELC algorithm. Without the iterative calculation process, this linear approach can significantly reduce the computational burden at the upper level. Fig. 4.9 shows the normalised comparison of CPU time between Scenario 3 and 4 at the coordination level. The CPU time of Scenario 3 are selected as the 100%. This figure indicates an apparent decrease of CPU time at the coordination level in Scenario 4. This decrease is more apparent on the IEEE 118-bus system.

Finally, according to Table 4.5, the CPU time in Scenario 4 (Case D and H) is the smallest in four scenarios. This can conclude that the proposed DSELC algorithm has the best computational efficiency in this case study.

4.3.5 Bad Data Processing

The case study in this sub-section is conducted to validate the bad data processing of

the DSELC algorithm. Both of bad data detection and identification are tested at two

levels individually. Because the bad data may appear in any kind of measurements, all

sorts of bad data need to be checked. Case D is used to perform the bad data test.
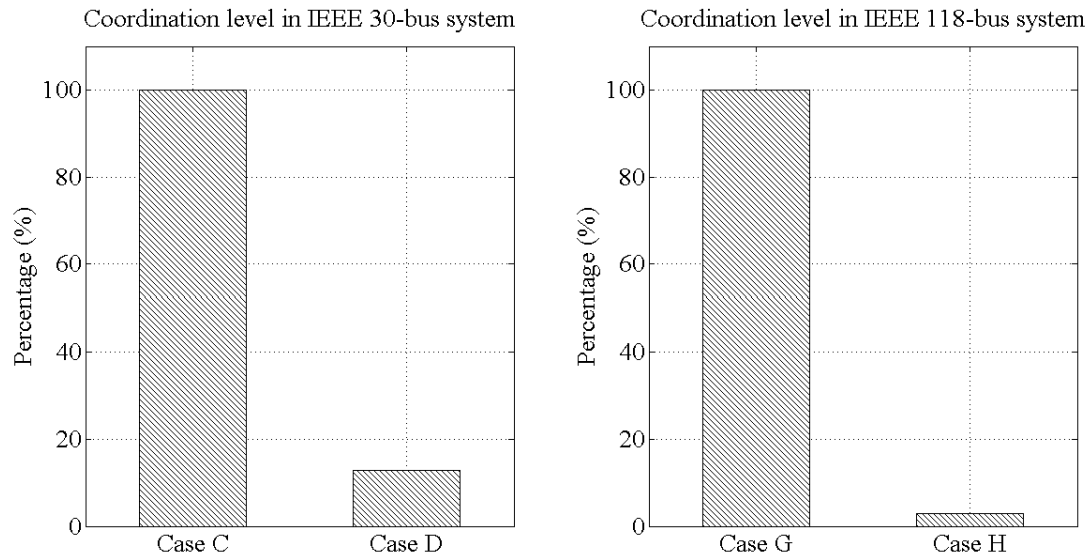
Fig. 4. 9. Comparison of normalised CPU time at the coordination level between the

DSELC algorithm and another distributed state estimation algorithm

Subsystem 1 is selected as an example at the subsystem level. There are seven sorts of

measurements in this system: voltage magnitudes, active and reactive power flows

from RTUs; voltage magnitudes, phase angles, real and imaginary part of current

phasors from PMUs. The aggregated system at the coordination level is also tested.

PMU and pseudo phasor measurements are both considered in this test.

The Chi-square method and the LNR method in Section 4.2.3 are used to detect and

identify the bad data. After the identification of bad data, the filtered estimation is

re-executed, and the bad data detection process is performed again to check whether

the bad data is eliminated or not. The test results for Subsystem 1 and the aggregated

system in Case D are shown in Table 4.6 and 4.7, respectively.

The detection confidence is set as 0.95. From Table 4.2, the degree of freedom in

Subsystem 1 is 45, and it is 8 in the aggregated system. Thus, the thresholds in these

two systems are 61.66 and 15.51, respectively.

	Bad Data	Exact Value	Bad Value	$J(x)$	
		Maximum r_i^N	Locate Error	New $J(x)$ after elimination	
	No bad data			13.44	
RTUs	P_{2-4}	0.1609	0.12	1598.24	Detected
		39.8	P_{24}	13.98	Identified
	Q_{4-6}	0.1161	0.20	6653.79	Detected
		81.5	Q_{46}	13.82	Identified
	V_7	0.9670	0.90	4293.38	Detected
		65.4	V_7	12.26	Identified
PMUs	V_4	0.9800	1.10	82637.6	Detected
		287.44	V_4	12.22	Identified
	θ_4	-1.795	-3.0	89.91	Detected
		8.63	θ_4	15.64	Identified
	$Re(I_{2-4})$	0.1604	0.20	4098.27	Detected
		63.99	$Re(I_{24})$	14.36	Identified
	$Im(I_{3-4})$	-0.047	-0.10	2707.74	Detected
		51.91	$Im(I_{34})$	13.88	Identified

Table 4. 6. Bad data tests in Subsystem 1 in Case D

According to Table 4.6 and 4.7, when there is no bad data in the test, the value of the

objective function is 13.44 in Subsystem 1 and 7.39 in the aggregated system. Both of

them are smaller than corresponding thresholds, which means no bad data is detected.

When the bad data is added into selected measurements, all the values of $J(x)$ are

larger than the threshold. It indicates the bad data is detected successfully. The bad data identification is then performed to locate the bad data. Through the LNR test in Section 4.2.3, the bad data can be identified. After the elimination of identified bad data, the filtered state estimation is executed, and all the new $J(x)$ obtained are smaller than the thresholds. This demonstrates the effectiveness of the bad data identification.

Therefore, both of the bad data detection and identification in the proposed DSELC algorithm are validated from the above numerical simulations.

	Bad Data	Exact Value	Bad Value	$J(x)$	
		Maximum r_i^N	Locate Error	New $J(x)$ after elimination	
	No bad data			7.39	
PMUs	$\tilde{V}_4$	$0.98\angle{-1.795}$	$0.93\angle{-1.795}$	40005.56	Detected
		508.09	$\tilde{V}_4$	5.74	Identified
	$\tilde{V}_4$	$0.98\angle{-1.795}$	$0.98\angle{-3}$	6802.22	Detected
		212.07	$\tilde{V}_4$	5.49	Identified
	$\tilde{I}_{6-10}$	$0.039\angle{27.35}$	$0.1\angle{27.35}$	1914.01	Detected
		100.72	$\tilde{I}_{6-10}$	7.40	Identified
	$\tilde{I}_{6-10}$	$0.039\angle{27.35}$	$0.039\angle{20}$	407.70	Detected
		45.56	$\tilde{I}_{6-10}$	7.44	Identified
Pseudo	$\tilde{V}_6$	$0.973\angle{-2.267}$	$1.05\angle{-2.267}$	15185.5	Detected
		127.64	$\tilde{V}_6$	7.02	Identified
	$\tilde{V}_6$	$0.973\angle{-2.267}$	$0.973\angle{-1.5}$	441.39	Detected
		21.56	$\tilde{V}_6$	7.49	Identified

Table 4. 7. Bad data tests in the aggregated system in Case D

4.3.6 Improvement of the WLS Algorithm by PMU Measurements

PMU measurements are more accurate compared with traditional RTU measurements. This higher accuracy can increase the estimation accuracy. The improvement in the WLS algorithm is demonstrated by the comparison between Scenario 1 (Case A and E) and 2 (Case B and F) in this case study. The difference between these two scenarios is that Scenario 1 considers RTU measurements only, whilst both RTU and PMU measurements are utilised in Scenario 2. The comparison of the error level for both voltage magnitudes and phase angles in Case A and B are illustrated in Fig. 4.10.
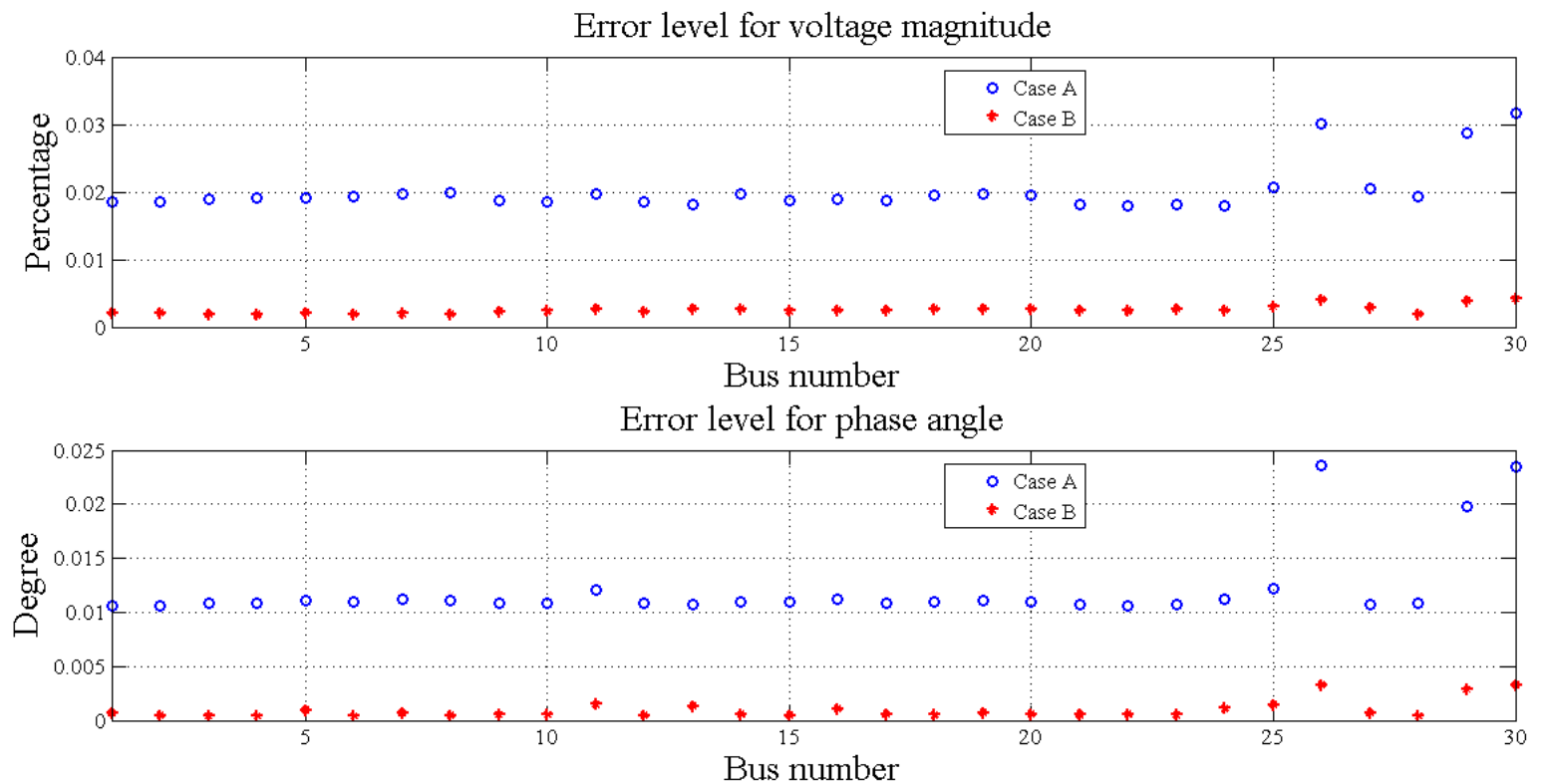
Fig. 4. 10. Comparison of error level between Case A and Case B

Fig. 4.10 shows that the error level in Case B is generally smaller than those in Case A, which means Case B has better estimation accuracy. It demonstrates the benefit of

PMU measurements in the estimation accuracy of the WLS algorithm. The same conclusion can be drawn by the comparison of the error level in Case E and F as in Fig. 4.11.
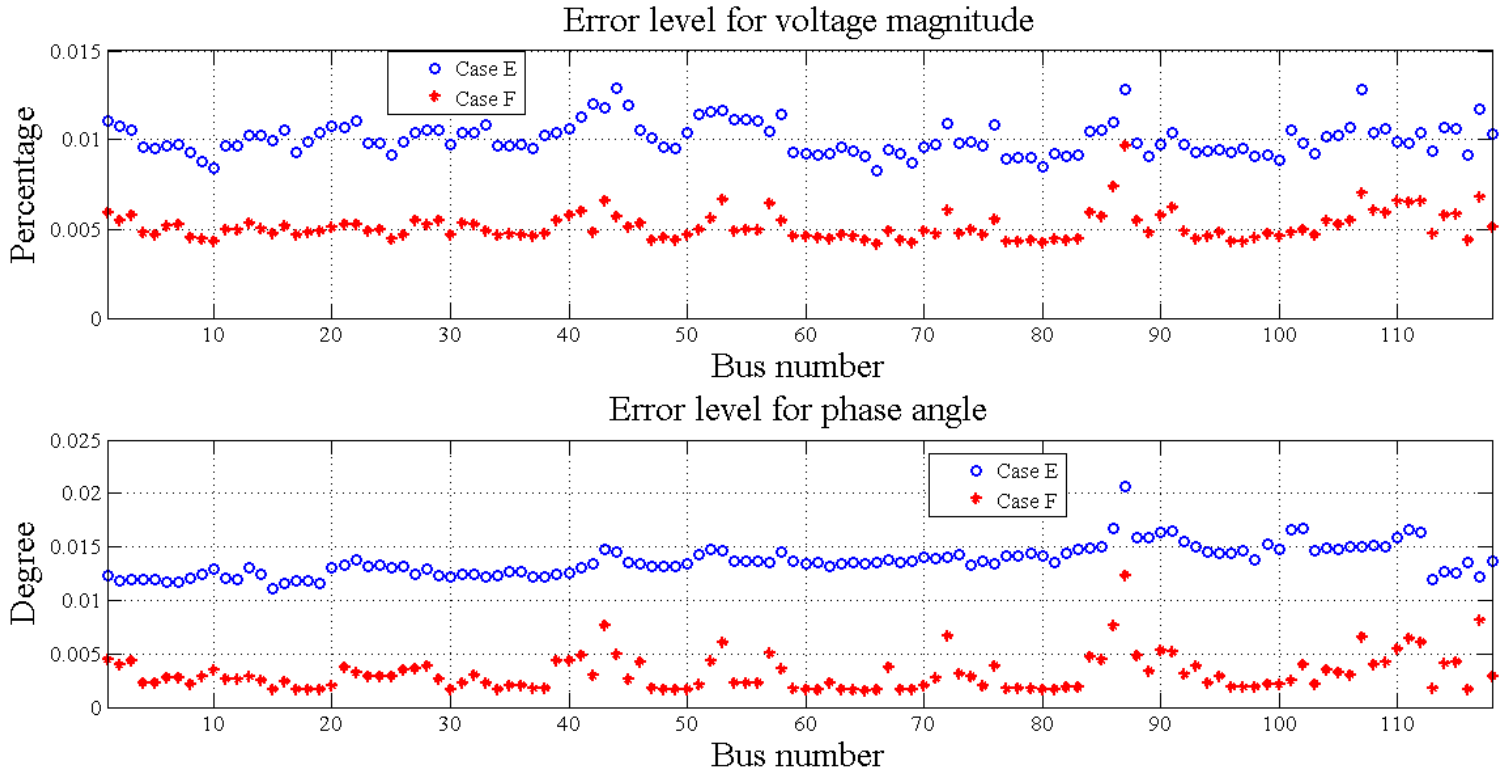
Fig. 4. 11. Comparison of error level between Case E and Case F

Two main reasons are summarised to explain this improvement in the estimation accuracy. At first, PMU measurements have higher accuracy. In this case study, the revenue accuracy of RTU measurements is set to 0.1% and that of PMU measurements is about 0.025% [131]. Measurements with higher accuracy can improve the estimation accuracy naturally. Additionally, the redundancy of the WLS estimation is increased through the introduction of PMU measurements. According to Table 4.4, Case B (3.87) has larger redundancy than Case A (3.33), and the

redundancy of Case F (4.26) is larger than that in Case E (3.68). Higher redundancy can lead to higher estimation accuracy in state estimation.

Moreover, the improvement in the estimation accuracy for phase angles is more apparent. PMUs can provide the measurements of phase angles, and it is certain that these phase angle measurements can benefit the estimation for phase angles directly.

4.4 Summary

In the last two decades, PMUs, as novel meters, have attracted more attention in modern power systems. In state estimation, the more precise PMU measurements can improve the estimation accuracy. This improvement in the WLS estimation was demonstrated by numerical tests in this chapter.

However, in the near future, it may not possible to replace RTUs with PMUs at all substations due to the high cost of PMUs. The most likely circumstance is that both RTU and PMU measurements are used in the estimation at the same time. In this situation, the computational burden is observed to greatly increase, and the computational efficiency of the estimation may be beyond industry expectations. In a large scale power system, the problem becomes even worse. To mitigate this, the chapter proposes a novel distributed state estimation algorithm, named as Distributed State Estimation with Linear Coordination (DSELC).

A two-level distributed configuration is employed in the proposed DSELC algorithm. At the subsystem level, the large power system is decomposed into several

subsystems, and local estimations are performed with both RTU and PMU measurements individually. The parallel calculation process is employed naturally at this level, and it can significantly improve computational efficiency. The states of boundary buses are coordinated in a virtual aggregated system at the coordination level. The linear estimation approach based on PMU measurements is utilised to perform the coordination. Without the iterative calculation process, the computational burden at this level can be further reduced.

The performance of the proposed DSELC algorithm is evaluated through the case studies on the IEEE 30-bus and 118-bus systems. Test results are compared with other centralised and distributed state estimation algorithms. The proposed DSELC algorithm has acceptable estimation accuracy and improved computational efficiency. Hence, this proposed algorithm can effectively solve the problem of low computational efficiency. Furthermore, the bad data processing in the DSELC algorithm is also verified. All the bad data at two levels can be successfully detected and identified.

Due to hardware limitations, the communication time between the subsystem level and the coordination level was ignored in the current research. The communication time will be considered in a future work.

CHAPTER 5 FAST ALGORITHM FOR DISTRIBUTED STATE ESTIMATION WITH PMU MEASUREMTNS

5.1 Introduction

The DSELC algorithm in Chapter 4 is proposed to solve the problem of low efficiency in state estimation, when both RTU and PMU measurements are considered. This algorithm employs a distributed configuration and the linear estimation approach to improve computational efficiency. According to Section 4.3.4, the efficiency of the DSELC algorithm is much improved compared with centralised algorithms, but it can only save about one third computational cost from the distributed state estimation algorithm [118].

Two levels have been mentioned in the distributed configuration of the DSELC algorithm, the subsystem level and the coordination level. At the coordination level of the DSELC algorithm, the linear estimation approach is performed, and this approach has greatly improved computational efficiency. Fig. 4.9 compares the CPU time of the DESLC algorithm and the distributed algorithm [118] at the coordination level. The result demonstrates that the DSELC algorithm has much higher efficiency at this level. On the other hand, a nonlinear WLS estimation is conducted at the subsystem level of the DSELC algorithm. The computational burden of this method is comparatively large, and it would limit the overall computational efficiency of the DSELC algorithm.

To further improve the computational efficiency of the DSELC algorithm, a faster method is introduced to replace the WLS estimation at the subsystem level. This method is chosen as the fast decoupled state estimation. Through this replacement, a novel distributed algorithm, named as Fast Distributed State Estimation with Linear Coordination (FDSELC), is proposed in this chapter. The FDSELC algorithm is developed from the DSELC algorithm. In the FDSELC algorithm, the fast decoupled estimation can reduce the computational burden at the subsystem level, which can improve the overall computational efficiency consequently.

5.2 Conventional Fast Decoupled State Estimation

In the load flow calculation, the technique of fast decoupled load flow is one of the successful methods to reduce computational cost. Combined this technique with state estimation, the fast decoupled state estimation was developed. The computational burden in the fast decoupled state estimation can be greatly reduced as a consequence of the decoupled estimation process and some assumed constant matrices.

5.2.1 Development of Fast Decoupled State Estimation

The first attempt to present the fast decoupled state estimation was proposed in [61]. It described the fundamental concepts, models and configuration of the fast decoupled state estimation. The overall estimation process was decoupled into active and reactive estimation processes. As a result of this decoupling, both computational burden and memory storage were reduced.

Another work in the fast decoupled state estimation was presented in [95]. Four decoupled algorithms with different decoupling schemes were compared. The bad data processing in these fast decoupled estimations, and the relationship between the convergence sensitivity and the X/R ratios of branches were also discussed.

The [96] presented a new framework in the fast decoupled state estimation. A procedure of two steps was established to solve the full Newton equations, and traditional approximations can be avoided in this procedure. This new method had better performance in the power system with critical R/X ratio. Other important developments of the fast decoupled state estimation can be referred to in [97, 133-136].

5.2.2 Conventional Solution for Fast Decoupled State Estimation

In conventional methods of fast decoupled state estimation, the method in [61] has the advantages of simplicity and flexibility. Thus, this method is chosen to use at the subsystem level of the FDSELC algorithm. The model and solution of this method are introduced in this section.

The method in [61] introduces the fast load flow technique to the WLS estimation. The estimation in this method is decoupled into active and reactive processes. Correspondingly, the states in this estimation are also divided into active and reactive groups. Phase angles are related to the active estimation process, and voltage magnitudes associate with the reactive estimation process.

Regarding the measurements in this method, RTUs provide all the measurements in the estimation. These measurements can be also divided into active and reactive measurements. Active measurements consist of active power flows and active power injections. Reactive measurements include voltage magnitudes, reactive power flows and reactive power injections. Hence, considering these active and reactive measurements, the measurement model in (3.4) can be revised as follows:

$$z = \begin{bmatrix} z_a \\ z_r \end{bmatrix} = \begin{bmatrix} h_a(x) + e_a \\ h_r(x) + e_r \end{bmatrix} \tag{5.1}$$

The subscribe a and r denote the variables associating with the active and reactive estimation process, respectively. Because the measurement errors in the above model (e_a and e_r) are both Gaussian noise, their corresponding covariance matrices R_a and R_r are both diagonal and have the same configuration in (3.5).

The Jacobian matrix is the next to be decoupled. In the WLS estimation, the Jacobian matrix is the first order differential of nonlinear function. Because the nonlinear function in (5.1) is decoupled as h_a and h_r and the states are also decoupled as voltage magnitudes and phase angles, the corresponding Jacobian matrix in the fast decoupled state estimation would have the following configuration.

$$H = \begin{bmatrix} \dfrac{\partial h_a}{\partial \theta} & \dfrac{\partial h_a}{\partial v} \\ \dfrac{\partial h_r}{\partial \theta} & \dfrac{\partial h_r}{\partial v} \end{bmatrix} = \begin{bmatrix} H_{aa} & H_{ar} \\ H_{ra} & H_{rr} \end{bmatrix} \tag{5.2}$$

In practical power systems, the values of H_{aa} and H_{rr} are much larger than those of H_{ar} and H_{ra} [61]. Accordingly, the matrices H_{ar} and H_{ra} can be ignored in the

estimation process. This is the first important assumption in the fast decoupled state estimation. The modified Jacobian matrix is then obtained as:

$$H = \begin{bmatrix} H_{aa} & 0 \\ 0 & H_{rr} \end{bmatrix} \tag{5.3}$$

In the normal condition of power systems, the voltage magnitudes at all buses are close to the reference voltage magnitude v_o, and the phase angles at two terminals of a branch are almost the same. Thus, the following approximations can be made and used to calculate H_{aa} and H_{rr} in the fast decoupled state estimation. These approximations can further reduce computational burden [61].

$$v_i \approx v_j = v_o \tag{5.4}$$

$$\sin\theta_{ij} \approx 0, \cos\theta_{ij} \approx 1 \tag{5.5}$$

The entries in H_{aa} and H_{rr} are constant during the process of iterative calculations according to the above assumptions. Two constant matrices, denoted by B_a and B_r, are introduced to express H_{aa} and H_{rr} as:

$$H_{aa} = -v_o^2 \cdot B_a \tag{5.6}$$

$$H_{rr} = -v_o \cdot B_r \tag{5.7}$$

After the decoupling of the Jacobian matrix, the gain matrix can be modified correspondingly. The gain matrix in the WLS estimation is calculated from the Jacobian matrix and the covariance matrix by (3.13). In the fast decoupled estimation, the modified gain matrix is obtained similarly as [61]:

$$G(x) = H^T \cdot R^{-1} \cdot H = \begin{bmatrix} H_{aa} & 0 \\ 0 & H_{rr} \end{bmatrix}^T \cdot \begin{bmatrix} R_a & 0 \\ 0 & R_r \end{bmatrix}^{-1} \cdot \begin{bmatrix} H_{aa} & 0 \\ 0 & H_{rr} \end{bmatrix}$$
$$= \begin{bmatrix} H_{aa} \cdot R_a^{-1} \cdot H_{aa} & 0 \\ 0 & H_{rr} \cdot R_r^{-1} \cdot H_{rr} \end{bmatrix} = \begin{bmatrix} G_a & 0 \\ 0 & G_r \end{bmatrix} \tag{5.8}$$

Substituted (5.6) and (5.7) into (5.8), the active and reactive gain matrices can be formulated in (5.9) and (5.10), respectively. According to these equations, the gain matrices are comprised of the reference voltage magnitude (v_o), the constant matrix (B_a and B_r) and the constant covariance matrix (R_a and R_r). Because the reference voltage magnitude is normally unchanged during the estimation process, both active and reactive gain matrices are constant during the fast decoupled state estimation.

$$G_a = v_o^4 \cdot [(-B_a)^T \cdot R_a^{-1} \cdot (-B_a)] \tag{5.9}$$

$$G_r = v_o^2 \cdot [(-B_r)^T \cdot R_r^{-1} \cdot (-B_r)] \tag{5.10}$$

Through the decoupling of the Jacobian and gain matrices, the WLS estimation process can be finally decoupled into the active and reactive estimation. Phase angles are estimated in the active estimation, and voltage magnitudes are determined in the reactive process. According to the solution of the WLS algorithm in (3.14), corresponding Normal Equations in the active and reactive estimation processes are formulated respectively.

$$G_a \cdot \Delta\theta = H_{aa}^T \cdot R_a^{-1} \cdot [z_a - h_a(x)] \tag{5.11}$$

$$G_r \cdot \Delta v = H_{rr}^T \cdot R_r^{-1} \cdot [z_r - h_r(x)] \tag{5.12}$$

Where

$\Delta\theta$ solved by the active estimation process, and $\Delta\theta = \theta^{k+1} - \theta^k$;

Δv solved by the reactive estimation process, and $\Delta v = v^{k+1} - v^k$.

The solutions of the fast decoupled state estimation can be obtained through the following iterative process. In each iteration, $\Delta\theta$ is solved by (5.6), (5.9) and (5.11) at first. The updated phase angles are substituted into (5.7), (5.10) and (5.12) to calculate Δv. These updated results of phase angles and voltage magnitudes would be utilised in the next iteration. The iterative process will continue until the maximum value in $\Delta\theta$ and Δv is smaller than the tolerance limit. Thereafter, corresponding values of voltage magnitudes and phase angles at the last iteration are the estimated solutions of the fast decoupled estimation.

Two main reasons can explain the improved computational efficiency in the fast decoupled estimation. The overall estimation process is decoupled into the active and reactive processes, and both processes are performed once in each iterative step. The number of states and measurements in these two processes is much reduced compared with the original overall estimation process. Thus, the computational burden can be reduced significantly.

In addition, the Jacobian matrix, H_{aa} and H_{rr} in (5.6) and (5.7), and the gain matrix, G_a and G_r in (5.9) and (5.10), are all constant in the fast decoupled estimation. These matrices can be factorised once, saved in the computer memory, and then substituted in each step of the estimation. This can greatly reduce computational burden and memory storage. Hence, the computational efficiency in the fast decoupled estimation is further improved.

5.3 Fast Distributed State Estimation with Linear Coordination (FDSELC) Algorithm

Conventional fast decoupled state estimation in previous section has high computational efficiency. The FDSELC algorithm is proposed based on this advantage. The model, solution, and bad data processing of the FDSELC algorithm are described in this section. The similarities and differences between the FDSELC and DSELC algorithm are also discussed.

5.3.1 FDSELC Algorithm

Similar to the DSELC algorithm, the FDSELC algorithm employs a distributed configuration with two levels: the subsystem level and the coordination level.

- Subsystem Level:

In the FDSELC algorithm, the non-overlapping decomposition strategy in the last chapter is used to divide the large system at the subsystem level. This strategy is shown in Fig. 4.1, and more details about this strategy can be referred to in Section 4.2.1. In each subsystem, the fast decoupled estimation is performed individually. Because both RTU and PMU measurements are considered in the FDSELC algorithm, the method of fast decoupled state estimation in [61] is not suitable, and it should be modified to include PMU measurements. Similar to traditional RTU measurements, PMU measurements can also be divided into active and reactive measurements.

PMU measurements include the voltage phasors of buses and the current phasors of

branches. In nonlinear state estimation, the voltage phasors are usually expressed as voltage magnitudes and phase angles. These phase angles are active measurements and these voltage magnitudes belong to reactive measurements. As for the current phasors, their real and imaginary parts associated with active and reactive measurements, respectively.

The measurement model in (5.1) can be modified to involve both RTU and PMU measurements in the following equation. The superscripts *RTU* and *PMU* denote that the variables related to RTU and PMU measurements, respectively.

$$
z' = \begin{bmatrix} z'_a \\ \cdots \\ z'_r \end{bmatrix} = \begin{bmatrix} z_a^{RTU} \\ z_a^{PMU} \\ \cdots \\ z_r^{RTU} \\ z_r^{PMU} \end{bmatrix} = \begin{bmatrix} h_a^{RTU}(x) + e_a^{RTU} \\ h_a^{PMU}(x) + e_a^{PMU} \\ \cdots \\ h_r^{RTU}(x) + e_r^{RTU} \\ h_r^{PMU}(x) + e_r^{PMU} \end{bmatrix}
\tag{5.13}
$$

The consideration of PMU measurements does not affect the fast decoupled estimation process actually. The important assumptions in section 5.2 are feasible, and the overall estimation at this level can be also decoupled into the active and reactive process.

- Active Process

Phase angles are estimated in the active estimation process. The active measurements used in the FDSELC algorithm consist of the active power flows from RTUs (z_a^{RTU}), and the phase angles and real parts of current phasors from PMUs (z_a^{PMU}). Because the errors of these measurements are Gaussian noise, two

diagonal covariance matrices $R_a{}^{RTU}$ and $R_a{}^{PMU}$ can be established in this process.

Considering PMU measurements, the active Jacobian matrix is modified from (5.6), and it is formulated in (5.14). According to the assumptions in (5.4) and (5.5), this active Jacobian matrix is also constant during the estimation. The constant matrix $B_a{}'$ is used to express the active Jacobian matrix.

$$H'_{aa} = -v_o{}^2 \cdot \begin{bmatrix} B_a{}^{RTU} \\ B_a{}^{PMU} \end{bmatrix} = -v_o{}^2 \cdot B'_a \tag{5.14}$$

Combined (5.9) with (5.14), the corresponding active gain matrix is formed in (5.15). This gain matrix is also constant because all the parameters in it do not change during the estimation process.

$$\begin{aligned} G'_a &= v_o{}^4 \cdot \left[\left(-\begin{bmatrix} B_a{}^{RTU} \\ B_a{}^{PMU} \end{bmatrix} \right)^T \cdot \begin{bmatrix} R_a{}^{RTU} & 0 \\ 0 & R_a{}^{RTU} \end{bmatrix}^{-1} \cdot \left(-\begin{bmatrix} B_a{}^{RTU} \\ B_a{}^{PMU} \end{bmatrix} \right) \right] \\ &= v_o{}^4 \cdot \left[\left(-B'_a \right)^T \cdot R'_a{}^{-1} \cdot \left(-B'_a \right) \right] \end{aligned} \tag{5.15}$$

Finally, based on (5.11), the active Normal equation at the subsystem level of the FDSELC algorithm is formulated in (5.16). This equation is used to solve $\Delta\theta$ in each iterative step, and the results of $\Delta\theta$ can update phase angles.

$$\begin{aligned} G'_a \cdot \Delta\theta &= H'_{aa}{}^T \cdot \begin{bmatrix} R_a{}^{RTU} & 0 \\ 0 & R_a{}^{RTU} \end{bmatrix}^{-1} \cdot \begin{bmatrix} z_a{}^{RTU} - h_a{}^{RTU}(x) \\ z_a{}^{PMU} - h_a{}^{PMU}(x) \end{bmatrix} \\ &= H'_{aa}{}^T \cdot R'_a \cdot \left[z'_a - h'_a(x) \right] \end{aligned} \tag{5.16}$$

- Reactive Process

The reactive estimation process at the subsystem level of the FDSELC algorithm is similar to the active estimation process. In the reactive process, the reactive measurements are provided from RTUs ($z_r{}^{RTU}$) and PMUs ($z_r{}^{PMU}$). RTU measurements include voltage magnitudes and reactive power flows, and PMU measurements contain voltage magnitudes and the imaginary parts of current phasors. The measurement errors in this reactive estimation are also Gaussian noise, so two diagonal covariance matrices can be constructed, denoted by $R_r{}^{RTU}$ and $R_r{}^{PMU}$.

The reactive Jocabian matrix, reactive gain matrix and reactive Normal equation are formulated in (5.17) ~ (5.19). These matrices are constant during the estimation with the assumptions in (5.4) and (5.5). $\varDelta v$ can be calculated by (5.19) and used to update voltage magnitudes in each iterative step.

$$H'_{rr} = -v_o \cdot \begin{bmatrix} B_r{}^{RTU} \\ B_r{}^{PMU} \end{bmatrix} = -v_o \cdot B'_r \tag{5.17}$$

$$G'_r = v_o{}^2 \cdot \left[\left(- \begin{bmatrix} B_r{}^{RTU} \\ B_r{}^{PMU} \end{bmatrix}' \right)^T \cdot \begin{bmatrix} R_r{}^{RTU} & 0 \\ 0 & R_r{}^{RTU} \end{bmatrix}^{-1} \cdot \left(- \begin{bmatrix} B_r{}^{RTU} \\ B_r{}^{PMU} \end{bmatrix}' \right) \right] \tag{5.18}$$

$$= v_o{}^2 \cdot \left[(-B'_r)^T \cdot R_r'^{-1} \cdot (-B'_r) \right]$$

$$G'_r \cdot \Delta v = H'_{rr}{}^T \cdot \begin{bmatrix} R_r{}^{RTU} & 0 \\ 0 & R_r{}^{RTU} \end{bmatrix}^{-1} \cdot \begin{bmatrix} z_r{}^{RTU} - h_r{}^{RTU}(x) \\ z_r{}^{PMU} - h_r{}^{PMU}(x) \end{bmatrix} \tag{5.19}$$

$$= H'_{rr}{}^T \cdot R'_r \cdot [z'_r - h'_r(x)]$$

In each iterative step of the fast decoupled estimation in the FDSELC algorithm, the active and reactive estimation processes are performed in turn. The incremental values of phase angles are calculated at first by (5.16). The updated phase angles are

thereafter substituted in (5.19) to solve the incremental values of voltage magnitudes. These updated phase angles and voltage magnitudes are then used in the next iteration of the estimation. Finally, local states can be estimated in each subsystem through this fast decoupled state estimation.

In this fast decoupled state estimation with PMU measurements, the active and reactive Jacobian matrices (H_{aa}' and H_{rr}'), and the active and reactive gain matrices (G_a' and G_r') are all constant during the estimation. They can be factorised once before the estimation and saved in memory. In each step, they would be substituted in the estimation. This can significantly reduce the computational burden of local estimations and guarantee the high computational efficiency at the subsystem level of the FDSELC algorithm.

According to the practical experience, the entries in Ba' are generally selected as the reciprocal of branch reactance, and the imaginary part of branch admittances are used to form Br'. Through this selection, the convergence speed of the fast decoupled estimator can be guaranteed.

In the FDSELC algorithm, the states of internal buses are well estimated at the subsystem level, but the states of boundary buses need to be coordinated at the upper level. An aggregated system is established to involve all boundary buses, shown in Fig. 4.1. Similar to the DSELC algorithm, local solutions of boundary buses in the FDSELC algorithm are also imported into the coordinator to form pseudo measurements, which can increase the redundancy of the coordination.

- Coordination Level:

At the coordination level of the FDSELC algorithm, the linear estimation approach based on PMU measurements is employed. The coordination process including states, measurements and solutions at this level is the same with that at the upper level of the DSELC algorithm in Section 4.2.2. The (4.12) can be also used to coordinate states at the coordination level of the FDSELC algorithm.

A simple process of the FDSELC algorithm is outlined as follows. The original large power system is decomposed into a number of small subsystems at the subsystem level. In each subsystem, buses are classified as internal and boundary buses. The states of internal buses are well estimated by local estimations in subsystems through a modified fast decoupled state estimation considering both RTU and PMU measurements. Boundary buses can form an aggregated system at the upper level, where the linear estimation approach is used to coordinate local solutions of boundary buses. Only PMU measurements and pseudo measurements are utilised in this coordination. A function diagram of the FDSELC algorithm is illustrated in Fig. 5.1.

5.3.2 Bad Data Processing

In the practical operation of the FDSELC algorithm, bad data may exist in RTU and PMU measurements, and the bad data can reduce the estimation accuracy. To prevent these potential damages, bad data detection and identification are necessary. Because the two-level distributed configuration is employed in the FDSELC algorithm, the bad data should be detected at two levels independently. The procedure of bad data

processing at the coordinated level in this algorithm is the same as the DSELC algorithm. This procedure is described in Section 4.2.3.
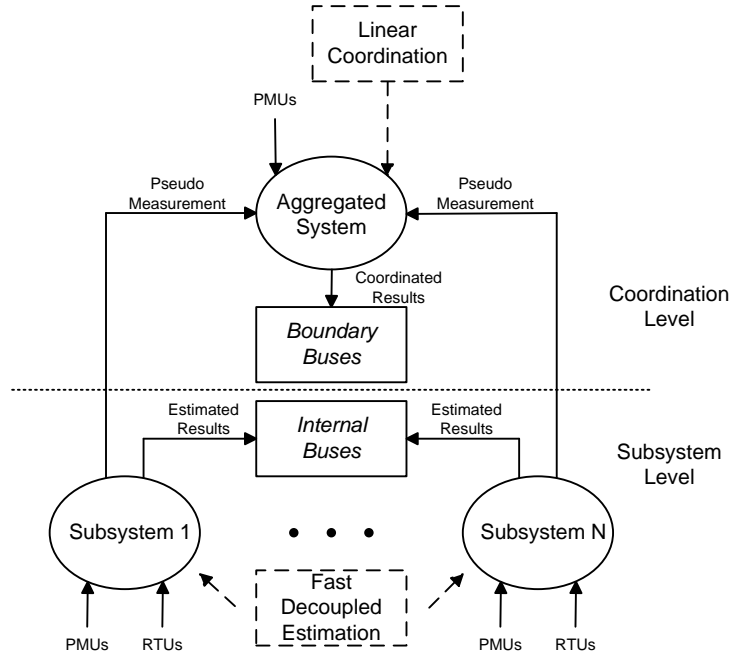
Fig. 5. 1. Function diagram of the FDSELC algorithm

The process to detect and identify bad data at the subsystem level of the FDSELC algorithm would be introduced as follows. At this level, the fast decoupled state estimation is performed, and this method is developed based on the WLS estimation. Thus, the Chi-squares approach and the LNR approach are suitable for detecting and identifying bad data at this level. However, as a result of the decoupled estimation in the fast decoupled method, the processes of bad data detection and identification need to be decoupled correspondingly. In this situation, the bad data can be detected in the active and reactive estimation individually. Based on the aforementioned Section 3.2, the objective functions in the active and reactive estimations can be calculated by the

following equations, where r'_a and r'_r are the residuals in the active and reactive estimations.

$$J_a(\hat{x}) = (z'_a - h'_a(\hat{x}))^T \cdot R'^{-1}_a \cdot (z'_a - h'_a(\hat{x})) = r'^T_a \cdot R'^{-1}_a \cdot r'_a \qquad (5.20)$$

$$J_r(\hat{x}) = (z'_r - h'_r(\hat{x}))^T \cdot R'^{-1}_r \cdot (z'_r - h'_r(\hat{x})) = r'^T_r \cdot R'^{-1}_r \cdot r'_r \qquad (5.21)$$

Afterwards, the results of (5.20) and (5.21) are compared with the corresponding Chi-squares thresholds. These thresholds are calculated based on the number of states and measurements involved in each estimation process. The number of measurements and states are denoted as m_a and n_a in the active estimation, and the threshold in the active estimation is $\chi^2_{m_a - n_a, p}$. On the other hand, the threshold is $\chi^2_{m_r - n_r, p}$ in the reactive estimation, where m_r and n_r are the numbers of the measurements and states in this estimation. The criterions of bad data detection are summarised as follows:

If $J_a(\hat{x}) > \chi^2_{m_a - n_a, p}$, the bad data is existed in the active measurements.

If $J_r(\hat{x}) > \chi^2_{m_r - n_r, p}$, the bad data is existed in the reactive measurements.

Through the above processes, the bad data can be located in the active or reactive measurements. Thus, the bad data identification process only considers active measurements or reactive measurements, rather than all the measurements. This means the number of measurements to be identified is significantly reduced, and the computational efficiency is improved consequently. The processes of bad data identification in the active or reactive estimation are the same. This section describes the process in the active estimation. The LNR approach is utilised to recognise the

bad data. The first step is to calculate the residual covariance matrix in the active estimation as:

$$\Omega'_a = R'_a - H'_{aa} \cdot G'^{-1}_a \cdot H'^T_{aa} \tag{5.22}$$

This residual covariance matrix is an off-diagonal and symmetric matrix. Its diagonal entries are used to form the normalised residuals of active measurements as:

$$r^N_{ai} = \frac{\left| r'_{ai} \right|}{\sqrt{\Omega'_{aii}}} \tag{5.23}$$

The normalised residual for each active measurement can be calculated by (5.23). The measurement with the largest normalised residual is recognised as the bad data. If the bad data exists in the reactive measurements, a similar process related to the reactive estimation can be used to identify the bad data. Finally, all the bad data at the subsystem level of the FDSELC algorithm can be identified.

5.3.3 Comparison between the FDSELC and DSELC Algorithms

The FDSELC algorithm in this chapter is developed from the DSELC algorithm in previous chapter. This section compares these two algorithms.

The main similarities between two algorithms are summarised as: both algorithms employ the same distributed configuration, which comprises of the subsystem level and the coordination level. At the subsystem level, the same non-overlapping decomposition strategy is used to separate the large system. At the coordination level, the same linear estimation approach is conducted to coordinate the states of boundary

buses. Thus, the procedures of bad data processing are the same at this level. In addition, two algorithms consider the same measurements at both levels. RTU and PMU measurements are utilised at the subsystem level, and PMU and pseudo phasor measurements are employed at the coordination level.

On the other hand, compared with the DSELC algorithm, the FDSELC algorithm has improved computational efficiency. One key reason for this improvement is that the fast decoupled state estimation is performed in the subsystems of the FDSELC algorithm. This approach is much faster than the nonlinear WLS approach, which is used at the subsystem level of the DSELC algorithm. At the subsystem level of the FDSELC algorithm, the processes of the bad data detection and identification are also decoupled, and this can reduce the computational burden in local estimations.

5.4 Case Studies

The feasibility of the FDSELC algorithm is validated at first in this section. Afterwards, the estimation accuracy and computational efficiency of the proposed FDSELC algorithm are compared with centralised fast decoupled state estimation algorithm, another distributed state estimation algorithm [118] and the DSELC algorithm. The capability of detecting and identifying the bad data in the FDSELC algorithm is demonstrated by numerical simulations. The impact of PMU measurements on the estimation accuracy of the fast decoupled estimation is also investigated. The following case studies are performed by the MATLAB R2009b on the desktop with Intel Core 2 Quad CPU Q9550 of 2.83 GHz.

5.4.1 Test Systems and Case Description

To simulate a large scale power system, the IEEE 118-bus and 300-bus system are utilised in these case studies. Their details can be referred to in [130, 137]. According to different algorithms and measurements, five scenarios are designed, and ten cases are established correspondingly, as shown in Table 5.1. Through the comparison among these five scenarios, the estimation accuracy and computational efficiency of the FDSELC algorithm can be evaluated.

- Scenario 1: Centralised state estimation by the fast decoupled algorithm [61] with RTU measurements.

- Scenario 2: Centralised state estimation by the fast decoupled algorithm with both RTU and PMU measurements.

- Scenario 3: Distributed state estimation by the algorithm in [118] with both RTU and PMU measurements.

- Scenario 4: Distributed state estimation by the DSELC algorithm with both RTU and PMU measurements.

- Scenario 5: Distributed state estimation by the proposed FDSELC algorithm with both RTU and PMU measurements.

RTU and PMU measurements are utilised in these case studies. Scenario 1 considers RTU measurements only, whilst both of RTU and PMU measurements are used in

other scenarios. RTUs can provide the measurements of voltage magnitudes and the power flows at the sending and receiving ends of branches. PMU measurements consist of voltage and current phasors. These measurements are sampled as many as possible to guarantee the best estimation accuracy. To simulate the practical situation, white Gaussian noise is added to each measurement. RTU and PMU measurements have revenue accuracy of 0.1% and 0.025%, respectively [131, 132]. Due to the randomness, test results are evaluated based on the average value of 1000 tests.

	Centralised state estimation		Distributed state estimation		
	Scenario 1	Scenario 2	Scenario 3	Scenario 4	Scenario 5
IEEE 118-bus	Case A	Case B	Case C	Case D	Case E
IEEE 300-bus	Case F	Case G	Case H	Case I	Case J

Table 5. 1. Case description in Chapter 5

Three different distributed state estimation algorithms are performed in Scenario 3, 4 and 5, respectively. The same distributed configuration is applied in these three scenarios. The IEEE 118-bus system is divided into four subsystems, and the decomposition scheme is shown in Fig. 4.5. PMUs are installed at Bus 15, 17, 19, 23, 38, 49, 59, 64, 69, 80, 82 and 100, to meet the requirement of the DSELC and FDSELC algorithm.

The redundancy in Case E is discussed then. Because the fast decoupled state estimation is executed at the subsystem level in this case, the redundancy degrees for the active and reactive estimations are calculated individually. The total redundancy in each subsystem is the combination of the degrees in these estimations. The

redundancy degree of all subsystems and the aggregated system in Case E are listed in the following table, where the 'S', 'M', and 'R' denote the number of states, measurements and redundancy degrees, respectively.

	Active Process			Reactive Process			Total		
	S	M	R	S	M	R	S	M	R
Subsystem 1	29	87	3.00	29	114	3.93	58	201	3.47
Subsystem 2	30	109	3.63	30	135	4.5	60	244	4.07
Subsystem 3	30	98	3.27	30	124	4.13	60	222	3.70
Subsystem 4	29	96	3.31	29	123	4.24	58	219	3.78
Aggregated System							29	49	1.69

Table 5. 2. Redundancy degrees in Case E

The IEEE 300-bus system is decomposed into four small subsystems. The buses with comparatively close distance are grouped in one subsystem. 36 PMUs are installed at selected boundary buses. The detailed decomposition scheme is listed in Table 5.3.

	Bus	PMU Installed
Subsystem 1	1~44, 46~47, 52, 60~64, 68, 72~75, 87, 92, 110, 129, 173~174, 198, 231~232, 238~242, 247~257 and 266.	44, 61, 64, 72, 74, 75, 174, 198 and 266
Subsystem 2	45, 48~51, 53~59, 65~67, 69~71, 76~86, 88~91, 93~106, 108, 111, 123, 136~139, 180, 183, 185~186, 190, 233~237, 243~245 and 258~262	48, 54, 59, 71, 81, 86, 89, 105, 106, 111, 183, 185 and 190
Subsystem 3	107, 109, 112~122, 124~128, 130~135, 140~172, 175~176, 184, 187~189, 204, 206, 208~210, 219, 230, 246 and 263~265	109, 112, 122, 184, 189, 204 and 210
Subsystem 4	179~179, 181~182, 191~197, 199~203, 205, 207, 211~218, 220~229 and 267~300	177, 203, 207, 211, 270, 271 and 273

Table 5. 3. Decomposition scheme on the IEEE 300-bus system

Similar to Case E, Case I also employs the fast decoupled state estimation at its lower level. Table 5.4 shows the redundancy degrees of all subsystems and the aggregated system in Case I.

	Active Process			Reactive Process			Total		
	S	M	R	S	M	R	S	M	R
Subsystem 1	83	246	2.96	83	320	3.86	166	566	3.41
Subsystem 2	72	215	2.99	72	274	3.81	144	489	3.40
Subsystem 3	74	212	2.86	74	279	3.77	148	491	3.32
Subsystem 4	71	168	2.37	71	232	3.27	142	400	2.82
Aggregated System							71	124	1.75

Table 5. 4. Redundancy degrees in Case I

In addition to Case E and I, the redundancy degrees of other cases can be calculated through the process described in Section 4.3.1. Combined these results with Table 5.2 and 5.4, the overall degrees of redundancy for all cases are finally obtained and they are listed in Table 5.5. Because only RTU measurements are considered in Case A and Case F, one slack bus has to be selected to balance phase angles in the system. This slack bus is excluded from the estimation, and this is the reason why the states of those cases are reduced by 2 from Case B and Case G, respectively.

	IEEE 118-bus system					IEEE 300-bus system				
	Case A	Case B	Case C	Case D	Case E	Case F	Case G	Case H	Case I	Case J
S	234	236	294	265	265	598	600	742	671	671
M	861	1006	1064	935	935	1944	2264	2371	2070	2070
R	3.68	4.26	3.62	3.53	3.53	3.25	3.77	3.20	3.08	3.08

Table 5. 5. Overall redundancy degrees in Chapter 5

5.4.2 Feasibility of the FDSELC Algorithm

According to Table 5.1, the FDSELC algorithm is performed in Scenario 5 (Case E & J). These cases can demonstrate the feasibility of the FDSELC algorithm. Conventional fast decoupled state estimation in Scenario 1 (Case A & F) is chosen to be compared with the FDSELC algorithm, because the conventional algorithm has been already accepted. If Case E & J have similar estimation accuracy with Case A & F, the proposed FDSELC algorithm can be regarded as feasible. The error level in (4.19) and (4.20) are used to evaluate the estimation accuracy. The level in Case A & E are illustrated in Fig. 5.2.
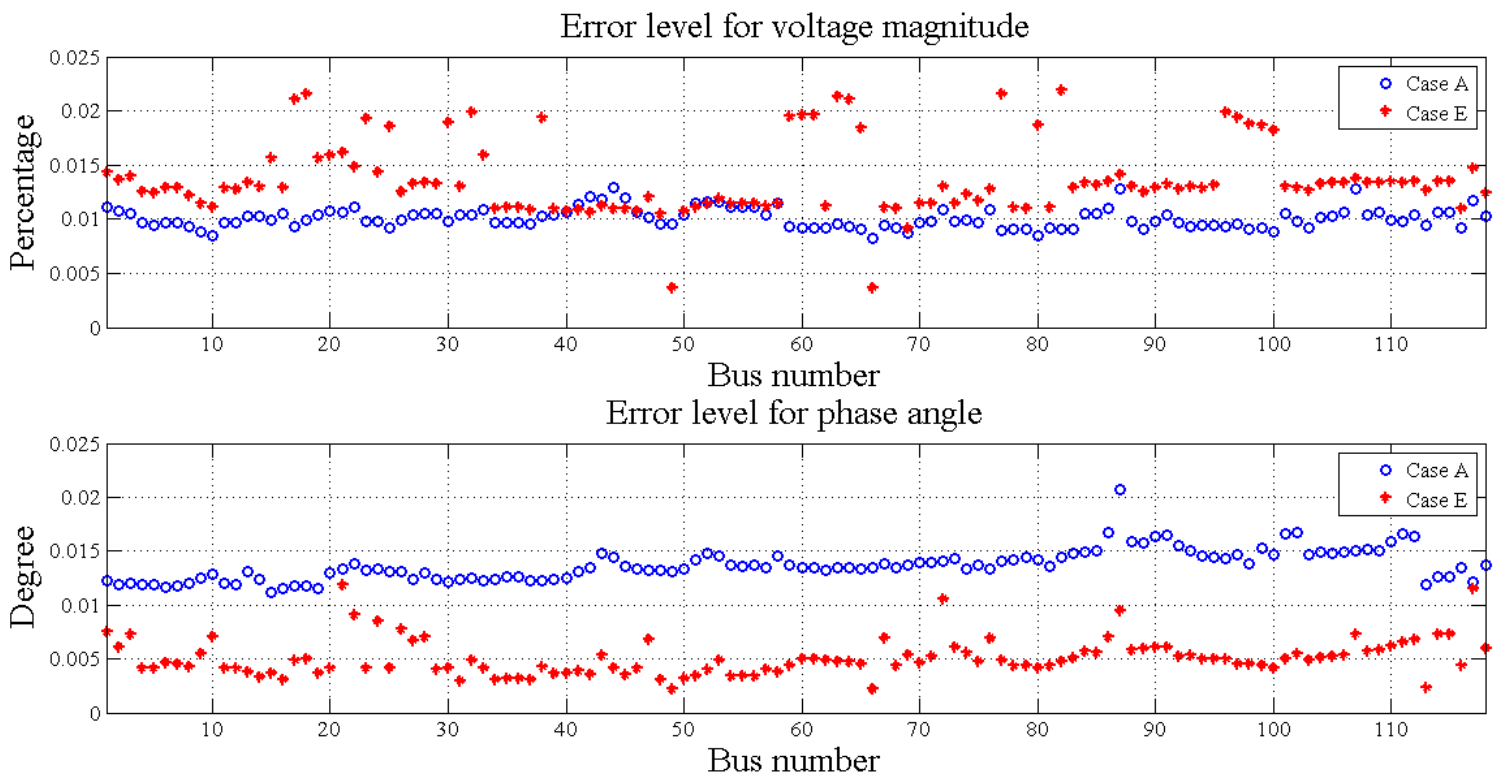
Fig. 5. 2. Comparison of error level between Case A and Case E

Fig. 5.2 shows that the maximum error level in Case E are about 0.022 for voltage

magnitudes and 0.012 for phase angles. This means the maximum estimation discrepancies are 0.022% for voltage magnitudes and 0.012 degree for phase angles. On the other hand, in Case A, the corresponding numbers are 0.014% and 0.018 degree. The differences between Case A and E are only 0.008% and 0.006 degree, which are really small in practice. Thus, the estimation accuracy of Case E is acceptable. On the IEEE 300-bus system, the same conclusion can be drawn that the estimation accuracy of Case J is satisfied.

Therefore, the proposed FDSELC algorithm has acceptable estimation accuracy compared with the conventional method, and the feasibility of the proposed algorithm is validated.

5.4.3 Comparison of Estimation Accuracy

The estimation accuracy of the proposed FDSELC algorithm is compared with other algorithms of centralised and distributed state estimation in this case study. The overall error level, E_V in (4.21) and E_A in (4.22), are calculated in each case to make the comparison quantitative. On the IEEE 118-bus system, the comparison results are illustrated in Fig. 5.3.

When the same measurement sets are considered in state estimation, higher redundancy usually lead to higher estimation accuracy. According to Table 5.5, Case B has the highest redundancy among the cases on the IEEE 118-bus system, so this case would have the best estimation accuracy as well as the lowest overall error level. Fig. 5.3 demonstrates this deduction.

On the IEEE 300-bus system, the same comparison is performed among five cases, and the results are shown in Fig. 5.4. In this comparison, Case G has the best estimation accuracy for voltage magnitude due to its highest redundancy. However, the estimation accuracy for phase angles in this case is lower than that in Case H, I and J. This can be explained as follows: It is a fact that the phase angle measurements from PMUs can improve the estimation accuracy for phase angles directly, but this improvement is related to the portion of phase angle measurements. In Case G, this portion is very small, and thus the improvement is limited. On the contrary, as a result of the distributed configuration and decoupled estimation process, the portion of phase angle measurements in Case J is much increased. So, the estimation accuracy for phase angles in Case J is higher than that in Case G.
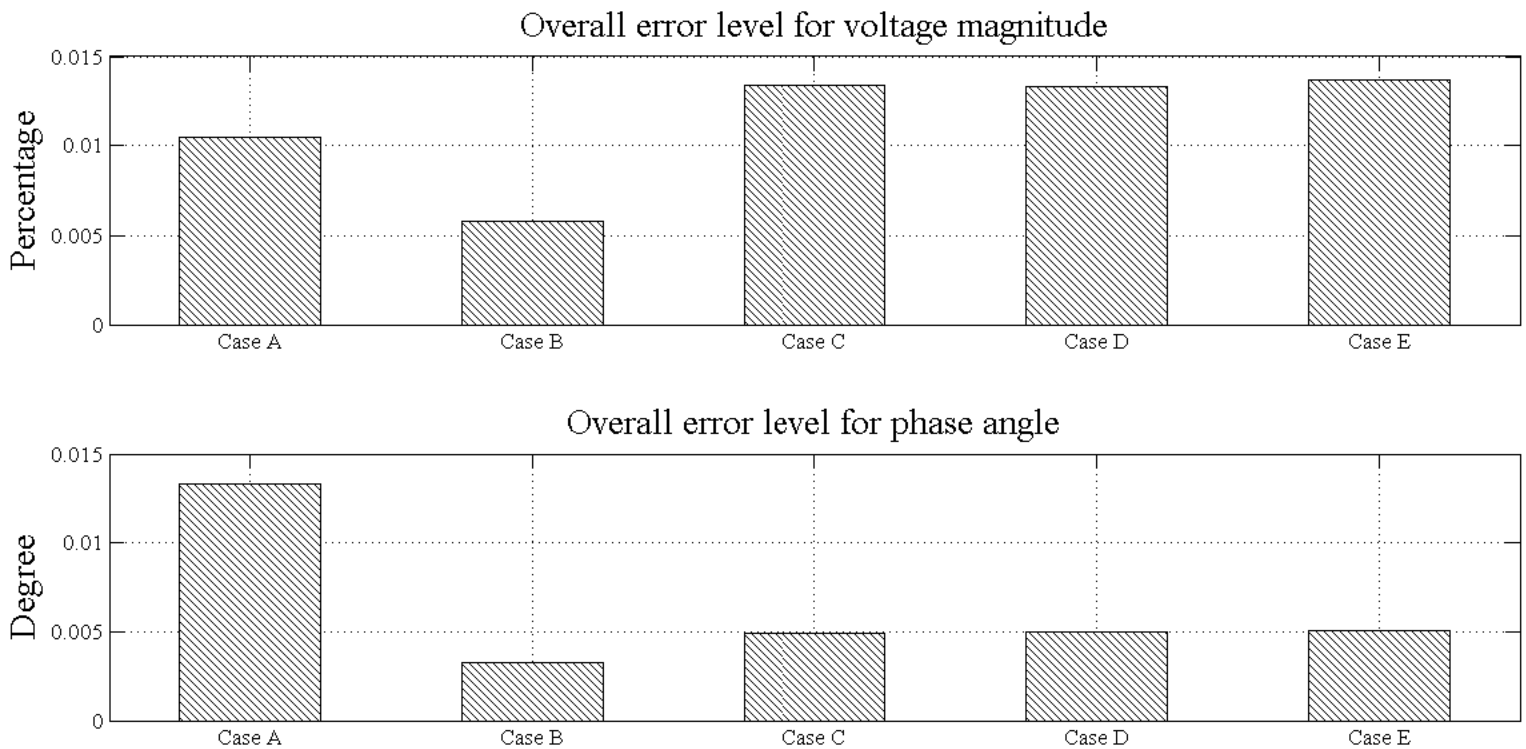
Fig. 5. 3. Comparison of overall error level on the IEEE 118-bus system

The accuracy of the proposed FDSELC algorithm is also evaluated by Case E and J through Fig. 5.3 and 5.4. On the IEEE 118-bus system, the estimation accuracy of Case E is lower than those of the centralised cases (Case A and B). This is because the redundancy degree in Case E is decreased by the distributed configuration. In the larger system, the IEEE 300-bus system, Case J has lower estimation accuracy for voltage magnitudes and higher one for phase angles. Compared with other distributed algorithms (Case C and D, Case H and I), the FDSELC algorithm (Case E and J) has similar estimation accuracies. Finally, it can conclude that the estimation accuracy of the proposed FDSELC algorithm is satisfied.
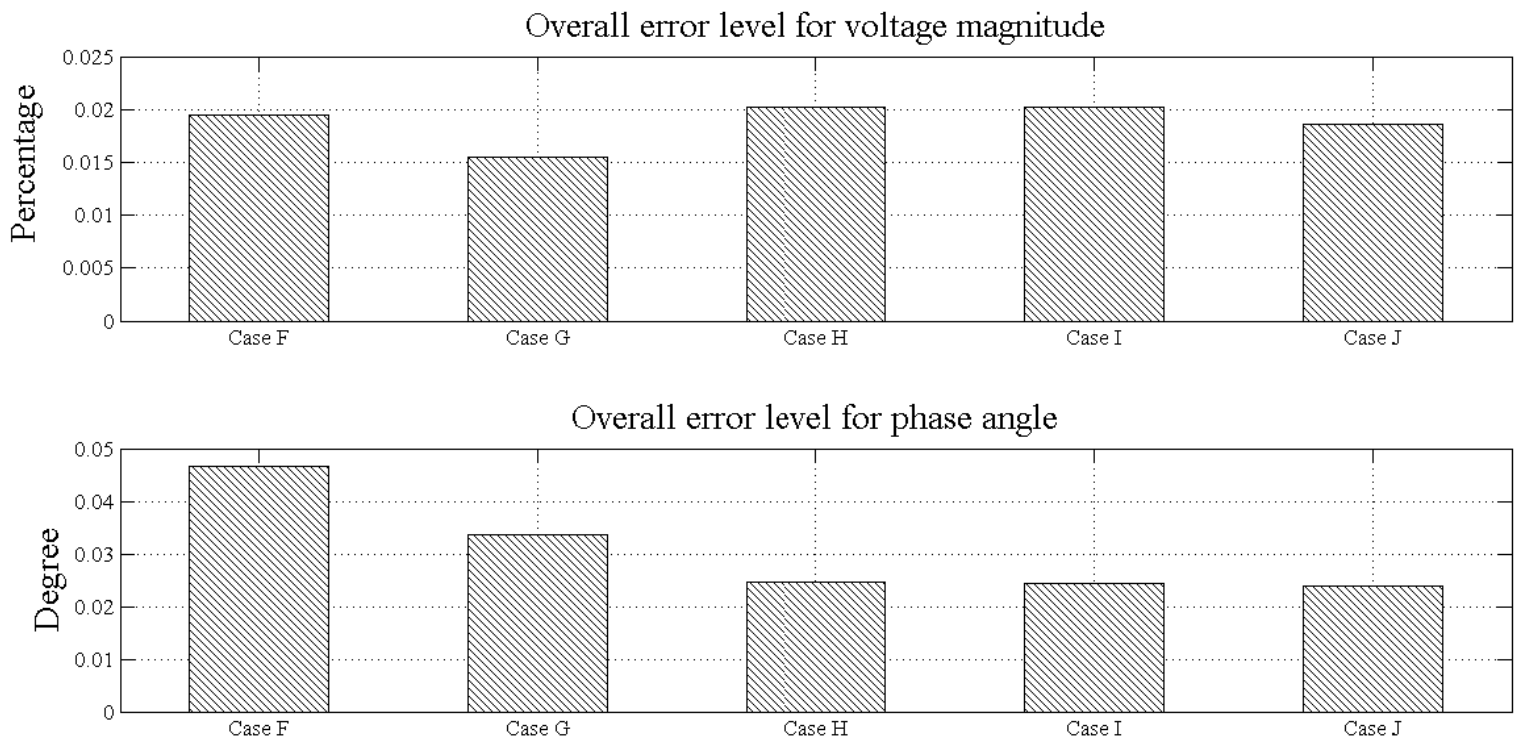
Fig. 5. 4. Comparison of overall error level on the IEEE 300-bus system

5.4.4 Comparison of Computational Efficiency

The FDSELC algorithm is proposed to further improve the computational efficiency of the DSELC algorithm. This improvement is demonstrated in this case study. Similar to case studies in Chapter 4, distributed scenarios (Scenario 3, 4 and 5) in this study are conducted with a parallel scheme, where local estimations are performed at the same time. The computational time at the subsystem level is then determined by the subsystem with the longest CPU time.

The tests are simulated in the MATLAB R2009b on the desktop with Intel Core 2 Quad CPU Q9550 of 2.83 GHz. The CPU time is recorded with the unit of millisecond. It should be noticed that the communication time between local estimators and the coordinator is not considered at current step due to hardware limitations. This communication time would be considered in the future work.

Table 5.6 shows the computational time in each case. The normalised values of CPU time are listed in brackets, and the time of Scenario 1 (Case A and F) is chosen as the standard in each test system.

	Centralised State estimation		Distributed State Estimation		
IEEE 118-bus	Case A	Case B	Case C	Case D	Case E
	18.32 (100%)	35.25 (192%)	5.23 (28.5%)	2.82 (15.4%)	2.08 (11.4%)
IEEE 300-bus	Case F	Case G	Case H	Case I	Case J
	352.89 (100%)	511.31 (144%)	77.85 (22.1%)	26.02 (7.4%)	12.47 (3.5%)

Table 5. 6. Comparison of computational efficiency in Chapter 5

According to Table 5.6, Scenario 5 (Case E and J) has the lowest computational time

in both IEEE 118-bus and 300-bus systems. This means the FDSELC algorithm has the highest computational efficiency in this case study. The improved computational efficiency of this algorithm is attributed to three reasons. The first and second reasons are the use of distributed configuration at the subsystem level and the use of linear estimation approach at the coordination level. Their effects in the improvement in computational efficiency are presented in Section 4.3.4. The third reason is the fast decoupled estimation employed at the subsystem level of the FDSELC algorithm. The computational burden is reduced in local estimations, and the overall computational efficiency of this algorithm can be enhanced consequently.

To demonstrate the effect of the third reason, the computational cost at the subsystem level is compared between Scenario 4 (DSELC algorithm) and Scenario 5 (FDSELC algorithm). The CPU time of Scenario 4 is selected as 100%, and a comparison of normalised CPU time is illustrated in Fig. 5.5.

It is clear that smaller CPU time is taken in Scenario 5. This can show the great reduction of the fast decoupled state estimation in computational cost. This improvement is more obvious on the IEEE 300-bus system. Therefore, the advantage of the FDSELC algorithm in computational efficiency is more apparent in a larger scale system.

5.4.5 Bad Data Processing

The proposed FDSELC algorithm can also deal with bad data. Numerical tests are executed in Case I to verify this capability. As a result of the distributed configuration,

the procedure of bad data processing in this case is performed at two levels separately. Because the same method is employed to coordinate states at the upper level of the DSELC and FDSELC algorithm, the processes to detect and identify bad data at this level are the same. These processes are described in Section 4.2.3, and their effectiveness is verified in Section 4.3.5. Thus, in this case study, the bad data is only checked at the subsystem level of the FDSELC algorithm, and Subsystem 1 in Case I is chosen to conduct the bad data tests.
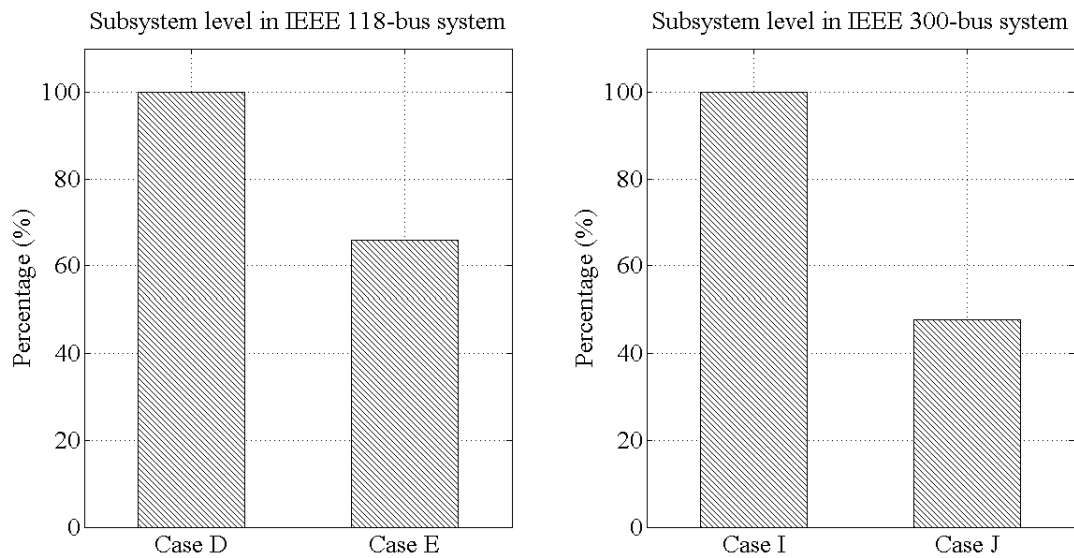
Fig. 5. 5. Comparison of normalised CPU time at the subsystem level between the DSELC and FDSELC algorithms

At the subsystem level of the FDSELC algorithm, the bad data can be detected in the active and reactive process, respectively as a consequence of the decoupled estimation. The objective functions in these processes are calculated by (5.20) and (5.21). The detection confidence is chosen as 0.95 in this case study, and the detection thresholds

used in the active and reactive estimations are 193.8 and 273.9 respectively. Selected single bad data is added to all types of measurements in turn. The tests for bad data detection and identification in Case I are summarised in Table 5.7.

When the bad data exists, the values of the objective function are increased sharply and far beyond the threshold. This means all the bad data can be detected successfully through the comparison in this case study.

Thereafter, these bad data can be also recognised effectively by the modified LNR approach in Section 5.3.2. After the elimination of identified bad data, the value of the objective function comes back to normal. The identification is successful. In conclusion, the bad data detection and identification at the subsystem level of the FDSELC algorithm are verified.

		Bad Data	Execute Value	Bad Value	$J(x)$	
			Maximum r_i^N	Locate Error	New $J(x)$ after elimination	
Active Estimation	No bad data				49.22	
	RTUs	$P_{11\text{-}12}$	0.3418	0.50	2316.14	Detected
			47.62	$P_{11\text{-}12}$	46.61	Identified
	PMUs	θ_{15}	11.474	15.0	29914.24	Detected
			172.01	θ_{15}	49.62	Identified
		$Re(I_{14\text{-}15})$	0.0547	0.03	96560.97	Detected
			300.83	$Re(I_{14\text{-}15})$	47.52	Identified
Reactive Estimation	No bad data				45.59	
	RTUs	$Q_{18\text{-}20}$	0.3978	0.50	6291.81	Detected
			79.03	$Q_{18\text{-}20}$	45.95	Identified
		V_{13}	0.968	0.93	1460.40	Detected
			37.64	V_{13}	43.83	Identified

	PMUs	V_{17}	0.995	1.05	35257.34	Detected
			187.38	V_{17}	43.48	Identified
		$Im(I_{17\text{-}26})$	-0.054	-0.03	566.57	Detected
			22.84	$Im(I_{17\text{-}26})$	45.40	Identified

Table 5. 7. Bad data tests in Case I

5.4.6 Improvement of the Fast Decoupled State Estimation by PMU Measurements

In the case study of Section 4.3.6, numerical tests demonstrate the benefits brought from PMU measurements in the WLS estimation. Similarly, this case study investigates the potential benefit from PMU measurements in the fast decoupled state estimation. This is investigated by the comparison between the estimation accuracy of Scenario 1 and 2. These two scenarios perform the fast decoupled state estimation with different measurement sets. Scenario 1 considers RTU measurements only, whilst both RTU and PMU measurements are used in Scenario 2.

On the IEEE 118-bus system, the error level at each bus in Case A and B are calculated by (4.19) and (4.20). Smaller error level means higher estimation accuracy. The comparison result is illustrated in Fig. 5.6.

According to Fig. 5.6, the error level for both voltage magnitudes and phase angles in Case B are lower than those in Case A. This means PMU measurements can actually improve the estimation accuracy of the fast decoupled estimation. A similar conclusion can be also drawn by the comparison between Case F and G on the IEEE 300-bus system. The estimation accuracy in Case G is higher than that in Case F, due

to the effect of PMU measurements.
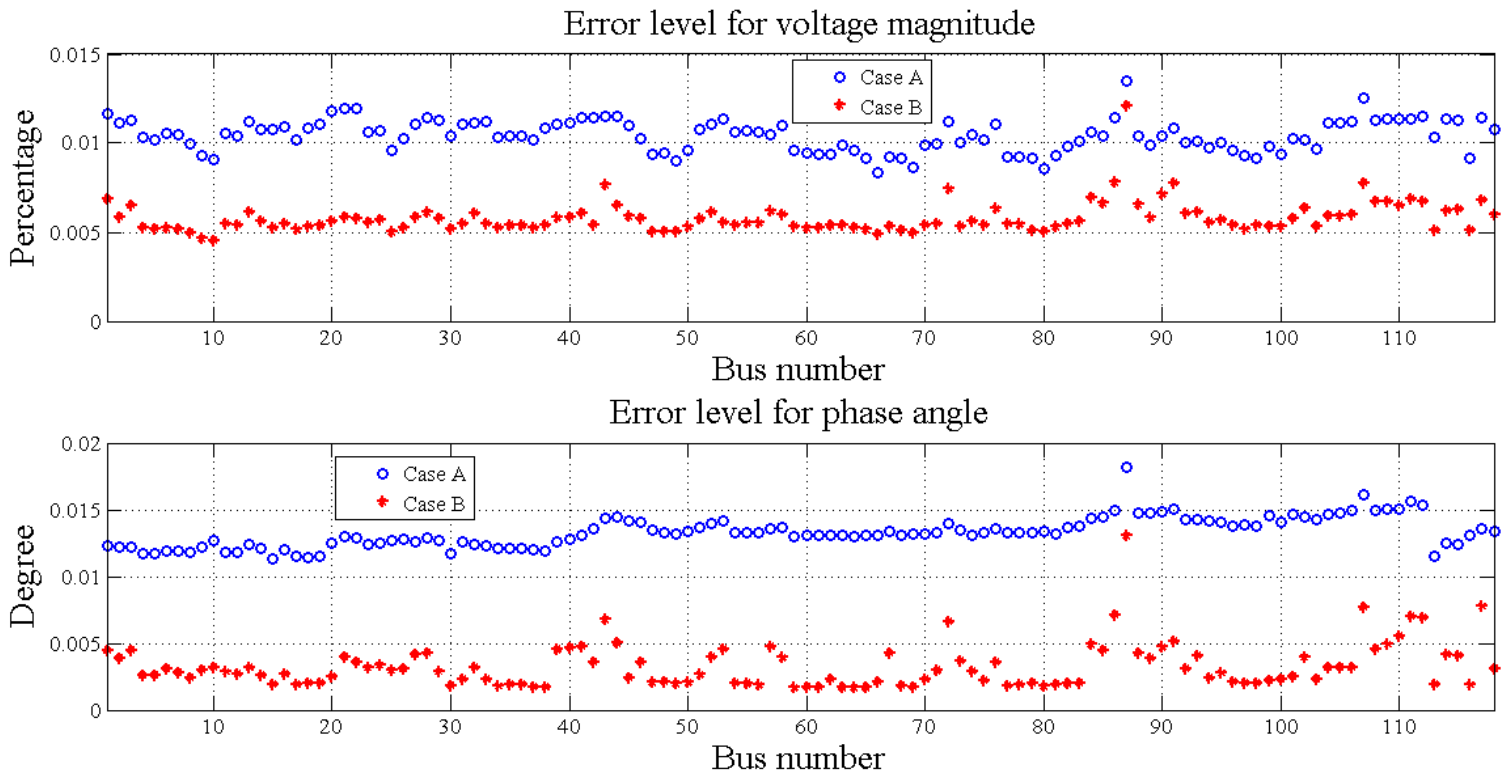
Fig. 5. 6. Comparison of error level between Case A and Case B

This improvement in the estimation accuracy of the fast decoupled estimation is reasonable because the redundancy is increased through the integration of PMU measurements with the estimation. Table 5.5 can indicate the increase of redundancy from Case A to B and from Case F to G. In addition, PMU measurements have better accuracy than RTU measurements. The more accurate measurements can lead to higher estimation accuracy consequently.

Additionally, focused on the upper and bottom figure in Fig. 5.6, the differences of the error level between Case A and B in the bottom figure are more apparent. This indicates that PMUs can bring more benefits on the accuracy of the estimation for

phase angles in the fast decoupled state estimation.

5.6 Summary

This chapter proposes a novel FDSELC algorithm based on the DSELC algorithm described in previous chapter. In the FDSELC algorithm, the fast decoupled state estimation is employed at the subsystem level, and thereafter the computational burden is reduced in local estimations. Thus, a further improved computational efficiency can be achieved in the FDSELC algorithm.

The performance of the FDSELC algorithm is evaluated through the case studies on the IEEE 118-bus and 300-bus system. Compared with other centralised and distributed state estimation algorithms, simulations indicate that the FDSELC algorithm has acceptable estimation accuracy and improved computational efficiency. The advantage on the computational efficiency of the FDSELC algorithm would be more obvious in larger systems.

In addition, a corresponding procedure is also presented to deal with bad data in the FDSELC algorithm. Numerical results demonstrate that the bad data are detected and identified successfully through this procedure. Hence, the effectiveness of this procedure is verified. At last, the improvement in the accuracy of the fast decoupled state estimation by PMU measurements is demonstrated in this chapter.

It should be noticed that the communication time between estimators and the coordinator is not included in this chapter, due to hardware limitations.

CHAPTER 6 DISTRIBUTED ALGORITHM FOR TRANSIENT STATE ESTIMATION WITH PMU MEASUREMENTS

6.1 Introduction

As aforementioned in Chapter 1, there are two main contributions in this thesis. The first one is to solve the low efficiency problem in static state estimation caused by a huge computational burden. This burden is produced by the use of both RTU and PMU measurements in the estimation at the same time. Two newly developed algorithms are proposed in Chapters 4 and 5, and these algorithms can mitigate the problem effectively.

The other main contribution is to propose a method to perform transient state estimation. When a system disturbance occurs, the voltage and current waveforms in the power system are not sinusoidal longer. Conventional methods of static state estimation using voltage and current phasors are not working effectively or not working at all. Thus, the methods of transient state estimation are necessary in this condition. The research of the transient state estimation is still in the processing, and there are no methods can be implemented in actual power systems so far. This chapter proposes a novel algorithm, namely the Distributed Space State Estimation (DSSE), to perform transient state estimation in practice.

The proposed DSSE algorithm is the first of its kind, which can be performed in practical power systems. The algorithm is supposed to estimate transient states with actual PMU measurements. Current hardware conditions can meet the requirement of the DSSE approach, and this is one of the most important features of the algorithm. In addition, a distributed configuration is employed in the proposed approach, and therefore the computational burden can be much reduced in local estimations. This configuration can also reduce the hardware requirements for computation and data transmission in the DSSE approach.

Three main characterises can be summarised from the DSSE algorithm:

- The DSSE approach considers the model of the power system during the transient condition, and the non-sinusoidal voltage and current waveforms can be used in the estimation through this model;

- The DSSE approach is based on practical PMU measurements, including the sampling rate and scanning cycle;

- The DSSE approach employs a distributed configuration.

6.2 PMU Measurements in Transient Conditions

The appearance of PMUs can greatly improve the state estimation research. The introduction of PMU measurements can enhance the estimation accuracy, and this improvement has been demonstrated in Chapters 4 and 5. In addition, the faster sampling rate of PMU measurements can also benefit state estimation. The proposed

DSSE algorithm is based on this benefit, and all the measurements in this algorithm are provided from PMUs. Before the description of the DSSE algorithm, it is necessary to introduce the standards of practical PMU measurements and the use of these measurements during the transient condition of power systems.

6.2.1 Sampling Rate and Scanning Cycle

In practice, PMUs always provide voltage and current phasor measurements, which are formed by the magnitude and phase angle. The magnitude is the Root Mean Square (RMS) values of the signal, and the phase angle equals the angle between the reporting instant of PMUs and the peak of the sinusoid. The reporting instant is the time when PMUs export measurements. PMUs can only capture raw data from power systems. The background noise in these raw data needs to be filtered in PMUs at first. The filtered data, called sampled data, are used to estimate phasors, which are the outputs of PMUs. This process of producing phasor measurements in PMUs is shown in a simple function diagram in Fig. 6.1 [13].

Phasor Measurement Unit (PMU)

Filters → Sampled Data → Phasor Estimator

Raw Samples

Phasor Measurements
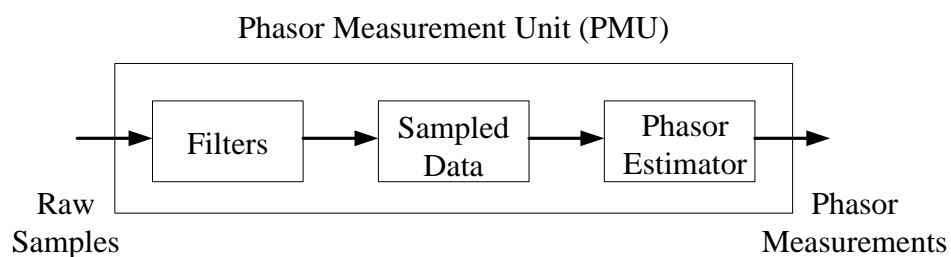
Fig. 6. 1. Function diagram of producing phasor measurements in PMUs

Two important parameters need to be distinguished in practical PMU measurements. One is the sampling rate. The sampling rate is related to the process of capturing raw

data in PMUs. The raw data are sampled as the instantaneous magnitudes of the measured signal in different time instants. These samples during a short period can estimate a phasor measurement. This period is the scanning cycle of PMU measurements or named as the reporting time, which is the other important parameter. In each scanning cycle, PMUs can capture a multitude of raw sampling and produce one phasor measurement. The relationship between these two parameters is illustrated in Fig. 6.2. According to the IEC 61850 standard, there are always 80 samples per scanning cycle.
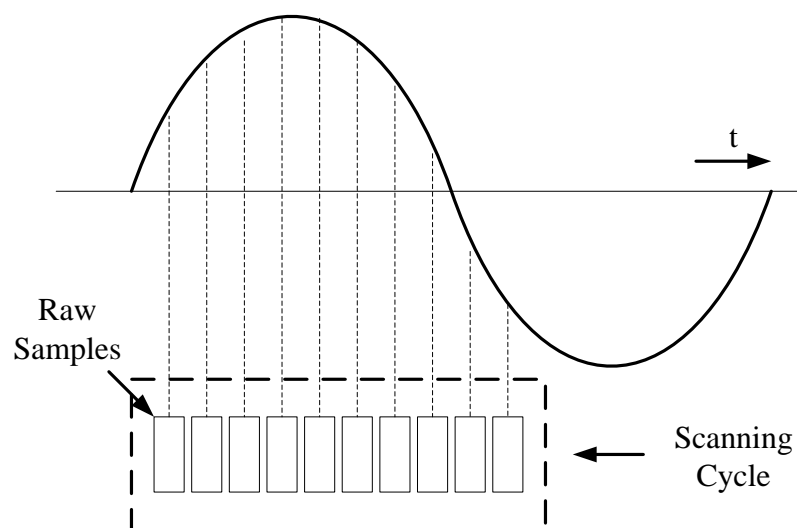
Fig. 6. 2. Relationship between samples and the scanning cycle of PMU measurements

Conventional RTUs have a scanning cycle of 580ms under the frequency of 50 Hz [132]. This is too slow for a typical transient state estimation, because the period of a transient is usually smaller than this scanning cycle. According to the IEEE Std C37.118-2011 [37], the scanning cycle of PMUs can be decreased to 10ms or even

less if needed. Therefore, PMU measurements have a shorter scanning cycle than conventional RTU measurements, and this shorter scanning cycle can lead to a faster sampling rate. Thus, PMU measurements may meet the requirement of transient state estimation.

6.2.2 PMU Measurements in Transient Conditions

Normally, PMU phasor measurements are based on the static operation of power systems. However, in the transient condition, the precondition of phasor measurements is not effective. The phasor measurements are produced from a sine wave at the fundamental frequency. This sine wave has time-invariant amplitude in steady state. During the transient condition, both amplitude and fundamental frequency of the signal are time-variant, and this signal cannot be treated as a sinusoid. Hence, conventional phasor measurements of PMUs are not suitable in transient state estimation.

In the proposed DSSE algorithm, the instantaneous magnitudes of the samples from PMUs are used instead of phasor measurements. This is feasible because the instantaneous magnitudes are also captured in existing PMUs. These instantaneous magnitudes are utilised to estimate phasor measurements in steady state. Therefore, existing PMUs can provide these instantaneous magnitudes after a small modification.

It has to be noticed that the filters employed in PMUs in Fig. 6.1 might be low-pass or band-pass filters. They are used to clean the background noise of the raw samples, but at the same time, they are required to pass the samples during the transient condition.

For example, if the stop band of the filters is set to about 20k Hz, the filters are able to filter the undesired noise and pass the desired transient samples.

According to Fig. 6.2, there are n samples in one scanning cycle. This means the sampling rate of instantaneous magnitudes is much faster than that of phasor measurements. When these instantaneous magnitudes are provided from PMUs, the concept of scanning cycle is also effective, which indicates that all the instantaneous measurements in one scanning cycle are transmitted at the end of this scanning cycle. In steady state, PMUs can provide voltage and current phasor measurements. Correspondingly, under the transient condition, PMU measurements consist of the instantaneous magnitudes of voltage and current.

6.3 Model of Transient State Estimation

Traditional state estimation was established on the static model of power systems [9], but these static methods cannot perform the state estimation during the transient condition. In future Smart Grids, the system will be more complex and the system disturbance will be prone to occur, because more power electronics devices will be deployed. Thus, the transient condition will be more usual. The static methods are not suitable or even not working at all in that condition. This makes transient state estimation becoming more significant in future power systems. In transient state estimation, the state space model is usually used to express the relationship between states and measurements, and this model is discussed at first.

6.3.1 State Space Model

In power system research, a coupled PI model is normally employed to represent a short segment of transmission line. This PI model is also applied in the proposed DSSE algorithm. According to the practical experience, the shunt conduct in the model is not considered in this algorithm. Fig. 6.3 illustrates a typical configuration of the single phase PI model used in this section.
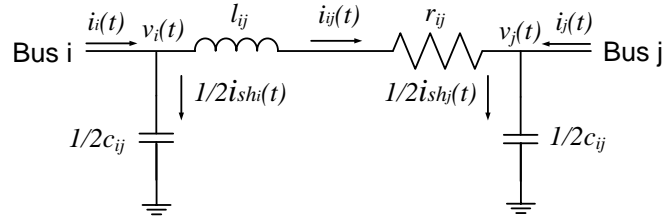
Fig. 6. 3. PI model of the transmission line

In Fig. 6.3, l_{ij}, r_{ij} and c_{ij} are the inductance, resistance and susceptance of branch ij, respectively. $v_i(t)$ and $v_j(t)$ are instantaneous voltages at Bus i and j. $i_i(t)$, $i_j(t)$, and $i_{ij}(t)$ represent the instantaneous values of the current at the sending-end, the receiving-end and the branch for the branch ij, respectively. $i_{shi}(t)$ and $i_{shj}(t)$ denote the shunt current at the sending-end and receiving-end of the branch.

Hence, the following equations can formulate the state space model of branch ij during the transient condition.

$$\frac{di_{ij}(t)}{dt} = \frac{1}{l_{ij}} \cdot (v_i(t) - v_j(t) - r_{ij} \cdot i_{ij}(t)) \tag{6.1}$$

$$\frac{dv_i(t)}{dt} = \frac{2}{c_{ij}} \cdot (i_i(t) - i_{ij}(t)) \tag{6.2}$$

$$\frac{dv_j(t)}{dt} = \frac{2}{c_{ij}} \cdot (i_{ij}(t) - i_j(t)) \tag{6.3}$$

6.3.2 Discretised Space Model

The above state space model constitutes of some first order differential equations as shown in (6.1) ~ (6.3). To transfer the state space model into a discrete one, the calculator *dx/dt* can be written as:

$$\frac{dx(t)}{dt} \approx \frac{x(t) - x(t - \Delta t)}{\Delta t} \tag{6.4}$$

where

Δt	interval time between two steps
x(t)	variables at time *t*
x(t-Δt)	variables at time *t-Δt*

Substituted (6.4) into (6.1) ~ (6.3), the discretised state model of branch *ij* during the transient condition can be obtained as follows:

$$v_i(t) - v_j(t) = (r_{ij} + \frac{l_{ij}}{\Delta t}) \cdot i_{ij}(t) - \frac{l_{ij}}{\Delta t} \cdot i_{ij}(t - \Delta t) \tag{6.5}$$

$$i_i(t) = \frac{c_{ij}}{2 \cdot \Delta t} \cdot v_i(t) - \frac{c_{ij}}{2 \cdot \Delta t} \cdot v_i(t - \Delta t) + i_{ij}(t) \tag{6.6}$$

$$i_j(t) = -\frac{c_{ij}}{2 \cdot \Delta t} \cdot v_j(t) + \frac{c_{ij}}{2 \cdot \Delta t} \cdot v_j(t - \Delta t) + i_{ij}(t) \tag{6.7}$$

The above discretised equations describe the relationships between voltage and current at time *t* and time *t-Δt* in the PI model of branch *ij*, as shown in Fig. 6.3. According to these equations, the history variables (variables at *t-Δt*) can be used to estimate the current states (variables at *t*).

6.4 Distributed Space State Estimation (DSSE) Algorithm

A transient state estimation algorithm, namely the Transient State Estimation (TSE), was proposed based on the above state space model and the discretised state model [87]. Its effectiveness was verified by numerical tests. However, this approach is not able to be implemented in current power systems because its hardware requirements cannot be met in practice. For example, the interval time between two samples of measurements is supposed as 50μs in this approach, and thus the computational time of each estimation process in the TSE algorithm is smaller than 50μs. These requirements are beyond the level of current measuring and computer technology.

The DSSE algorithm is proposed to conduct transient state estimation in actual power systems. All the key requirements of the algorithm can be met in the modern technology of power systems. The concept of scanning cycle is used in this approach. PMU measurements are only imported to the estimator every scanning cycle (10ms or even less if needed). Hence, the interval time between two estimation processes in this approach can be greatly increased. This fact can actually reduce the hardware requirements of the DSSE algorithm, and make it possible to implement the approach in practical power systems.

6.4.1 States and Measurements

Similar to other state estimation algorithms, states and measurements are two essential factors in the DSSE algorithm. These two factors are introduced in this sub-section at first.

Because the DSSE algorithm considers the model of the power system during the transient condition, its states and measurements are different from those in static estimation methods. In static estimation methods, the states contain voltage magnitudes and phase angles [9]. However, during the transient condition, the phase angles are no longer meaningful because the measuring objective cannot be treated as a sinusoid. In this situation, the instantaneous voltage magnitudes of buses and the instantaneous current magnitudes of branches are selected as states in the DSSE approach. Regarding the PI model shown as Fig. 6.3, $v_i(t)$, $v_j(t)$ and $i_{ij}(t)$ are the states of branch ij at time instant t. These states can be formulated as:

$$x_{ij}(t) = \begin{bmatrix} v_i(t) & v_j(t) & i_{ij}(t) \end{bmatrix}^T \tag{6.8}$$

All the instantaneous measurements in the DSSE approach are provided from PMUs. Practical PMUs can measure the voltage of buses and the current at the sending-end and receiving-end of branches. At time instant t, these measurements for the branch ij are expressed as:

$$z_{ij}(t) = \begin{bmatrix} v_i(t) & v_j(t) & i_i(t) & i_j(t) \end{bmatrix} \tag{6.9}$$

In a single estimation process of the DSSE algorithm, the measurements in one scanning cycle of PMUs are considered to estimate transient states in this scanning cycle. These measurements are transmitted to the estimator at the end of the scanning cycle. According to Fig. 6.2, there are n samples in a scanning cycle. Each sample means a time step in the discretised state model, as shown in (6.5) ~ (6.7), and every step contain several individual states and measurements. All these states and

122

measurements at n time steps are considered in one estimation process in the DSSE algorithm.

On the contrary, the TSE algorithm only estimates the states at one time step in each estimation process [87]. Hence, in one scanning cycle, the DSSE algorithm is performed once to estimate all states in this cycle, whilst the TSE algorithm needs to be conducted for n times to estimate these states. This is the reason why the interval time between two estimation processes in the DSSE algorithm is much longer than that in the TSE algorithm. Correspondingly, the hardware requirements in the DSSE algorithm can be greatly reduced.

6.4.2 Measurement Model

At each time step in the DSSE algorithm, the measurement model is formed by (6.5) ~ (6.7) to represent the relationship among current measurements, current states and history states. To give a more detail explanation, the measurement model for the PI section ij at time step t is constructed as:

$$
\begin{bmatrix}
v_i(t) \\
v_j(t) \\
i_i(t) + \dfrac{c_{ij}}{2 \cdot \Delta t} \cdot v_i(t - \Delta t) \\
i_j(t) - \dfrac{c_{ij}}{2 \cdot \Delta t} \cdot v_i(t - \Delta t) \\
- \dfrac{l_{ij}}{\Delta t} \cdot i_{ij}(t - \Delta t)
\end{bmatrix}
=
\begin{bmatrix}
1 & 0 & 0 \\
0 & 1 & 0 \\
\dfrac{c_{ij}}{2 \cdot \Delta t} & 0 & 1 \\
0 & -\dfrac{c_{ij}}{2 \cdot \Delta t} & 1 \\
1 & -1 & -(r_{ij} + \dfrac{l_{ij}}{\Delta t})
\end{bmatrix}
\cdot
\begin{bmatrix}
v_i(t) \\
v_j(t) \\
i_{ij}(t)
\end{bmatrix}
+ e_{ij}(t) \quad (6.10)
$$

$$
\tilde{z}_{ij}(t) = H_{ij}(t) \cdot x_{ij}(t) + e_{ij}(t) \tag{6.11}
$$

In the above measurement model, the measurements vector $\tilde{z}_{ij}$ is formed by PMU

measurements at time step t and history states. H_{ij} is the measurement matrix, and it relates measurements to states. The entries in this measurement matrix only depend on the parameters of the branch (b_{ij}, r_{ij} and l_{ij}) and the interval time between two samples (Δt). Therefore, if the topology of the system does not change and the interval time remains the same, the measurement matrix in the DSSE algorithm is constant during the transient condition. It can be factorised once, saved in the memory and substituted in each estimation process of the DSSE algorithm. Consequently, the computational burden in the algorithm can be significantly reduced.

The measurement model for the overall system can be constructed by the combination of the above model in (6.11), and it has the following forms at the time instant t.

$$
\begin{bmatrix} \widetilde{z}_{12}(t) \\ \vdots \\ \widetilde{z}_{ij}(t) \\ \vdots \end{bmatrix} = \begin{bmatrix} H_{12}(t) & & & \\ & \ddots & & \\ & & H_{ij}(t) & \\ & & & \ddots \end{bmatrix} \cdot \begin{bmatrix} x_{12}(t) \\ \vdots \\ x_{ij}(t) \\ \vdots \end{bmatrix} + \begin{bmatrix} e_{12}(t) \\ \vdots \\ e_{ij}(t) \\ \vdots \end{bmatrix} \tag{6.12}
$$

$$
\widetilde{z}(t) = H(t) \cdot x(t) + e(t) \tag{6.13}
$$

6.4.3 DSSE Algorithm

In the DSSE algorithm, PMU measurements are imported to the estimator at the end of every scanning cycle. The estimation process is performed once in each scanning cycle to estimate the states during this cycle. As aforementioned, the estimation process considers n time steps of states and measurements. Regarding each time step, an individual measurement model of the system can be constructed by (6.13). Combined all these models at n time steps, the measurement model for the overall

scanning cycle can be obtained. This overall measurement model is used in the estimation of the DSSE algorithm to execute transient state estimation. The overall measurement model is expressed in the following equation, and its compact form is also formulated as:

$$
\begin{bmatrix}
\tilde{z}(t - n \cdot \Delta t) \\
\tilde{z}(t - (n-1) \cdot \Delta t) \\
\cdots \\
\tilde{z}(t - \Delta t) \\
\tilde{z}(t)
\end{bmatrix}
=
\begin{bmatrix}
H(t - n \cdot \Delta t) & & \\
& \ddots & \\
& & H(t)
\end{bmatrix}
\cdot
\begin{bmatrix}
x(t - n \cdot \Delta t) \\
x(t - (n-1) \cdot \Delta t) \\
\cdots \\
x(t - \Delta t) \\
x(t)
\end{bmatrix}
+ \tilde{e} \quad (6.14)
$$

$$
\tilde{Z} = \tilde{H} \cdot \tilde{X} + \tilde{e} \quad (6.15)
$$

where

$\tilde{H}$ overall measurement matrix in a scanning cycle;

$\tilde{e}$ vector of measurement errors in a scanning cycle;

$\tilde{Z}$ vector of instantaneous measurements in a scanning cycle;

$\tilde{X}$ vector of states in a scanning cycle.

The measurement errors $\tilde{e}$ in the above model can be regarded as Gaussian noise, and they are independent and have zero mean. Thus, their covariance matrix $\tilde{R}$ is diagonal and comprised of σ_i^2. The σ_i is the standard deviation for the instantaneous measurement i from PMUs.

Another important matrix in the above model is $\tilde{H}$. This matrix relates measurements to states in the overall scanning cycle. The measurements at each time step can add a set of rows into this matrix, as shown in (6.12) ~ (6.15). According to

(6.10), the measurements at time step t ($z(t)$) only associates with the states at the current step and the previous step, ($x(t)$ and $x(t-\varDelta t)$). Hence, $\tilde{H}$ would be very sparse. If the non-zero entries in this matrix are denoted by 'X', and the zero entries remain blank, $\tilde{H}$ has the structure in Fig. 6.4. Each 'X' symbol would contain a set of rows in the measurement matrix and these rows are established by (6.10) ~ (6.14).
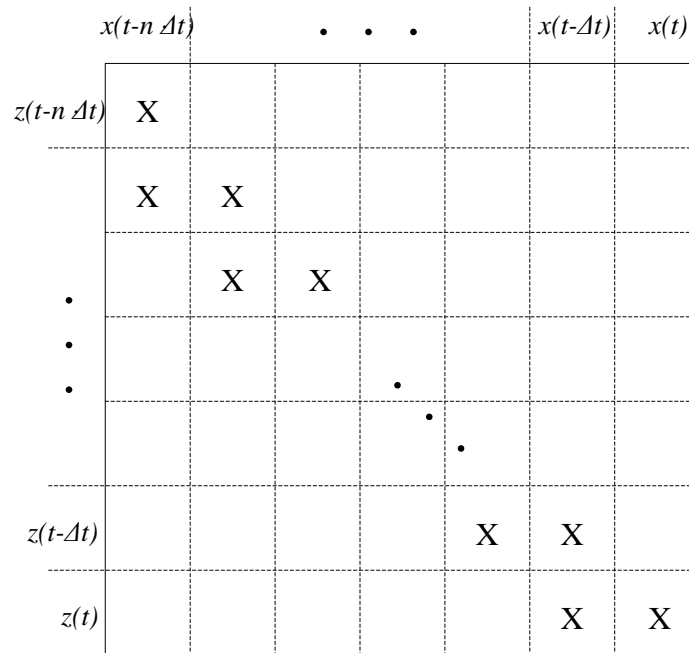
Fig. 6. 4. Structure of the measurement matrix $\tilde{H}$

According to (6.10), the entries in the measurement matrix $\tilde{H}$ only depend on the network parameter values and the interval time between two samples. The sampling rate and scanning cycle of PMUs can determine the interval time, and therefore can affect the size of the measurement matrix. Normally, all of them remain unchanged during the short transient condition, and the measurement matrix would be constant in this condition. Consequently, $\tilde{H}$ only needs to be factorised once. The factorised

result can be saved in the memory and utilised to perform the DSSE approach in each estimation process. Hence, the memory cost of the DSSE approach is saved and the computational burden is reduced.

It can be found that the measurement model for branch *ij* at time step *t* is a linear model, as shown in (6.10). Thus, the overall measurement model for the system during the scanning cycle, as shown in (6.15), is also linear, and it has a linear solution as:

$$\widetilde{X} = (\widetilde{H}^T \cdot \widetilde{R}^{-1} \cdot \widetilde{H})^{-1} \cdot \widetilde{H}^T \cdot \widetilde{R}^{-1} \cdot \widetilde{Z} \qquad (6.16)$$

In the DSSE algorithm, the states in one scanning cycle can be estimated through the above solution. The estimated results can form the snapshot of the power system during the scanning cycle. Based on the snapshots of many scanning cycles, the transient state estimation can be achieved through the DSSE approach.

Considering two facts of PMU measurements, the DSSE algorithm can be implemented in practical power systems. However, the amount of data communication is greatly increased due to the higher sampling rate of measurements. This may lead to huge memory cost and unacceptable computational burden in the transient state estimation. To reduce the amount of data communication and improve computational efficiency, a distributed configuration is introduced to the DSSE algorithm.

6.4.4 Distributed Configuration

In the distributed configuration of the DSSE algorithm, the non-overlapping decomposition strategy is utilised to divide the large system. Neighbouring buses can form a small subsystem, called as DSSE group, and thus a large system is decomposed into many independent DSSE groups. The information between a DSSE group and its neighbouring groups is only exchanged via tie-lines. Detailed information about this non-overlapping strategy including the measurements and states are summarised in [49].

Although the same non-overlapping strategy in Section 4.2.1 is used to decompose the large system, the distributed configuration in the DSSE algorithm is different from that of the DSELC and FDSELC algorithm. Because the DSSE algorithm is based on transient state estimation, its distributed configuration focuses on the reduction of computational burden and the requirement of hardware. On the contrary, the distributed configuration in static algorithms (DSELC and FDSELC algorithms) pays more attention to the guarantee of the estimation accuracy. Therefore, two main differences can be identified between these two distributed configurations.

The DSSE algorithm employs the decentralised configuration other than the hierarchical configuration in the DSELC and FDSELC algorithm. The details about these two configurations are described in Section 2.2.3. In the decentralised configuration, the states of boundary buses are not necessary to be coordinated. In this situation, the final solutions of the DSSE algorithm are obtained through the local

transient estimations in DSSE groups. This configuration can improve computational efficiency, but also decrease estimation accuracy.

The other difference is that the mutual influence between DSSE groups is not considered in the distributed configuration of the DSSE algorithm, because the signals during the transient condition changes too fast. If a local estimation considers the exchanged information from its neighbouring groups, the requirements of hardware such as transmission speed and bandwidth in this estimation can increase sharply, and these requirements may not be met by current technology. The ignorance of mutual influence would have a negative effect on the estimation accuracy, but the compromise of the estimation accuracy is acceptable through case studies. Based on this ignorance, each DSSE group can be regarded as an independent one, and the transient state estimation is conducted in each group individually. This can greatly reduce the hardware requirements of data transmission between DSSE groups. The distributed configuration in the DSSE algorithm is illustrated in Fig. 6.5.

In each DSSE group, the observability should be guaranteed to perform local transient estimations. The decomposition scheme of the DSSE algorithm has to provide enough redundant measurements in each group. In addition, local DSSE estimations must make sure that their corresponding measurement matrix $\tilde{H}$ are non-singular. These two requirements should be met at the same time in the decomposition scheme of the DSSE algorithm.
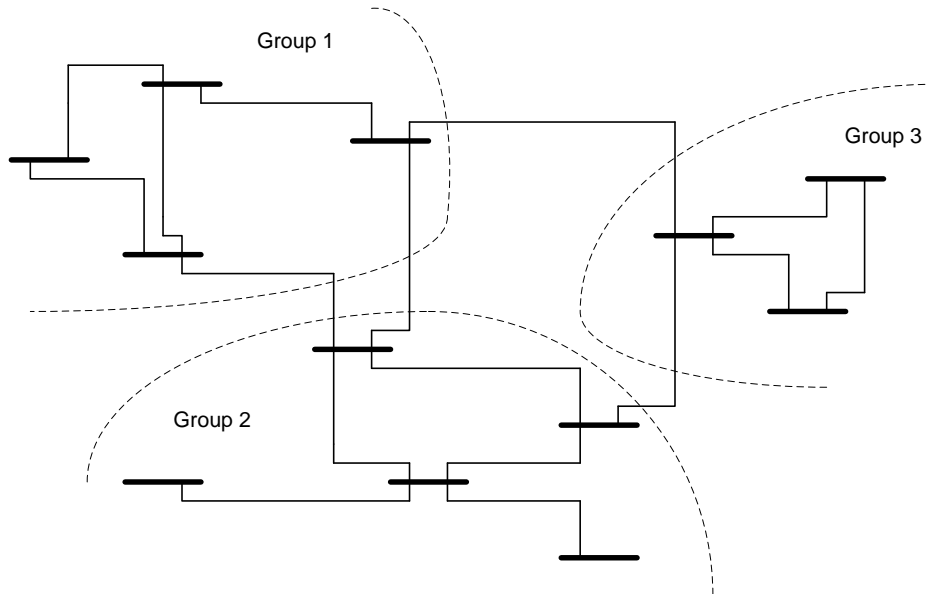
Fig. 6. 5. Distributed configuration in the DSSE algorithm

6.5 Case Studies

In this section, the following case studies are conducted for three aims. The feasibility of the proposed DSSE algorithm is validated at first. The performance of the proposed algorithm is then compared with the TSE algorithm [87] in estimation accuracy and computational efficiency. According to the requirements of the DSSE algorithm in previous section, three different decomposition schemes are applied in the DSSE algorithm to investigate their influence in the performance of the DSSE algorithm at last.

6.5.1 Test System and Case Description

The test platform in these case studies is the IEEE 14-bus system. The single line diagram of this system is shown in Fig. 6.6, and details about this system can be referred to in [138].

Because these case studies focus on transient state estimation, a three-phase grounded fault at Bus 5 is simulated in PSCAD/EMTDC to produce the transient condition. PMUs are installed at all the buses in the system, and provide instantaneous measurements of the voltage and current. White Gaussian noise at 5% is added to all measurements to simulate the practical condition. Each case is performed for 100 times to evaluate the average performance of estimation accuracy and computational efficiency.
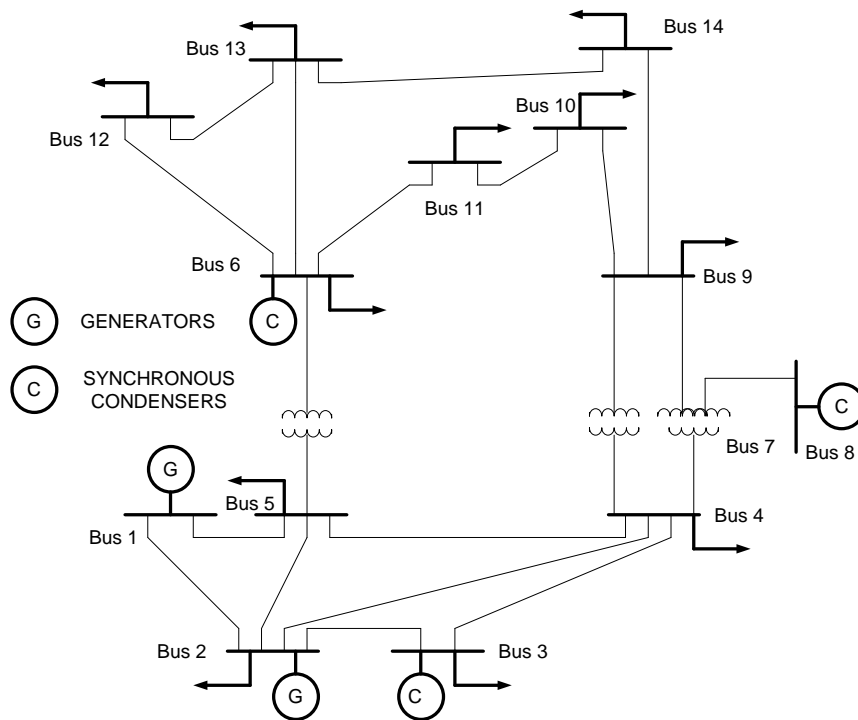
Fig. 6. 6. IEEE 14-bus test system

Four cases (one centralised case and three distributed cases) are established in these case studies, listed as follows. Case A uses TSE algorithm to estimate states during the transient condition. Case B, C and D employ the proposed DSSE algorithm to conduct transient state estimation. Different decomposition schemes are applied in these three

distributed cases.

- Case A: Centralised state estimation by the TSE algorithm [87].

- Case B: Distributed state estimation by the DSSE algorithm with the decomposition scheme 1.

- Case C: Distributed state estimation by the DSSE algorithm with the decomposition scheme 2.

- Case D: Distributed state estimation by the DSSE algorithm with the decomposition scheme 3.

The following table shows the different decomposition schemes employed in Case B, C and D. The Arabic numerals in the table denote the bus number, and the Roman numerals are the DSSE group number. Case B decomposes the IEEE 14-bus system into two groups identically, and each group contains 7 buses and 9 branches. Case C and D have 4 and 5 groups, respectively. Thus, the size of DSSE groups is smaller in Case C and D than that in Case B.

DSSE group	Case B	Case C	Case D
I	1, 2, 3, 4, 5, 7 and 8	1, 2 and 5	1, 2 and 5
II	6, 9, 10, 11, 12, 13 and 14	3, 4, 7 and 8	3 and 4
III	N/A	6, 12 and 13	6, 12 and 13
IV		9, 10, 11, and 14	7, 8 and 9
V		N/A	10, 11 and 14

Table 6. 1. Decomposition schemes on the IEEE 14-bus system

The scanning cycle of PMUs is set to 2ms in these case studies. According to the IEC 618500 standard, there are normally 80 samples per scanning cycle, so the interval between each sample of PMU instantaneous measurements is 0.025ms (2ms/80). Correspondingly, in Case A, the interval time between two estimation processes in the TSE algorithm is 0.025ms. On the other hand, regarding Case B, C and D, the interval time between two estimation processes in the DSSE algorithm equals the scanning cycle of PMUs, which is 2ms.

6.5.2 Feasibility of the DSSE algorithm

The feasibility of the proposed DSSE algorithm is validated in this section. If the proposed DSSE approach can estimate states during the transient condition accurately, this approach is feasible. This transient condition is simulated as the recovery stage of a three-phase grounded fault at Bus 5. Because the fault occurs at Bus 5, the transient fluctuation at this bus is more serious than that at any other bus. This bus is chosen as an example to demonstrate the estimation accuracy of the proposed approach. The estimated results at Bus 5 in Case B are drawn in Fig. 6.7, denoted by the square markers. The solid line is the exact values of the states at Bus 5 from the simulation.

Fig. 6.7 demonstrates that the estimated results can track the exact values effectively. The same conclusion can be drawn for other buses in Case B. Hence, Case B can perform transient state estimation with acceptable estimation accuracy. Similarly, Case C and D are also successful in the estimation of transient states. Therefore, the proposed DSSE approach is feasible.
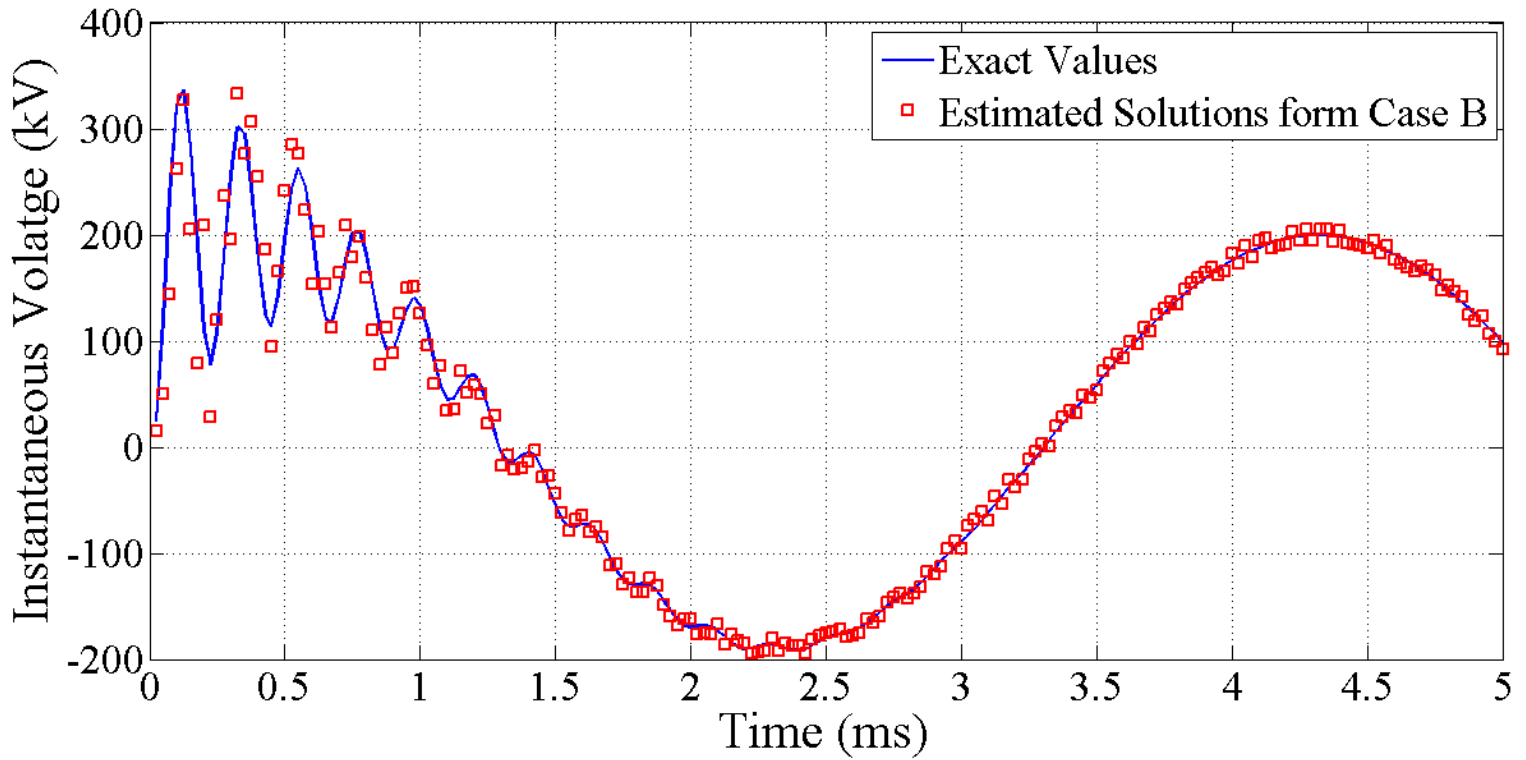
Fig. 6. 7. Estimated results at the Bus 5 in Case B

It can be also found from Fig. 6.7 that the discrepancies between the estimated results and the exact values are more obvious at the beginning period (0~0.5ms). This can be explained by the fact that the fluctuation of the voltage is more serious at the begging of the transient condition, and the more serious fluctuation can decrease the estimation accuracy of the DSSE algorithm.

6.5.3 Comparison of Estimation Accuracy

The estimation accuracy of the proposed DSSE algorithm (Case B, C and D) is compared with the TSE algorithm (Case A) in this section. The absolute discrepancies between the estimated results and the exact values are used to evaluate the estimation accuracy. It is obvious that lower absolute discrepancies mean higher estimation

accuracy. The comparison of the absolute discrepancies at Bus 5 between Case A and B during the transient condition is conducted at first. The comparison is shown in Fig. 6.8.

According to Fig. 6.8, it illustrates that the absolute discrepancies in Case B are smaller. Because Bus 5 has the most serious fluctuation in the system, the conclusion can be achieved that the DSSE approach can estimate states more accurately than the TSE algorithm at the bus with the most severe fluctuation.
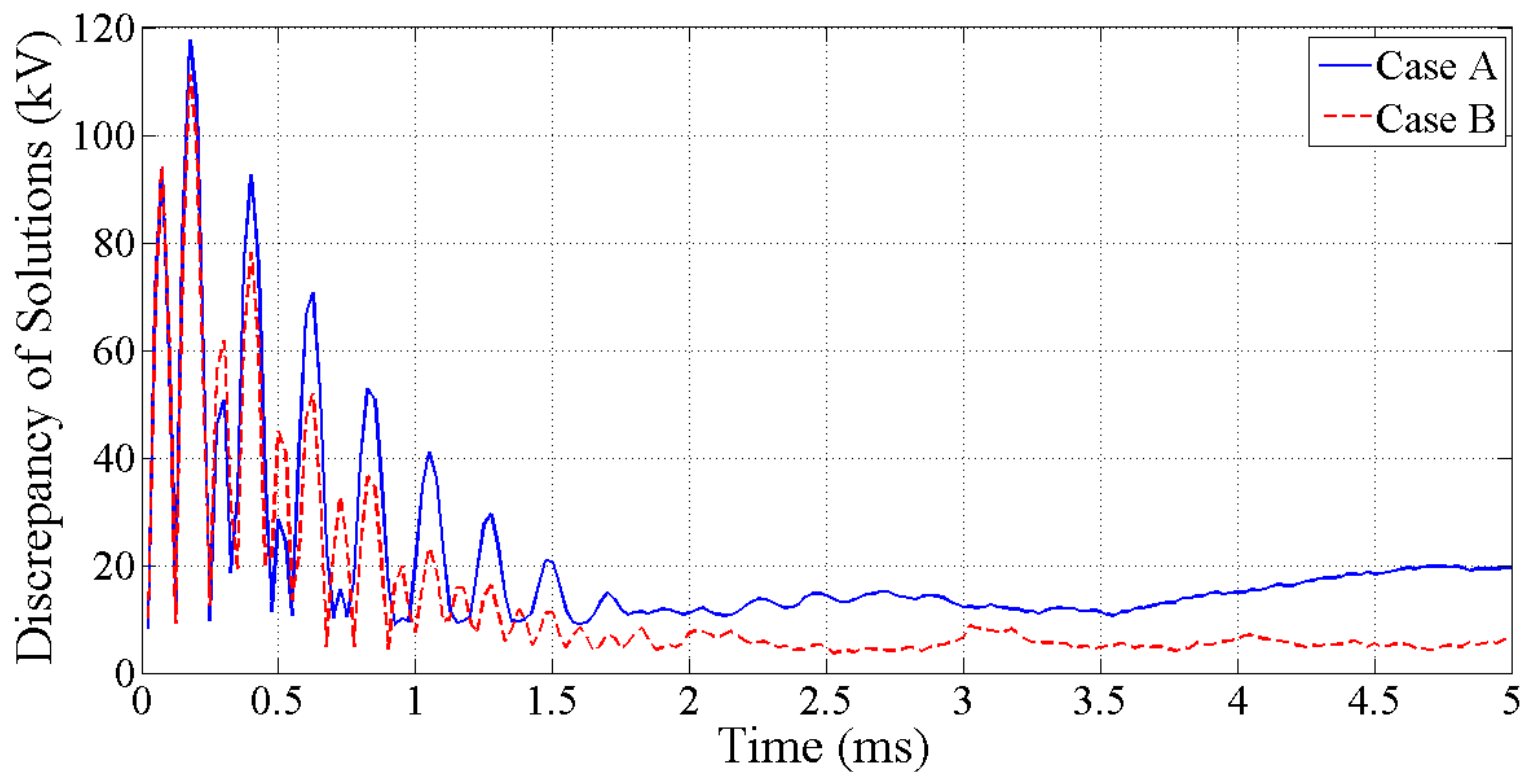
Fig. 6. 8. Comparison of discrepancies of the estimated results at Bus 5 between Case A and Case B

Afterwards, the estimation accuracy in four cases are quantised and compared. The transient error level, $\tilde{E}_{Vi}$, is introduced to evaluate the average value of the absolute

discrepancies at bus i. This level is formulated in (6.17), and it is certain that the small value of $\tilde{E}_{Vi}$ indicates higher accuracy of the estimation.

$$\tilde{E}_{Vi} = \frac{1}{N} \sum_{t=1}^{N} \left| \hat{V}_i(t) - V_i^{EX}(t) \right| \tag{6.17}$$

where

$\hat{V}_i(t)$ estimated result at Bus i at the time t.

$V_i^{EX}(t)$ exact value at Bus i at the time t.

In this case study, the transient error level at each bus is calculated by (6.17). The sum of the level for all 14 buses is used to indicate the overall estimation accuracy in each case. Table 6.2 lists the degrees for all buses and their sum in four cases.

Bus	Case A	Case B	Case C	Case D
1	8.9127	2.8999	3.1905	3.1905
2	8.3254	3.0389	3.3379	3.3379
3	8.2621	1.9754	2.9806	3.0926
4	7.9784	1.6714	2.1087	2.3743
5	20.255	12.832	17.4536	17.4536
6	5.0441	4.9609	4.9582	4.9582
7	4.8586	4.8179	4.7561	4.8277
8	5.0792	5.0935	5.1401	5.2109
9	4.7559	4.7021	4.6709	4.8293
10	4.7427	4.7586	4.7122	4.8869
11	4.8844	4.8311	4.9099	4.8735
12	4.9181	4.9026	4.9054	4.9054
13	4.9305	4.8681	4.8186	4.8186
14	4.7594	4.7202	4.7003	4.7815
Sum	97.7071	66.0726	72.6430	73.5409

Table 6. 2. Comparison of error level on the IEEE 14-bus system

Two conclusions can be drawn from the above table:

Focused on the last line of the table, the sum of transient error level in Case B, C and D (66.0726, 72.6430 and 73.5409) are all smaller than that in Case A (97.7071). This means the estimations in Case B, C and D are more accurate, and so the proposed DSSE algorithm has higher estimation accuracy than the TSE algorithm.

In comparison of Case B, C and D, the sum of transient error level in Case B is the minimum, whilst that in Case D is the maximum. According to Table 6.1, the number of DSSE groups in Case B, C and D are 2, 4 and 5, respectively. In conclusion, the estimation accuracy of the DSSE algorithm will decrease if more DSSE groups are formed from the original large system.

6.5.4 Comparison of Computational Efficiency

Compared with the TSE algorithm, the proposed DSSE algorithm has improved computational efficiency because a distributed configuration is employed in the DSSE algorithm. This case study demonstrates this improvement through the comparison of CPU time among four cases. Due to the distributed configuration, the proposed DSSE algorithm can be implemented in a parallel processing scheme naturally. In this parallel processing scheme, local estimations in all DSSE groups are performed concurrently, and the final computational time depends on the estimation with the maximum CPU time.

These case studies are simulated by MATLAB R2009b in the desktop PC with an

Intel Core 2 Quad 2.83GHz CPU. The communication time between PMUs and estimators is not considered at the present work. The average computational time of 100 tests in each case is normalised according to the time in Case A. The comparison of normalised CPU time is depicted in Fig. 6.9.
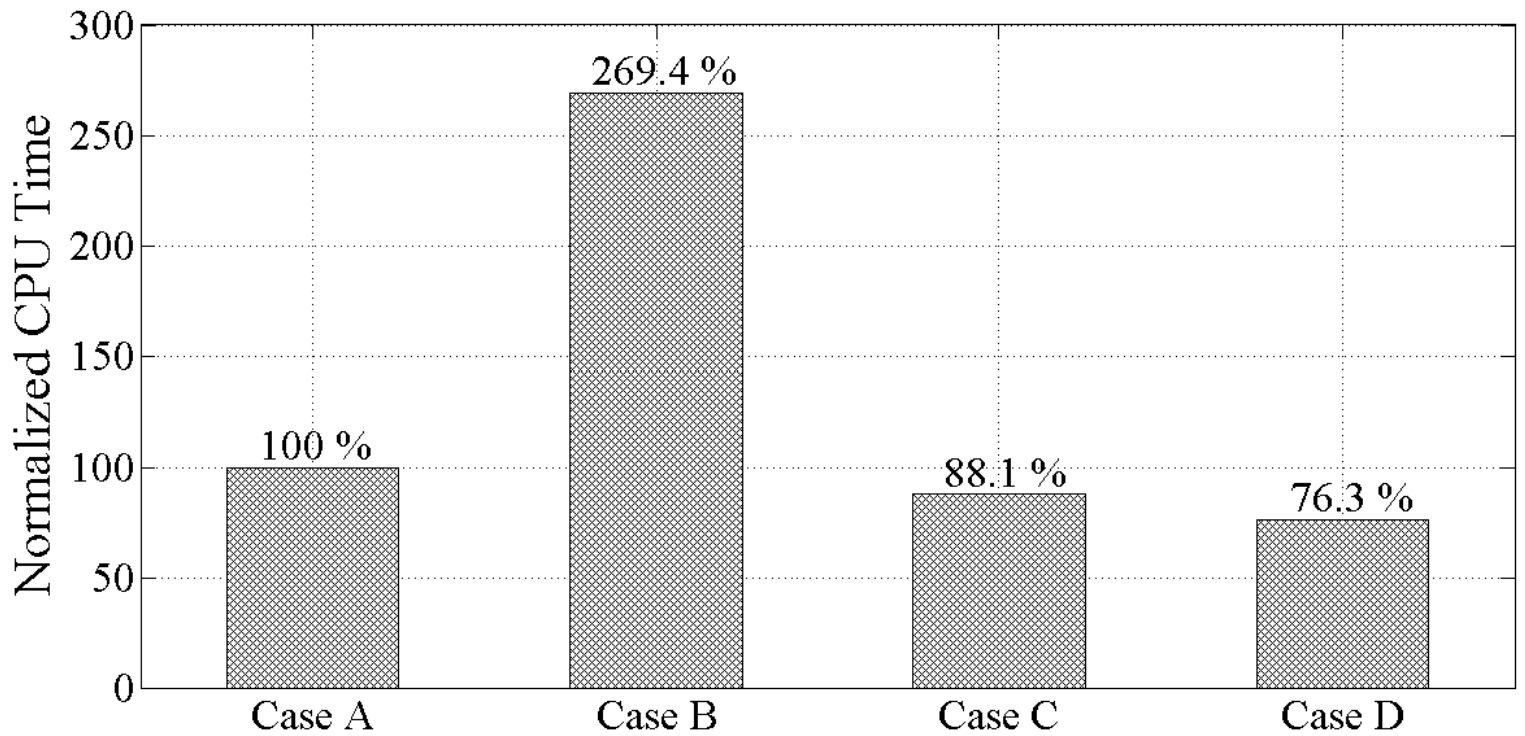
Fig. 6. 9. Comparison of normalised CPU time on the IEEE 14-bus system

Fig. 6.9 can illustrate two results:

1) Compared the DSSE algorithm with the TSE algorithm, Case B takes longer CPU time than Case A, whilst Case C and D cost less. This means that the proposed DSSE algorithm, with a reasonable decomposition scheme, can have higher computational efficiency than the TSE algorithm.

2) In comparison of the cases with the DSSE algorithms (Case B, C and D), it shows

that the computational time is decreased from Case B, C to D. On the other hand, the number of DSSE groups in Case B, C and D are 2, 4 and 5 as shown in Table 6.1. Therefore, the computational efficiency of the DSSE algorithm is enhanced when more DSSE groups are formed from the original large system.

In practice, the scale of power systems is much larger than the IEEE 14-bus system, and more DSSE groups can be formed. Correspondingly, this can further strength the improvement of the DSSE algorithm in computational efficiency.

6.5 Summary

The DSSE algorithm is proposed in this chapter, and it is the algorithm to conduct transient state estimation. This algorithm considers practical PMU measurements to estimate transient states, and thus it is the first method of its kind, which can be implemented in actual power systems.

A distributed configuration is employed in the DSSE algorithm. The large system is decomposed into a number of DSSE groups, where local DSSE estimations can be performed individually. Consequently, the computational efficiency in local estimations can be improved. In addition, the DSSE algorithm is more suitable for future power systems as a result of the distributed control and distributed operation in the Smart Grid.

The proposed DSSE algorithm is validated through the case studies on the IEEE 14-bus system, and its estimation accuracy and computational efficiency are

compared with the existing TSE algorithm. According to the simulation results, with a reasonable decomposition scheme, the DSSE algorithm can have higher accuracy and higher computational efficiency.

In addition to the performance, the DSSE algorithm has a more important advantage compared with the TSE algorithm. The DSSE algorithm is able to be implemented in practical power systems because its requirements can be met by current technology. On the contrary, the TSE algorithm is based on ideal measurements and data transmission, and therefore it may not be considered practical.

Similar to the proposed algorithms in previous chapters, the communication time in the DSSE algorithm between PMUs and estimators has not been considered, and this communication time will be included in the future.

CHAPTER 7 CONCLUSION AND FUTURE RESEARCH

7.1 Conclusion

As the power system is becoming larger and more complex, its security faces more severe challenges than ever before, and therefore the corresponding security analysis is even more necessary and important. The EMS system can provide the tool to analyse security and control functions, and as such it is widely employed in modern power systems. State estimation, as the backbone of the EMS/SCADA system, has attracted more attention in recent years. A great amount of progress has been achieved to promote the development of state estimation in software and hardware. One crucial breakthrough in hardware is the introduction of PMU measurements. PMUs are novel measurement tools, which can provide more accurate measurements than conventional ones. This introduction of PMU measurements can be regarded as a revolution in the state estimation in the last decade.

PMU measurements can improve state estimation in several aspects, including estimation accuracy and synchronisation of states in different systems. A large amount of research contributes to the development of the integration of PMU measurements with state estimation, but several unresolved problems remain. This was the primary motivation in this thesis. Two algorithms were proposed to solve the problem of low efficiency caused by the introduction of PMU measurements to state estimation. In addition, an applicable transient state estimation algorithm was proposed based on

PMU measurements.

The conclusion of this thesis covers the following aspects:

1. PMU measurements can provide the voltage and current phasor measurements directly. A linear estimation approach can be used to perform state estimation with PMU measurements. This linear approach is a simple solution and has higher computational efficiency, but it requires that all the measurements are provided from PMUs. This requirement is impossible in practice due to high cost of PMUs. In Chapter 4, a virtual aggregated system was created at the upper level of the DSELC algorithm, and the requirement of the linear approach can be met in this system. Through this virtual system, the linear estimation can be applied with a limited number of PMUs, and thus its applicability is improved.

2. One prediction is that PMU measurements could replace all conventional RTU measurements in state estimation. However, this replacement cannot be achieved in the near future, due to economic reasons. The most likely situation is that both PMU and RTU measurements are used in the estimation together. In this situation, PMU measurements are integrated into conventional WLS estimation approach and fast decoupled estimation approach, as shown in Chapters 4 and 5, respectively. Corresponding procedures of bad data processing in these two cases were also described. Numerical results demonstrate the improvements in estimation accuracy in both approaches.

3. There appear to be two main problems after the integration of PMU

measurements with state estimation. One problem is that a limited number of PMUs can be installed in the system. Much progress has been made to place these limited number of PMUs to achieve the optimal observability and estimation accuracy. The other problem is low computational efficiency caused by the integration. Litter progress has been made in this problem. To deal with this problem, two novel algorithms, named DSELC and FDSELC, were proposed in Chapters 4 and 5. Numerical results show that both algorithms are feasible and can mitigate the problem effectively.

4. The proposed DSELC and FDSELC algorithms employ a distributed configuration, and these algorithms belong to the distributed state estimation. The distributed state estimation is flexible in practice, because it is easy to adapt to the distributed generation and control paradigm in future power systems. This has become more favourable in recent years. It is considered that the distributed state estimation will act as the fundamental function in the Smart Grid. Therefore, the proposed DSELC and FDSELC algorithms would have better applicability in future power systems.

5. The synchronised measurements from PMUs can also be introduced to transient state estimation. Compared with static methods, transient state estimation is more meaningful in practice. However, there is no transient state estimation algorithm to date that could be implemented in actual power systems. A novel algorithm in transient state estimation, named as DSSE, was proposed in Chapter 6. The proposed

algorithm considers the facts of synchronised measurements from PMUs including the scanning cycle and sampling rate, etc. This algorithm is more applicable because its requirement can be met by current hardware conditions. Hence, the proposed DSSE algorithm can be employed in actual power systems to estimate the states of buses during the transient condition. Simulation results verify the performance of the DSSE algorithm. With a reasonable decomposition strategy, the proposed algorithm has improved accuracy and efficiency compared with the existing algorithm in transient state estimation.

7.2 Future Research

In this thesis, there are three main advances identified that could be achieved in the future.

Three distributed algorithms in state estimation are proposed based on PMU measurements in Chapters 4, 5 and 6. Due to hardware limitations, the communication time between subsystems, and the time between subsystems and the coordinator in these three algorithms are not considered in this current work. This issue can affect the analysis of computational efficiency in case studies. To make it more practical, the inclusion of this variable would be introduced in future research.

The proposed DSELC, FDSELC and DSSE algorithms only focus on the estimation and the bad data processing. Other auxiliary functions are not considered in these three algorithms. To improve the reliability and applicability of the proposed algorithms, some processes, such as distributed observability analysis and the

144

distributed topology processor, would be investigated in the future and combined with

the proposed algorithms.

Regarding the DSSE algorithm in Chapter 6, it provides the theoretical possibility to

perform the transient state estimation in practice. However, some actual problems still

need to be considered including the communication speed and the hardware cost.

These problems would be also involved in the next step.

APPENDIX

A.1 Equations in Static State Estimation

A.1.1 Measurement Model

In static state estimation, the measurement model is described as:

$$\begin{bmatrix} z_1 \\ z_2 \\ \vdots \\ z_m \end{bmatrix} = \begin{bmatrix} h_1(x_1, x_2, \cdots, x_n) \\ h_2(x_1, x_2, \cdots, x_n) \\ \vdots \\ h_m(x_1, x_2, \cdots, x_n) \end{bmatrix} + \begin{bmatrix} e_1 \\ e_2 \\ \vdots \\ e_n \end{bmatrix} \tag{A.1}$$

$$z = h(x) + e \tag{A.2}$$

The states in static state estimation are defined as the voltage magnitude and phase angle at each bus. In mathematic expression, they can be formulated as:

$$x_i = \begin{bmatrix} v_i & \theta_i \end{bmatrix}^T \tag{A.3}$$

In the proposed algorithms in Chapters 4 and 5, the measurements consist of RTU and PMU measurements. According to Section 4.2.2, RTUs can provide the measurements of voltage magnitudes, active and reactive power flows, and active and reactive power injections. PMU measurements are comprised of voltage magnitudes, phase angles, real parts and imaginary parts of the current phasors. Hence, details of RTU and PMU measurements are expressed as:

$$z_{RTU} = \begin{bmatrix} z_v & z_{pf} & z_{qf} & z_{pinj} & z_{qinj} \end{bmatrix}^T \tag{A.4}$$

$$z_{PMU} = \begin{bmatrix} z_v & z_a & z_{i\,\mathrm{Re}} & z_{i\,\mathrm{Im}} \end{bmatrix}^T \tag{A.5}$$

For each type of measurements in (A.4) and (A.5), there is a nonlinear function h_i relating the measurements to the states. These nonlinear functions are shown in this appendix in a typical example of the PI branch ij. The voltage magnitudes and phase angles at two terminals are v_i, v_j and θ_i, θ_j, respectively. Both RTUs and PMUs can measure voltage magnitudes, and the corresponding nonlinear functions are the same. Thus, they are only formulated in (A.6) and (A.7).

In practical transmission system, the values of grounded parts can be ignored, and the PI branch has the admittance of $y_{ij}=g_{ij}+i*b_{ij}$. The angle difference at this branch is denoted as $\theta_{ij}=\theta_i-\theta_j$, and the corresponding entry in Node Admittance Matrix is expressed as $Y_{ij}=G_{ij}+i*B_{ij}$. Hence, the equations for the nonlinear function associated with each type of measurements are listed as follows:

- RTU measurements:

$$z_{v,i} = v_i \tag{A.6}$$

$$z_{v,j} = v_j \tag{A.7}$$

$$z_{pf,ij} = v_i^2 g_{ij} - v_i v_j (g_{ij}\cos\theta_{ij} + b_{ij}\sin\theta_{ij}) \tag{A.8}$$

$$\begin{aligned} z_{pf,ji} &= v_j^2 g_{ji} - v_j v_i (g_{ji}\cos\theta_{ji} + b_{ji}\sin\theta_{ji}) \\ &= v_j^2 g_{ij} - v_i v_j (g_{ij}\cos\theta_{ij} - b_{ij}\sin\theta_{ij}) \end{aligned} \tag{A.9}$$

$$z_{qf,ij} = -v_i^2 b_{ij} - v_i v_j (g_{ij}\sin\theta_{ij} - b_{ij}\cos\theta_{ij}) \tag{A.10}$$

$$\begin{aligned} z_{qf,ji} &= -v_j^2 b_{ji} - v_j v_i (g_{ji}\sin\theta_{ji} - b_{ji}\cos\theta_{ji}) \\ &= -v_j^2 b_{ij} - v_i v_j (-g_{ij}\sin\theta_{ij} + b_{ij}\cos\theta_{ij}) \end{aligned} \tag{A.11}$$

$$z_{pinj,i} = \sum_{j=1}^{n} v_i v_j (G_{ij}\cos\theta_{ij} + B_{ij}\sin\theta_{ij}) \tag{A.12}$$

$$z_{qinj,i} = \sum_{j=1}^{n} v_i v_j (G_{ij} \sin \theta_{ij} - B_{ij} \cos \theta_{ij}) \qquad (A.13)$$

- PMU measurements:

As for the measurements of voltage magnitudes from PMUs, the formulations are the same as (A.6) and (A.7).

$$z_{a,i} = \theta_i \qquad (A.14)$$

$$z_{a,j} = \theta_j \qquad (A.15)$$

$$z_{i\,\mathrm{Re}} = v_i (g_{ij} \cos \theta_i - b_{ij} \sin \theta_i) - v_j (g_{ij} \cos \theta_j - b_{ij} \sin \theta_j) \qquad (A.16)$$

$$z_{i\,\mathrm{Im}} = v_i (g_{ij} \sin \theta_i + b_{ij} \cos \theta_i) - v_j (g_{ij} \sin \theta_j + b_{ij} \cos \theta_j) \qquad (A.17)$$

A.1.2 Jacobian Matrix

The entries in the Jacobian matrix are the first order differential of the nonlinear functions formulated above to states. In the PI branch model, the states are v_i, v_j θ_i, and θ_j. Thus, regarding each nonlinear function, there are four entries may not be zero, and others would be zero. These entries can be formulated as follows:

- Jacobian matrix entries for RTU measurements:

$$\frac{\partial z_{v,i}}{\partial v_i} = 1 \qquad (A.18)$$

$$\frac{\partial z_{v,i}}{\partial v_j} = 0 \qquad (A.19)$$

$$\frac{\partial z_{v,i}}{\partial \theta_i} = 0 \qquad (A.20)$$

$$\frac{\partial z_{v,i}}{\partial \theta_j} = 0 \tag{A.21}$$

$$\frac{\partial z_{v,j}}{\partial v_i} = 0 \tag{A.22}$$

$$\frac{\partial z_{v,j}}{\partial v_j} = 1 \tag{A.23}$$

$$\frac{\partial z_{v,j}}{\partial \theta_i} = 0 \tag{A.24}$$

$$\frac{\partial z_{v,j}}{\partial \theta_j} = 0 \tag{A.25}$$

$$\frac{\partial z_{pf,ij}}{\partial v_i} = 2v_i g_{ij} - v_j (g_{ij} \cos \theta_{ij} + b_{ij} \sin \theta_{ij}) \tag{A.26}$$

$$\frac{\partial z_{pf,ij}}{\partial v_j} = -v_i (g_{ij} \cos \theta_{ij} + b_{ij} \sin \theta_{ij}) \tag{A.27}$$

$$\frac{\partial z_{pf,ij}}{\partial \theta_i} = -v_i v_j (-g_{ij} \sin \theta_{ij} + b_{ij} \cos \theta_{ij}) \tag{A.28}$$

$$\frac{\partial z_{pf,ij}}{\partial \theta_j} = -v_i v_j (g_{ij} \sin \theta_{ij} - b_{ij} \cos \theta_{ij}) \tag{A.29}$$

$$\frac{\partial z_{pf,ji}}{\partial v_i} = -v_j (g_{ij} \cos \theta_{ij} + b_{ij} \sin \theta_{ij}) \tag{A.30}$$

$$\frac{\partial z_{pf,ji}}{\partial v_j} = 2v_j g_{ij} - v_i (g_{ij} \cos \theta_{ij} - b_{ij} \sin \theta_{ij}) \tag{A.31}$$

$$\frac{\partial z_{pf,ji}}{\partial \theta_i} = -v_i v_j (-g_{ij} \sin \theta_{ij} - b_{ij} \cos \theta_{ij}) \tag{A.32}$$

$$\frac{\partial z_{pf,ji}}{\partial \theta_j} = -v_i v_j (g_{ij} \sin \theta_{ij} + b_{ij} \cos \theta_{ij}) \tag{A.33}$$

$$\frac{\partial z_{qf,ij}}{\partial v_i} = -2v_i b_{ij} - v_j (g_{ij} \sin \theta_{ij} - b_{ij} \cos \theta_{ij}) \tag{A.34}$$

$$\frac{\partial z_{qf,ij}}{\partial v_j} = -v_i(g_{ij}\sin\theta_{ij} - b_{ij}\cos\theta_{ij}) \tag{A.35}$$

$$\frac{\partial z_{qf,ij}}{\partial \theta_i} = -v_i v_j(g_{ij}\cos\theta_{ij} + b_{ij}\sin\theta_{ij}) \tag{A.36}$$

$$\frac{\partial z_{qf,ij}}{\partial \theta_j} = -v_i v_j(-g_{ij}\cos\theta_{ij} - b_{ij}\sin\theta_{ij}) \tag{A.37}$$

$$\frac{\partial z_{qf,ji}}{\partial v_i} = -v_j(-g_{ij}\sin\theta_{ij} + b_{ij}\cos\theta_{ij}) \tag{A.38}$$

$$\frac{\partial z_{qf,ji}}{\partial v_j} = -2v_j b_{ij} - v_i(-g_{ij}\sin\theta_{ij} + b_{ij}\cos\theta_{ij}) \tag{A.39}$$

$$\frac{\partial z_{qf,ji}}{\partial \theta_i} = -v_i v_j(-g_{ij}\cos\theta_{ij} - b_{ij}\sin\theta_{ij}) \tag{A.40}$$

$$\frac{\partial z_{qf,ji}}{\partial \theta_j} = -v_i v_j(g_{ij}\cos\theta_{ij} + b_{ij}\sin\theta_{ij}) \tag{A.41}$$

$$\frac{\partial z_{pinj,i}}{\partial v_i} = \sum_{j=1}^{n} v_j(G_{ij}\cos\theta_{ij} + B_{ij}\sin\theta_{ij}) \tag{A.42}$$

$$\frac{\partial z_{pinj,i}}{\partial v_j} = \sum_{j=1}^{n} v_i(G_{ij}\cos\theta_{ij} + B_{ij}\sin\theta_{ij}) \tag{A.43}$$

$$\frac{\partial z_{pinj,i}}{\partial \theta_i} = \sum_{j=1}^{n} v_i v_j(-G_{ij}\sin\theta_{ij} + B_{ij}\cos\theta_{ij}) \tag{A.44}$$

$$\frac{\partial z_{pinj,i}}{\partial \theta_j} = \sum_{j=1}^{n} v_i v_j(G_{ij}\sin\theta_{ij} - B_{ij}\cos\theta_{ij}) \tag{A.45}$$

$$\frac{\partial z_{qinj,i}}{\partial v_i} = \sum_{j=1}^{n} v_j(G_{ij}\sin\theta_{ij} - B_{ij}\cos\theta_{ij}) \tag{A.46}$$

$$\frac{\partial z_{qinj,i}}{\partial v_j} = \sum_{j=1}^{n} v_i(G_{ij}\sin\theta_{ij} - B_{ij}\cos\theta_{ij}) \tag{A.47}$$

$$\frac{\partial z_{qinj,i}}{\partial \theta_i} = \sum_{j=1}^{n} v_i v_j(G_{ij}\cos\theta_{ij} + B_{ij}\sin\theta_{ij}) \tag{A.48}$$

$$\frac{\partial z_{qinj,i}}{\partial \theta_j} = \sum_{j=1}^{n} v_i v_j (-G_{ij} \cos \theta_{ij} - B_{ij} \sin \theta_{ij}) \tag{A.49}$$

- Jacobian matrix entries for PMU measurements:

$$\frac{\partial z_{a,i}}{\partial v_i} = 0 \tag{A.50}$$

$$\frac{\partial z_{a,i}}{\partial v_j} = 0 \tag{A.51}$$

$$\frac{\partial z_{a,i}}{\partial \theta_i} = 1 \tag{A.52}$$

$$\frac{\partial z_{a,i}}{\partial \theta_j} = 0 \tag{A.53}$$

$$\frac{\partial z_{a,j}}{\partial v_i} = 0 \tag{A.54}$$

$$\frac{\partial z_{a,j}}{\partial v_j} = 0 \tag{A.55}$$

$$\frac{\partial z_{a,j}}{\partial \theta_i} = 1 \tag{A.56}$$

$$\frac{\partial z_{a,j}}{\partial \theta_j} = 0 \tag{A.57}$$

$$\frac{\partial z_{i\,\mathrm{Re}}}{\partial v_i} = g_{ij} \cos \theta_i - b_{ij} \sin \theta_i \tag{A.58}$$

$$\frac{\partial z_{i\,\mathrm{Re}}}{\partial v_j} = -(g_{ij} \cos \theta_j - b_{ij} \sin \theta_j) \tag{A.59}$$

$$\frac{\partial z_{i\,\mathrm{Re}}}{\partial \theta_i} = v_i(-g_{ij} \sin \theta_i - b_{ij} \cos \theta_i) \tag{A.60}$$

$$\frac{\partial z_{i\,\mathrm{Re}}}{\partial \theta_j} = -v_j(-g_{ij} \sin \theta_j - b_{ij} \cos \theta_j) \tag{A.61}$$

$$\frac{\partial z_{i\,\text{Im}}}{\partial v_i} = g_{ij}\sin\theta_i + b_{ij}\cos\theta_i \tag{A.62}$$

$$\frac{\partial z_{i\,\text{Im}}}{\partial v_j} = -(g_{ij}\sin\theta_j + b_{ij}\cos\theta_j) \tag{A.63}$$

$$\frac{\partial z_{i\,\text{Im}}}{\partial \theta_i} = v_i(g_{ij}\cos\theta_i - b_{ij}\sin\theta_i) \tag{A.64}$$

$$\frac{\partial z_{i\,\text{Im}}}{\partial \theta_j} = -v_j(g_{ij}\cos\theta_j - b_{ij}\sin\theta_j) \tag{A.65}$$

A.2 Test Results in the Thesis

A.2.1 Case Results in Chapter 4

In Chapter 4, there are two test systems, the IEEE 30-bus and 118-bus system. According to Table 4.1, four cases are established in each test system. Two cases apply centralised methods, whilst other two employ distributed algorithms. In distributed cases, the IEEE 30-bus system and 118-bus system are decomposed into 3 and 4 subsystems, respectively. The estimated solutions for all subsystems and the aggregated system are also recorded. Because the same algorithm is performed at the subsystem level in two distributed cases, the test results at this level are the same in these two cases. Thus, they would be listed once. The test results for each case are listed in terms of the maximum, minimum and average error level for voltage magnitudes and phase angles.

- IEEE 30-Bus System

	Maximum		Minimum		Average
	Value	Bus	Value	Bus	

			Maximum		Minimum		Average
			Value	Bus	Value	Bus	
Case A	Voltage		0.03166	30	0.01787	22	0.02014
	Angle		0.00415	30	0.00183	4	0.00253
Case B	Voltage		0.02365	26	0.01059	22	0.01211
	Angle		0.00327	30	0.00038	28	0.00092
Case C	Voltage		0.02932	26	0.01288	22	0.01882
	Angle		0.00271	11	0.00039	28	0.00103
Case D	Voltage		0.02932	26	0.01225	22	0.01874
	Angle		0.00271	11	0.00038	28	0.00103

Table A. 1. Error level on the IEEE 30-bus system in Chapter 4

			Maximum		Minimum		Average
			Value	Bus	Value	Bus	
Subsystem Level	Subsystem 1	Voltage	0.02166	11	0.01932	2	0.02007
		Angle	0.00271	11	0.00046	4	0.00105
	Subsystem 2	Voltage	0.01629	20	0.01573	13	0.01616
		Angle	0.00175	13	0.00069	15	0.00088
	Subsystem 3	Voltage	0.02932	26	0.02009	27	0.02565
		Angle	0.00280	23	0.00058	28	0.00208
Coordination Level	Case C	Voltage	0.02229	15	0.01288	22	0.01636
		Angle	0.00065	23	0.00039	28	0.00048
	Case D	Voltage	0.02268	4	0.01225	22	0.01613
		Angle	0.00065	23	0.00038	28	0.00047

Table A. 2. Error level in the distributed cases on the IEEE 30-bus system in Chapter

4

• IEEE 118-Bus System

		Maximum		Minimum		Average
		Value	Bus	Value	Bus	
Case E	Voltage	0.01293	44	0.00829	66	0.01009
	Angle	0.02071	87	0.01115	15	0.01370
Case F	Voltage	0.00969	87	0.00416	66	0.00513
	Angle	0.01233	87	0.00158	65	0.00315
Case G	Voltage	0.02124	18	0.00923	66	0.01224

	Angle	0.01219	117	0.00240	113	0.00484
Case H	Voltage	0.02299	63	0.00364	66	0.01335
	Angle	0.01219	117	0.00216	66	0.00497

Table A. 3. Error level on the IEEE 118-bus system in Chapter 4

			Maximum		Minimum		Average
			Value	Bus	Value	Bus	
Subsystem Level	Subsystem 1	Voltage	0.01452	117	0.01094	10	0.01289
		Angle	0.01219	117	0.00238	17	0.00536
	Subsystem 2	Voltage	0.00943	49	0.01098	33	0.01013
		Angle	0.00540	43	0.00260	49	0.00336
	Subsystem 3	Voltage	0.01666	20	0.00923	66	0.01117
		Angle	0.01344	20	0.00363	69	0.00566
	Subsystem 4	Voltage	0.01406	87	0.01223	100	0.01289
		Angle	0.00935	87	0.00453	100	0.00549
Coordination Level	Case G	Voltage	0.02221	82	0.01435	66	0.01797
		Angle	0.00500	18	0.00327	15	0.00418
	Case H	Voltage	0.02299	63	0.00364	66	0.01776
		Angle	0.00663	47	0.00216	66	0.00445

Table A. 4. Error level in the distributed cases on the IEEE 118-bus system in Chapter 4

A.2.2 Case Results in Chapter 5

In Chapter 5, larger test systems are employed to demonstrate the performance of the proposed FDSELC algorithm. The case studies are conducted on the IEEE 118-bus and 300-bus systems. Four subsystems are separated in both test systems. Based on Table 5.1, five cases are established in each system. Two cases apply the centralised algorithm, and other three are distributed cases. According to the algorithm employed, Case C and D, and Case H and I have the same results at the subsystem level. The test

results for each case are listed based on the maximum, minimum and average error level for voltage magnitudes and phase angles.

- IEEE 118-Bus System

		Maximum		Minimum		Average
		Value	Bus	Value	Bus	
Case A	Voltage	0.01350	87	0.00836	66	0.01045
	Angle	0.01822	87	0.01133	15	0.01332
Case B	Voltage	0.01213	87	0.00453	10	0.00580
	Angle	0.01305	87	0.00168	59	0.00327
Case C	Voltage	0.02124	18	0.00923	66	0.01224
	Angle	0.01219	117	0.00240	113	0.00484
Case D	Voltage	0.02299	63	0.00364	66	0.01335
	Angle	0.01219	117	0.00216	66	0.00497
Case E	Voltage	0.02191	82	0.00366	66	0.01368
	Angle	0.01184	21	0.00220	49	0.00510

Table A. 5. Error level on the IEEE 118-bus system in Chapter 5

			Maximum		Minimum		Average
			Value	Bus	Value	Bus	
Subsystem Level in Case C and D	Subsystem 1	Voltage	0.01452	117	0.01094	10	0.01289
		Angle	0.01219	117	0.00238	17	0.00536
	Subsystem 2	Voltage	0.00943	49	0.01098	33	0.01013
		Angle	0.00540	43	0.00260	49	0.00336
	Subsystem 3	Voltage	0.01666	20	0.00923	66	0.01117
		Angle	0.01344	20	0.00363	69	0.00566
	Subsystem 4	Voltage	0.01406	87	0.01223	100	0.01289
		Angle	0.00935	87	0.00453	100	0.00549
Subsystem Level in Case E	Subsystem 1	Voltage	0.01471	117	0.01115	10	0.01297
		Angle	0.01152	117	0.00228	17	0.00526
	Subsystem 2	Voltage	0.01205	33	0.01044	49	0.01114
		Angle	0.00554	33	0.00309	49	0.00366
	Subsystem 3	Voltage	0.01712	20	0.01018	66	0.01202
		Angle	0.01342	20	0.00419	80	0.00602

			Value	Bus	Value	Bus	
	Subsystem 4	Voltage	0.01417	87	0.01245	97	0.01315
		Angle	0.00950	87	0.00487	100	0.00579
Coordination Level	Case C	Voltage	0.02221	82	0.01435	66	0.01797
		Angle	0.00500	18	0.00327	15	0.00418
	Case D	Voltage	0.02299	63	0.00364	66	0.01776
		Angle	0.00663	47	0.00216	66	0.00445
	Case E	Voltage	0.02191	82	0.00366	66	0.01749
		Angle	0.00681	47	0.00220	49	0.00445

Table A. 6. Error level in the distributed cases on the IEEE 118-bus system in Chapter 5

- IEEE 300-Bus System

		Maximum		Minimum		Average
		Value	Bus	Value	Bus	
Case F	Voltage	0.11959	276	0.00656	33	0.01944
	Angle	0.84599	289	0.00737	44	0.04651
Case G	Voltage	0.18568	281	0.00213	191	0.01544
	Angle	0.96967	281	0.00219	191	0.03368
Case H	Voltage	0.11422	280	0.00764	33	0.02018
	Angle	0.44996	280	0.00224	191	0.02471
Case I	Voltage	0.11422	280	0.00764	33	0.02026
	Angle	0.44996	280	0.00196	174	0.02450
Case J	Voltage	0.11308	284	0.00510	79	0.01862
	Angle	0.57479	289	0.00126	53	0.02391

Table A. 7. Error level on the IEEE 300-bus system in Chapter 5

			Maximum		Minimum		Average
			Value	Bus	Value	Bus	
Subsystem Level in Case H and I	Subsystem 1	Voltage	0.04319	238	0.00764	33	0.01326
		Angle	0.03314	238	0.00666	74	0.01038
	Subsystem 2	Voltage	0.03119	245	0.01019	79	0.01505
		Angle	0.03895	245	0.00424	89	0.00794
	Subsystem	Voltage	0.03984	133	0.01172	263	0.01785

	3	Angle	0.04273	133	0.00360	109	0.01256
	Subsystem 4	Voltage	0.11422	280	0.01196	216	0.03679
		Angle	0.44996	280	0.00435	270	0.07564
Subsystem Level in Case J	Subsystem 1	Voltage	0.03781	238	0.00777	33	0.01371
		Angle	0.03308	240	0.00313	40	0.00767
	Subsystem 2	Voltage	0.01208	58	0.00488	76	0.00707
		Angle	0.01072	236	0.00126	53	0.00286
	Subsystem 3	Voltage	0.04742	133	0.00870	166	0.01539
		Angle	0.04933	133	0.00425	171	0.01285
	Subsystem 4	Voltage	0.11308	284	0.01036	220	0.03746
		Angle	0.57479	289	0.00398	205	0.07910
Coordination Level	Case C	Voltage	0.02685	148	0.00812	208	0.01546
		Angle	0.00921	187	0.00224	191	0.00442
	Case D	Voltage	0.02379	92	0.01007	174	0.01578
		Angle	0.00914	187	0.00196	174	0.00354
	Case E	Voltage	0.02432	92	0.00973	174	0.01551
		Angle	0.00761	187	0.00203	198	0.00339

Table A. 8. Error level in the distributed cases on the IEEE 300-bus system in Chapter 5

LIST OF PUBLICATIONS & OUTCOMES

1. X. Yang, X.-P. Zhang, GB Patent "The Distributed Space State Estimation," applied to Intellectual Property Office, UK, Patent Application Number: GB1314611.3, 2013.08

2. X. Yang, X.-P. Zhang, and S. Zhou, "Coordinated algorithms for distributed state estimation with synchronized phasor measurements," *Applied Energy,* vol. 96, pp. 253-260, 2012.

3. X. Yang and X. P. Zhang, "Fast decoupled multi area state estimation with PMUs measurements," in *Innovative Smart Grid Technologies - Asia (ISGT Asia), 2012 IEEE*, 2012, pp. 1-7.

4. X. Yang and X. P. Zhang, "Fast Distributed State Estimation with Synchronized Phasor Measurements," *IEEE Trans. Smart Grid,* Submitted.

5. X. Yang and X. P. Zhang, "Distributed Space Algorithm for Transient State Estimation with PMU Measurements," *IEEE Trans. Smart Grid,* Submitted.

6. S. Zhou, X. P. Zhang, and X. Yang, "Design of demand management system for household heating & cooling," in *Innovative Smart Grid Technologies (ISGT Europe), 2012 3rd IEEE PES International Conference and Exhibition on*, 2012, pp. 1-6.

REFERENCES

[1]   U. Department of Energy & Climate Change, "Historical electricity data: 1920 to 2011," 2013.

[2]   U. Department of Energy & Climate Change, "Digest of United Kingdom energy statistics 2012 Chapter 6: Renewable sources of energy," 2012.

[3]   I. E. A. I. Statistics, "Electricity Information (2010)," 2010.

[4]   H. Yunhe and Z. Jin, "Challenges Ahead: Currents Status and Future Prospects for Chinese Energy," *Power and Energy Magazine, IEEE,* vol. 10, pp. 38-47, 2012.

[5]   U. S. C. P. S. O. T. Force, "Final Report on the August 14, 2003 Blackout in the United States and Canada: Causes and Recommendations," Apr. 5, 2004.

[6]   K. Morison, L. Wang, and P. Kundur, "Power system security assessment," *Power and Energy Magazine, IEEE,* vol. 2, pp. 30-39, 2004.

[7]   A. Abur and A. G. Exposito, *Power System State Estimation – Theory and Implementation*. New York: Marcel Dekker, 2004.

[8]   F. F. Wu, "Power system state estimation: a survey," *International Journal of Electrical Power & Energy Systems,* vol. 12, pp. 80-87, 1990.

[9]   F. C. Schweppe and J. Wildes, "Power System Static-State Estimation, Part I: Exact Model," *IEEE Trans. Power App. Syst.,* vol. PAS-89, pp. 120-125, 1970.

[10]   F. C. Schweppe and D. B. Rom, "Power System Static-State Estimation, Part II: Approximate Model," *IEEE Trans. Power App. Syst.,* vol. PAS-89, pp. 125-130, 1970.

[11]   F. C. Schweppe, "Power System Static-State Estimation, Part III: Implementation," *IEEE Trans. Power App. Syst.,* vol. PAS-89, pp. 130-135, 1970.

[12]   F. C. Schweppe and E. J. Handschin, "Static state estimation in electric power systems," *Proceedings of the IEEE,* vol. 62, pp. 972-982, 1974.

[13]   A. G. Phadke and J. S. Thorp, *Synchronized Phasor Measurements and Their Applications*. New York: Springer, 2008.

[14]   S. Chakrabarti, E. Kyriakides, B. Tianshu, C. Deyu, and V. Terzija, "Measurements get together," *Power and Energy Magazine, IEEE,* vol. 7, pp. 41-49, 2009.

[15]   A. G. Phadke and R. M. de Moraes, "The Wide World of Wide-area Measurement," *Power and Energy Magazine, IEEE,* vol. 6, pp. 52-65, 2008.

[16]   P. M. Ashton, G. A. Taylor, M. R. Irving, A. M. Carter, and M. E. Bradley, "Prospective Wide Area Monitoring of the Great Britain Transmission System using Phasor Measurement Units," in *Power and Energy Society General Meeting, 2012 IEEE*, 2012, pp. 1-8.

[17]   A. G. Phadke, J. S. Thorp, and K. J. Karimi, "State Estimation with Phasor Measurements," *IEEE Trans. Power Syst.,* vol. 1, pp. 233-238, 1986.

[18]   J. S. Thorp, A. G. Phadke, and K. J. Karimi, "Real Time Voltage-Phasor Measurement For Static State Estimation," *IEEE Trans. Power App. Syst.,* vol. PAS-104, pp. 3098-3106, 1985.

[19]   A. Gomez-Exposito, A. Abur, A. de la Villa Jaen, and C. Gomez-Quiles, "A Multilevel State

Estimation Paradigm for Smart Grids," *Proceedings of the IEEE,* vol. 99, pp. 952-976, 2011.

[20]   C. Jian and A. Abur, "Placement of PMUs to Enable Bad Data Detection in State Estimation," *IEEE Trans. Power Syst.,* vol. 21, pp. 1608-1615, 2006.

[21]   X. Yang, X.-P. Zhang, and S. Zhou, "Coordinated algorithms for distributed state estimation with synchronized phasor measurements," *Applied Energy,* vol. 96, pp. 253-260, 2012.

[22]   X. Yang and X. P. Zhang, "Fast decoupled multi area state estimation with PMUs measurements," in *Innovative Smart Grid Technologies - Asia (ISGT Asia), 2012 IEEE*, 2012, pp. 1-7.

[23]   X. Yang and X. P. Zhang, "Fast Distributed State Estimation with Synchronized Phasor Measurements," *IEEE Trans. Smart Grid,* Submitted.

[24]   X. Yang and X. P. Zhang, "Distributed Space Algorithm for Transient State Estimation with PMU Measurements," *IEEE Trans. Power Syst.,* Submitted.

[25]   *Global   Positioning   System*.   Available: http://en.wikipedia.org/wiki/Global_Positioning_System

[26]   G. Missout and P. Girard, "Measurement of Bus Voltage Angle Between Montreal and SEPT-ILES," *IEEE Trans. Power App. Syst.,* vol. PAS-99, pp. 536-539, 1980.

[27]   P. Bonanomi, "Phase Angle Measurements with Synchronized Clocks-Principle and Applications," *IEEE Trans. Power App. Syst.,* vol. PAS-100, pp. 5036-5043, 1981.

[28]   G. Missout, J. Beland, G. Bedard, and Y. Lafleur, "Dynamic Measurement of the Absolute Voltage Angle on Long Transmission Lines," *IEEE Trans. Power App. Syst.,* vol. PAS-100, pp. 4428-4434, 1981.

[29]   A. G. Phadke, M. Ibrahim, and T. Hlibka, "Fundamental basis for distance relaying with symmetrical components," *IEEE Trans. Power App. Syst.,* vol. 96, pp. 635-646, 1977.

[30]   A. G. Phadke, J. S. Thorp, and M. G. Adamiak, "A New Measurement Technique for Tracking Voltage Phasors, Local System Frequency, and Rate of Change of Frequency," *IEEE Trans. Power App. Syst.,* vol. PAS-102, pp. 1025-1038, 1983.

[31]   A. G. Phadke, "Synchronized phasor measurements in power systems," *Computer Applications in Power, IEEE,* vol. 6, pp. 10-15, 1993.

[32]   Macrodyne, "Macrodyne Model 1690 PMU Distrubance Recorder," Clifton Park, NY, 120651991.

[33]   R. O. Burnett, Jr., M. M. Butts, T. W. Cease, V. Centeno, G. Michel, R. J. Murphy, and A. G. Phadke, "Synchronized phasor measurements of a power system event," *IEEE Trans. Power Syst.,* vol. 9, pp. 1643-1650, 1994.

[34]   X. Xiaorong, X. Yaozhong, X. Jinyu, W. Jingtao, and H. Yingdao, "WAMS applications in Chinese power systems," *Power and Energy Magazine, IEEE,* vol. 4, pp. 54-63, 2006.

[35]   "IEEE Standard for Synchrophasers for Power Systems," *IEEE Std 1344-1995(R2001),* p. i, 1995.

[36]   "IEEE Standard for Synchrophasors for Power Systems," *IEEE Std C37.118-2005 (Revision of IEEE Std 1344-1995),* pp. 0_1-57, 2006.

[37] "IEEE Standard for Synchrophasor Measurements for Power Systems," *IEEE Std C37.118.1-2011 (Revision of IEEE Std C37.118-2005),* pp. 1-61, 2011.

[38] "IEEE Standard for Synchrophasor Data Transfer for Power Systems," *IEEE Std C37.118.2-2011 (Revision of IEEE Std C37.118-2005),* pp. 1-53, 2011.

[39] J. De La Ree, V. Centeno, J. S. Thorp, and A. G. Phadke, "Synchronized Phasor Measurement Applications in Power Systems," *IEEE Trans. Smart Grid,* vol. 1, pp. 20-27, 2010.

[40] Z. Zhian, X. Chunchun, B. J. Billian, Z. Li, S. S. Tsai, R. W. Conners, V. A. Centeno, A. G. Phadke, and L. Yilu, "Power system frequency monitoring network (FNET) implementation," *IEEE Trans. Power Syst.,* vol. 20, pp. 1914-1921, 2005.

[41] J. S. Thorp, A. G. Phadke, S. H. Horowitz, and M. M. Begovic, "Some applications of phasor measurements to adaptive protection," *IEEE Trans. Power Syst.,* vol. 3, pp. 791-798, 1988.

[42] V. Centeno, J. De La Ree, A. G. Phadke, G. Michel, R. J. Murphy, and R. O. Burnett, Jr., "Adaptive out-of-step relaying using phasor measurement techniques," *Computer Applications in Power, IEEE,* vol. 6, pp. 12-17, 1993.

[43] M. Kezunovic and B. Perunicic, "Automated transmission line fault analysis using synchronized sampling at two ends," *IEEE Trans. Power Syst.,* vol. 11, pp. 441-447, 1996.

[44] L. Chih-Wen, L. Tzu-Chiao, Y. Chi-Shan, and Y. Jun-Zhe, "A Fault Location Technique for Two-Terminal Multisection Compound Transmission Lines Using Synchronized Phasor Measurements," *IEEE Trans. Smart Grid,* vol. 3, pp. 113-121, 2012.

[45] C. W. Taylor, D. C. Erickson, K. E. Martin, R. E. Wilson, and V. Venkatasubramanian, "WACS-Wide-Area Stability and Voltage Control System: R&D and Online Demonstration," *Proceedings of the IEEE,* vol. 93, pp. 892-906, 2005.

[46] N. Hui, G. T. Heydt, and L. Mili, "Power system stability agents using robust wide area control," *IEEE Trans. Power Syst.,* vol. 17, pp. 1123-1131, 2002.

[47] Z. Yang and A. Bose, "Design of Wide-Area Damping Controllers for Interarea Oscillations," *IEEE Trans. Power Syst.,* vol. 23, pp. 1136-1143, 2008.

[48] H. J. Koglin, T. Neisius, G. Beiβler, and K. D. Schmitt, "Bad data detection and identification," *International Journal of Electrical Power & Energy Systems,* vol. 12, pp. 94-103, 1990.

[49] A. Gómez-Expósito, A. de la Villa Jaén, C. Gómez-Quiles, P. Rousseaux, and T. Van Cutsem, "A taxonomy of multi-area state estimation methods," *Electric Power Systems Research,* vol. 81, pp. 1060-1069, 2011.

[50] M. Brown Do Coutto Filho and J. C. S. de Souza, "Forecasting-Aided State Estimation—Part I: Panorama," *IEEE Trans. Power Syst.,* vol. 24, pp. 1667-1677, 2009.

[51] A. Monticelli, *State Estimation in Electric Power Systems: A Generalized Approach*. Norwell: Springer, 1999.

[52] H. M. Merrill and F. C. Schweppe, "Bad Data Suppression in Power System Static State Estimation," *IEEE Trans. Power App. Syst.,* vol. PAS-90, pp. 2718-2725, 1971.

[53] J. F. Dopazo, S. T. Ehrmann, O. A. Klitin, A. M. Sasson, and L. S. Van Slyck, "Implementation of the AEP real-time monitoring system," *IEEE Trans. Power App. Syst.,* vol. 95, pp. 1618-1629, 1976.

[54] B. Porretta and R. S. Dhillon, "Performance Evaluation of State Estimation from Line Flow Measurements on Ontariio Hydro Power System," *IEEE Trans. Power App. Syst.,* vol. PAS-92, pp. 1702-1712, 1973.

[55] T. A. Stuart and C. J. Herczet, "A Sensitivity Analysis of Weighted Least Squares State Estimation for Power Systems," *IEEE Trans. Power App. Syst.,* vol. PAS-92, pp. 1696-1701, 1973.

[56] H. R. Sirisena and E. P. M. Brown, "Convergence analysis of weighted least-squares and fast decoupled weighted least-squares state estimation," *International Journal of Electrical Power & Energy Systems,* vol. 6, pp. 75-78, 1984.

[57] R. A. M. van Amerongen, "On convergence analysis and convergence enhancement of power system least-squares state estimators," *IEEE Trans. Power Syst.,* vol. 10, pp. 2038-2044, 1995.

[58] W. Hubbi and Y. Wang, "Effects of the weighting matrix on power system state estimation," *Electric Power Systems Research,* vol. 22, pp. 35-39, 1991.

[59] A. K. Al-Othman and M. R. Irving, "Uncertainty modelling in power system state estimation," *Generation, Transmission and Distribution, IEE Proceedings-,* vol. 152, pp. 233-239, 2005.

[60] A. K. Al-Othman and M. R. Irving, "A comparative study of two methods for uncertainty analysis in power system State estimation," *IEEE Trans. Power Syst.,* vol. 20, pp. 1181-1182, 2005.

[61] H. P. Horisberger, J. C. Richard, and C. Rossier, "A fast decoupled static state-estimator for electric power systems," *IEEE Trans. Power App. Syst.,* vol. 95, pp. 208-215, 1976.

[62] O. Alsac, N. Vempati, B. Stott, and A. Monticelli, "Generalized state estimation," *IEEE Trans. Power Syst.,* vol. 13, pp. 1069-1075, 1998.

[63] M. R. Irving, "Robust Algorithm for Generalized State Estimation," *IEEE Trans. Power Syst.,* vol. 24, pp. 1886-1887, 2009.

[64] Z. Shan and A. Abur, "Auto tuning of measurement weights in WLS state estimation," *IEEE Trans. Power Syst.,* vol. 19, pp. 2006-2013, 2004.

[65] A. Simoes-Costa and V. H. Quintana, "A Robust Numerical Technique for Power System State Estimation," *IEEE Trans. Power App. Syst.,* vol. PAS-100, pp. 691-698, 1981.

[66] A. Simoes-Costa and V. H. Quintana, "An Orthogonal Row Processing Algorithm for Power System Sequential State Estimation," *IEEE Trans. Power App. Syst.,* vol. PAS-100, pp. 3791-3800, 1981.

[67] J. W. Wang and V. H. Quintana, "A Decoupled Orthogonal Row Processing Algorithm for Power System State Estimation," *IEEE Trans. Power App. Syst.,* vol. PAS-103, pp. 2337-2344, 1984.

[68] N. Vempati, I. W. Slutsker, and W. F. Tinney, "Enhancement to Givens rotations for power system state estimation," *IEEE Trans. Power Syst.,* vol. 6, pp. 842-849, 1991.

[69]   A. Pandian, K. Parthasarathy, and S. A. Soman, "Towards faster Givens rotations based power system state estimator," *IEEE Trans. Power Syst.,* vol. 14, pp. 837-843, 1999.

[70]   F. F. Wu, W. H. E. Liu, and S. M. Lun, "Observability analysis and bad data processing for state estimation with equality constraints," *IEEE Trans. Power Syst.,* vol. 3, pp. 541-548, 1988.

[71]   K. A. Clements, G. W. Woodzell, and R. C. Burchett, "A new method for solving equality-constrained power system static-state estimation," *IEEE Trans. Power Syst.,* vol. 5, pp. 1260-1266, 1990.

[72]   A. F., P. N., and A. E., "State Estimation with Equality Constraints," presented at the 10th PICA Conference Proceedings, Toronto, 1977.

[73]   G. N. Korres, "A robust method for equality constrained state estimation," *IEEE Trans. Power Syst.,* vol. 17, pp. 305-314, 2002.

[74]   G. N. Korres, "A Robust Algorithm for Power System State Estimation With Equality Constraints," *IEEE Trans. Power Syst.,* vol. 25, pp. 1531-1541, 2010.

[75]   E. Handschin, F. C. Schweppe, J. Kohlas, and A. Fiechter, "Bad data analysis for power system state estimation," *IEEE Trans. Power App. Syst.,* vol. 94, pp. 329-337, 1975.

[76]   K. A. Clements and P. W. Davis, "Multiple Bad Data Detectability and Identifiability: A Geometric Approach," *IEEE Trans. Power Del.,* vol. 1, pp. 355-360, 1986.

[77]   E. Caro, A. J. Conejo, R. Minguez, M. Zima, and G. Andersson, "Multiple Bad Data Identification Considering Measurement Dependencies," *IEEE Trans. Power Syst.,* vol. 26, pp. 1953-1961, 2011.

[78]   N.-d. Xiang, S.-y. Wang, and E.-k. Yu, "A New Approach for Detection and Identification of Multiple Bad Data in Power System State Estimation," *IEEE Trans. Power App. Syst.,* vol. PAS-101, pp. 454-462, 1982.

[79]   T. Van Cutsem, M. Ribbens-Pavella, and L. Mili, "Hypothesis Testing Identification: A New Method For Bad Data Analysis In Power System State Estimation," *IEEE Trans. Power App. Syst.,* vol. PAS-103, pp. 3239-3252, 1984.

[80]   L. Mili and T. Van Cutsem, "Implementation of the hypothesis testing identification in power system state estimation," *IEEE Trans. Power Syst.,* vol. 3, pp. 887-893, 1988.

[81]   T. Van Cutsem, M. Ribbens-Pavella, and L. Mili, "Bad Data Identification Methods In Power System State Estimation-A Comparative Study," *IEEE Trans. Power App. Syst.,* vol. PAS-104, pp. 3037-3049, 1985.

[82]   A. Monticelli, F. F. Wu, and M. Yen, "Mutiple Bad Data Identwication for State Estimation by Combinatorial Oftimization," *IEEE Trans. Power Del.,* vol. 1, pp. 361-369, 1986.

[83]   A. Abur and A. Gomez Exposito, "Bad data identification when using ampere measurements," *IEEE Trans. Power Syst.,* vol. 12, pp. 831-836, 1997.

[84]   M. R. Irving, R. C. Owen, and M. J. H. Sterling, "Power-system state estimation using linear programming," *Electrical Engineers, Proceedings of the Institution of,* vol. 125, pp. 879-885, 1978.

[85]   R. Ueda, H. Takata, S. Nakagaki, and S. Takata, "On the estimation of transient state of power system by discrete nonlinear observer," *IEEE Trans. Power App. Syst.,* vol. 94, pp. 2135-2140, 1975.

[86]   C. K. Gharban and B. J. Cory, "Non-Linear Dynamic Power System State Estimation," *IEEE Trans. Power Syst.,* vol. 1, pp. 276-283, 1986.

[87]   K. K. C. Yu and N. R. Watson, "An Approximate Method for Transient State Estimation," *IEEE Trans. Power Del.,* vol. 22, pp. 1680-1687, 2007.

[88]   M. Zima-Bockarjova, M. Zima, and G. Andersson, "Analysis of the State Estimation Performance in Transient Conditions," *IEEE Trans. Power Syst.,* vol. 26, pp. 1866-1874, 2011.

[89]   P. Ashton, G. A. Taylor, M. R. Irving, I. Pisica, A. Carter, and M. E. Bradley, "Novel Application of Detrended Fluctuation Analysis for State Estimation Using Synchrophasor Measurements," *IEEE Trans. Power Syst.,* vol. 28, pp. 1930-1938, 2013.

[90]   J. D. Glover and M. Sheikoleslami, "State Estimation of Interconnected HVDC/AC Systems," *IEEE Trans. Power App. Syst.,* vol. PAS-102, pp. 1805-1810, 1983.

[91]   A. M. Leite da Silva, G. Perrotta, R. B. Prada, and D. M. Falcao, "State Estimation for Integrated Multi-Terminal DC/AC Systems," *IEEE Trans. Power App. Syst.,* vol. PAS-104, pp. 2349-2355, 1985.

[92]   D. Qifeng, T. S. Chung, and Z. Boming, "An improved sequential method for AC/MTDC power system state estimation," *IEEE Trans. Power Syst.,* vol. 16, pp. 506-512, 2001.

[93]   D. Qifeng, Z. Boming, and T. S. Chung, "State estimation for power systems embedded with FACTS devices and MTDC systems by a sequential solution approach," *Electric Power Systems Research,* vol. 55, pp. 147-156, 2000.

[94]   C. Rakpenthai, S. Premrudeepreechacharn, and S. Uatrongjit, "Power system with multi-type FACTS devices states estimation based on predictor–corrector interior point algorithm," *International Journal of Electrical Power & Energy Systems,* vol. 31, pp. 160-166, 2009.

[95]   A. Garcia, A. Monticelli, and P. Abreu, "Fast Decoupled State Estimation and Bad Data Processing," *IEEE Trans. Power App. Syst.,* vol. PAS-98, pp. 1645-1652, 1979.

[96]   A. Monticelli and A. Garcia, "Fast decoupled state estimators," *IEEE Trans. Power Syst.,* vol. 5, pp. 556-564, 1990.

[97]   L. Roy and T. A. Mohammed, "Fast super decoupled state estimator for power systems," *IEEE Trans. Power Syst.,* vol. 12, pp. 1597-1603, 1997.

[98]   T. Van Cutsem and M. Ribbens-Pavella, "Critical Survey of Hierarchical Methods for State Estimation of Electric Power Systems," *IEEE Trans. Power App. Syst.,* vol. PAS-102, pp. 3415-3424, 1983.

[99]   K.A. Clements, O.J. Denison, and R. J. Ringlee, "A multi-area approach to state estimation in power system networks," presented at the IEEE PES Summer Meeting, San Francisco, 1972.

[100]   T. Van Cutsem, J. L. Horward, and M. Ribbens-Pavella, "A Two-Level Static State Estimator for Electric Power Systems," *IEEE Trans. Power App. Syst.,* vol. PAS-100, pp. 3722-3732, 1981.

[101]   M. S. Kurzyn, "Real-Time State Estimation for Large-Scale Power Systems," *IEEE Trans. Power App. Syst.,* vol. PAS-102, pp. 2055-2063, 1983.

[102]   K. L. Lo, M. M. Salem, R. D. McColl, and A. M. Moffatt, "Two-level state estimation for large power system. I. Algorithms," *Generation, Transmission and Distribution, IEE Proceedings C,* vol. 135, pp. 299-308, 1988.

[103]   K. L. Lo, M. M. Salem, R. D. McColl, and A. M. Moffatt, "Two-level state estimation for large power system. II. Computational experience," *Generation, Transmission and Distribution, IEE Proceedings C,* vol. 135, pp. 309-318, 1988.

[104]   G. N. Korres and G. C. Contaxis, "Application of a reduced model to a distributed state estimator," in *Power Engineering Society Winter Meeting, 2000. IEEE*, 2000, pp. 999-1004 vol.2.

[105]   A. Gomez-Exposito and A. de la Villa Jaen, "Two-Level State Estimation With Local Measurement Pre-Processing," *IEEE Trans. Power Syst.,* vol. 24, pp. 676-684, 2009.

[106]   C. W. Brice and R. K. Cavin, "Multiprocessor Static State Estimation," *IEEE Trans. Power App. Syst.,* vol. PAS-101, pp. 302-308, 1982.

[107]   K. Seidu and H. Mukai, "Parallel Multi-Area State Estimation," *IEEE Trans. Power App. Syst.,* vol. PAS-104, pp. 1025-1034, 1985.

[108]   A. A. El-Keib, J. Nieplocha, H. Singh, and D. J. Maratukulam, "A decomposed state estimation technique suitable for parallel processor implementation," *IEEE Trans. Power Syst.,* vol. 7, pp. 1088-1097, 1992.

[109]   R. Ebrahimian and R. Baldick, "State estimation distributed processing [for power systems]," *IEEE Trans. Power Syst.,* vol. 15, pp. 1240-1246, 2000.

[110]   G. N. Korres, "A Distributed Multiarea State Estimation," *IEEE Trans. Power Syst.,* vol. 26, pp. 73-84, 2011.

[111]   S. Y. Lin, "A distributed state estimator for electric power systems," *IEEE Trans. Power Syst.,* vol. 7, pp. 551-557, 1992.

[112]   S. Y. Lin and C. H. Lin, "An implementable distributed state estimator and distributed bad data processing schemes for electric power systems," *IEEE Trans. Power Syst.,* vol. 9, pp. 1277-1284, 1994.

[113]   A. J. Conejo, S. de la Torre, and M. Canas, "An Optimization Approach to Multiarea State Estimation," *IEEE Trans. Power Syst.,* vol. 22, pp. 213-221, 2007.

[114]   Z. Ming, V. A. Centeno, J. S. Thorp, and A. G. Phadke, "An Alternative for Including Phasor Measurements in State Estimators," *IEEE Trans. Power Syst.,* vol. 21, pp. 1930-1937, 2006.

[115]   S. Chakrabarti and E. Kyriakides, "PMU Measurement Uncertainty Considerations in WLS State Estimation," *IEEE Trans. Power Syst.,* vol. 24, pp. 1062-1071, 2009.

[116]   S. Chakrabarti, E. Kyriakides, G. Ledwich, and A. Ghosh, "Inclusion of PMU current phasor measurements in a power system state estimator," *Generation, Transmission & Distribution, IET,* vol. 4, pp. 1104-1115, 2010.

[117]   L. Vanfretti, J. H. Chow, S. Sarawgi, and B. Fardanesh, "A Phasor-Data-Based State Estimator

Incorporating Phase Bias Correction," *IEEE Trans. Power Syst.,* vol. 26, pp. 111-119, 2011.

[118] Z. Liang and A. Abur, "Multi area state estimation using synchronized phasor measurements," *IEEE Trans. Power Syst.,* vol. 20, pp. 611-617, 2005.

[119] J. Weiqing, V. Vittal, and G. T. Heydt, "A Distributed State Estimator Utilising Synchronized Phasor Measurements," *IEEE Trans. Power Syst.,* vol. 22, pp. 563-571, 2007.

[120] J. Weiqing, V. Vittal, and G. T. Heydt, "Diakoptic State Estimation Using Phasor Measurement Units," *IEEE Trans. Power Syst.,* vol. 23, pp. 1580-1589, 2008.

[121] A. Bose, "Smart Transmission Grid Applications and Their Supporting Infrastructure," *IEEE Trans. Smart Grid,* vol. 1, pp. 11-19, 2010.

[122] J. Peng, Y. Sun, and H. F. Wang, "Optimal PMU placement for full network observability using Tabu search algorithm," *International Journal of Electrical Power & Energy Systems,* vol. 28, pp. 223-231, 2006.

[123] R. Chawasak, P. Suttichai, U. Sermsak, and R. W. Neville, "An Optimal PMU Placement Method Against Measurement Loss and Branch Outage," *IEEE Trans. Power Del.,* vol. 22, pp. 101-107, 2007.

[124] S. Chakrabarti and E. Kyriakides, "Optimal Placement of Phasor Measurement Units for Power System Observability," *IEEE Trans. Power Syst.,* vol. 23, pp. 1433-1440, 2008.

[125] M. Hurtgen and J. C. Maun, "Optimal PMU placement using Iterated Local Search," *International Journal of Electrical Power & Energy Systems,* vol. 32, pp. 857-860, 2010.

[126] S. M. Mahaei and M. T. Hagh, "Minimizing the number of PMUs and their optimal placement in power systems," *Electric Power Systems Research,* vol. 83, pp. 66-72, 2012.

[127] Z. Miljanić, I. Djurović, and I. Vujošević, "Optimal placement of PMUs with limited number of channels," *Electric Power Systems Research,* vol. 90, pp. 93-98, 2012.

[128] V. Kekatos, G. B. Giannakis, and B. Wollenberg, "Optimal Placement of Phasor Measurement Units via Convex Relaxation," *IEEE Trans. Power Syst.,* vol. 27, pp. 1521-1530, 2012.

[129] U. P. S. T. C. Archive. *30 Bus Power Flow Test Case*. Available: http://www.ee.washington.edu/research/pstca/pf30/pg_tca30bus.htm

[130] U. P. S. T. C. Archive. *118 Bus Power Flow Test Case*. Available: http://www.ee.washington.edu/research/pstca/pf118/pg_tca118bus.htm

[131] I. Arbiter System. *Model 1133A Power Sentinel Data Sheet*. Available: http://www.arbiter.com/files/product-attachments/1133a.pdf

[132] A. AG. (2012). *RTU560 Data Sheet Analog Input 23AE23*. Available: http://www05.abb.com/global/scot/scot258.nsf/veritydisplay/c4353aa0ba19f88ac1257a8b0034fd86/$file/E560_AE23_DS.pdf

[133] N. D. Rao and S. C. Tripathy, "A Variable Step Size Decoupled State Estimator," *IEEE Trans. Power App. Syst.,* vol. PAS-98, pp. 436-443, 1979.

[134] J. J. Allemong, L. Radu, and A. M. Sasson, "A Fast and Reliable State Estimation Algorithm for AEP's New Control Center," *IEEE Trans. Power App. Syst.,* vol. PAS-101, pp. 933-944, 1982.

[135]   K. L. Lo and Y. M. Mahmoud, "A Decoupled Linear Programming Technique for Power System State Estimation," *IEEE Trans. Power Syst.,* vol. 1, pp. 154-160, 1986.

[136]   I. O. Habiballah and V. H. Quintana, "Fast-decoupled rectangular co-ordinate state estimation with efficient data structure management," *Generation, Transmission and Distribution, IEE Proceedings C,* vol. 138, pp. 462-468, 1991.

[137]   U. P. S. T. C. Archive. *300 Bus Power Flow Test Case*. Available: http://www.ee.washington.edu/research/pstca/pf300/pg_tca300bus.htm

[138]   U. P. S. T. C. Archive. *14 Bus Power Flow Test Case*. Available: http://www.ee.washington.edu/research/pstca/pf14/pg_tca14bus.htm